THE DEVELOPMENT AND CHARACTERIZATION OF AN OSTEOINDUCTIVE PRE-VASCULARIZED SCAFFOLD FOR BONE TISSUE REGENERATION

by

BRITTANY LOUISE TAYLOR

A dissertation submitted to the

Graduate School-New Brunswick

Rutgers, The State University of New Jersey

and

The Graduate School of Biomedical Sciences

In partial fulfillment of the requirements

For the degree of

Doctor of Philosophy

Graduate Program in Biomedical Engineering

Written under the direction of

Joseph Freeman

And approved by

_____

_____

_____

_____

New Brunswick, New Jersey

May 2016

ABSTRACT OF DISSERTATION

The Development and Characterization of an Osteoinductive Pre-Vascularized Scaffold for Bone Tissue Regeneration

By BRITTANY LOUISE TAYLOR

Dissertation Director:

Joseph Freeman, Ph.D.

Bone loss and skeletal deficiencies due to traumatic injury or disease are major problems worldwide. In the U.S., approximately 500,000 bone-grafting procedures are performed annually. The main replacement options for bone loss are autografts, allografts, and bone cements. Unfortunately, autografts are limited in supply and require an invasive second surgery that can lead to donor site morbidity. Allografts are more abundant and do not require a harvesting surgery, but have there is a potential for disease transfer and decrease in mechanical strength leading to failure rates of 30-60% over a period of 10 years *in vivo*. Given these disadvantages, tissue engineering (TE) has been heavily explored as a promising alternative treatment. Most TE options for bone replacement seek to replace only the trabecular bone leading to low mechanical properties or lack the ability to promote early vascularization *in vivo.* To overcome these limitations, we have developed a novel osteoinductive pre-vascularized three-dimensional scaffold composed of electrospun synthetic and collagen-based materials with enhanced mechanics. We hypothesize the joining of a porous trabecular scaffold with the addition of hydroxyapatite (HAp), pre-vascularized cortical bone scaffold and HAp columns will promote the differentiation of human mesenchymal stem cells (hMSCs) along the

osteoblastic and angiogenic lineage for improved mechanics and graft viability *in vivo*.

Material characterization of the scaffold confirmed pore ranges necessary for neovascularization and osteoblast infiltration and mechanical properties comparable to native bone. The porous trabecular scaffold with HAp promoted osteogenic differentiation of hMSCs *in vitro*. The decellularized cortical scaffolds had a maintained collageneous pre-vascularized matrix, which promoted hMSCs to secrete vascular endothelial growth factor (VEGF), an early angiogenesis marker. Additionally, the hMSCs seeded on the pre-vascularized matrix developed morphology indicative of endothelial lumen development in 2D. Recent subcutaneous murine *in vivo* studies confirmed significant cellular infiltration and graft biocompatibility. This technology is transformative because it will be the first synthetic bone graft to contain both trabecular and cortical bone structures and be designed for vascularized bone growth and load-bearing applications.

DEDICATION

To my mother, I am who I am because of you.

ACKNOWLEDGEMENTS

The bone project is truly my baby and I am sad to move on, but I am grateful for the many people who played a part in maturing this project. I would first like to thank my advisor, Dr. Joseph Freeman, for making this dream possible back in 2010. Had it not been for him accepting me into his lab at that time, I would not be where I am today. He challenged me to be a better scientist and innovator than I ever could have imaged. This has been a fruitful experience working under his guidance and I am forever grateful for this opportunity. I look forward to one day collaborating with him! I would also like to thank Dr. Charles Gatt, Dr. Ronke Olabisi, and Dr. J. Christopher Fritton for serving on my thesis committee. Their insight on orthopedic surgeries, bone biology, and biomaterials has been extremely valuable to the progression of my thesis research. I would also like to acknowledge students I had the opportunity to mentor, Xiomara Perez, Sarah Indano, Pushpendra Patel and Apurva Limaye, who played a significant role on the bone project. The Musculoskeletal Tissue Regeneration Lab is a family and we all help each other in many ways and for that I would like to thank all the current and past members of the lab. Additionally, I would like to thank Dr. Greg Veronin and Dr. Barbara Perry for assisting with the animal protocols, providing their expertise on animal surgeries and always being a call or email away to answer any questions I had pertaining to the mouse surgery. I am also grateful for the friendship I created with fellow BME graduate students, Jennifer Winkler, Connie Wu, Yong Lee, Jack Zheng, Dan Browe, Margot Zevon and Kamua Pierre. Research is much easier when you have people you can talk to (and joke with) about science. Furthermore, I am grateful for

Linda Johnson, who was one of the first people in the department to offer her friendship and guidance.

Early in my journey, I realized that I needed to develop a 'family' here in New Jersey because moving away from my close knit family was very difficult for me. My life in Jersey was significantly enhanced when I met people who shared similar interest and passions. I have three particular friends who will forever be my PhD sisters: Renea Faulknor, Antionette Nelson and Joseanne Cudjoe. We prayed together, worked together, and managed to have a little bit of fun together. I am grateful for their friendship and I look forward to the day when we all have our doctorates! Special thanks to the members of the Council of Black Graduates (CBG) for all the laughs and support these past few years. I would also like to thank the members of the young adult ministry at First Baptist Church of Lincoln Gardens in Somerset, NJ. They are my brothers and sisters in Christ and they prayed for me when I was too tired to pray for myself. They challenged me to increase my faith and decrease the doubt.

This accomplishment would not have been possible without the support, motivation, and mentorship from many of people. These people make up my village and are the people who provide daily love, inspiration, and encouragement through their phone calls, emails, messages, and cards. I am thankful to the Womack and Lewis family for being the family away from home that I needed. I am especially thankful for the companionship and unconditional support I have received from Trey Womack. He has been alongside me this entire journey, all the while showering me with spiritual inspiration and love. I am grateful for my aunts, uncles, older cousins, and other ancestors who paved the way for me. It is because of their personal interest in my

success that I was able to get through these past few years. I would like to give special recognition to my grandparents, William and Alma Taylor and my aunts Sharon McGlone, Debbie Evans and Hester Clark for their willingness to also step in and make this journey as easy as possible. I am convinced I have the best cousins and for that I am extremely grateful. I would especially like to thank Rebekah Clark, Beth McGlone, Catherine Evans and Taylor Evans for making sure I enjoyed life no matter how demanding school was. I would like to thank my friends who have showed me unwavering love and support: MaRonda Jernigan, Gabrielle Quinn, Molissa Annuzi, Jamie Hurd, Portia Henry, Curretta Moon, Branden Albert, Mikell Simpson, Doniesha Foster and Dominique Fetherholf. I am also appreciative of the many mentors and role models I have had in my life: Alice Thompson, Dean Silvia Terry, Dr. Prosper Godonoo, Dr. Ed Smith, and Dr. Anne McNabb. I would also like to thank the members of Bethlehem Baptist Church in Spotsylvania, Va for being my spiritual family since birth.

I would not be the person I am today or have the personal motivation I have if it was not for my family. I have seven siblings and each of them play a significant role in my life and I am grateful for their support. My oldest sister, Cheri Rice, has always challenged me while my brother and sister-in-law, Eric and Jackie Taylor, have always protected me. My sisters, Samantha and Heidi Taylor, have always been there whenever I needed someone to vent to or for a trip to de-stress. My younger brother, Matthew Taylor, who keeps me silly and my youngest siblings, Kendall and Jarrett Taylor, who are a constant reminder of how to just live and love. I am thankful for my nieces and nephews, Alysia Harrison, Eric Taylor, Linden Tillery, King White and Jackson Taylor

who are the reasons I dream as big as I can and work as hard as I do. I am thankful for my father, William Taylor, Jr, who taught me to enjoy life and hang loose. It is because of him that I am as determined and competitive as I am.

Finally, I would like to thank my mother, Sharon Taylor. She sacrificed a lot so that my siblings and I could have the life we had. I am grateful for her multiple calls throughout the day and her willingness to drop everything just to come up here to make sure I am doing okay. I dedicate this dissertation to her, but I wish I could give her a doctorate as well. I model and admire her determination, perseverance, and giving nature. Last but not least, I would like to thank God for his grace, mercy, blessings, and unconditional love. God made ways when man said no. It is because of Him that I can go all things through Christ that strengthens me. This journey has been quite challenging, but I stood firm on my faith and believed that one day I would reap what I have sowed and receive my inheritance. I have fought the good fight, I have finished the race, and I have kept the faith.

TABLE OF CONTENTS

LIST OF TABLES

LIST OF FIGURES

CHAPTER 1: INTRODUCTION

Note: Excerpts from this chapter have been previously published and are the original work of the PhD Candidate, Brittany Taylor.

Taylor, B.L., Andric, T., Freeman, J.W. Recent Advances in Bone Graft Technologies. Recent Patents on Biomedical Engineering, 2013. 6(1):p.1-7

1.1. Bone Composition and Structure

Human bone is a complex hard tissue with a heterogeneous composition and structure. The main purpose of bone is to protect the body's vital organs by providing structural support and serve as a blood cell reservoir [1]. Bone is composed of an organic matrix of collagen fibers (20-30 wt%), inorganic calcium phosphate mineral crystals (60-70 wt%) and water (10 wt%) [1-3]. Each component plays a role in overall mechanical properties of bone. The organic matrix, mainly type I collagen, contributes to the toughness of bone. The hydrated inorganic mineral phase composed of mainly hydroxyapatite (HAp) and water are responsible for the stiffness and viscoelastic behaviors of bone, respectively. Bone is continuously remodeling and developed through the interaction of osteoclasts, osteoblasts and osteocytes [1]. Osteoclasts are multinucleated cells responsible for the adsorption of bone tissue, whereas osteoblasts are the group of cells responsible for forming the matrix of new bone. Osteocytes are inert cells derived from osteoblasts that are most commonly found in mature bone and responsible for bone molecular synthesis and modification [4].

Structurally, bone is organized into two distinct types based on their density and

location: cortical bone and trabecular bone [1, 3, 5]. Cortical bone, or compact bone, has a highly dense and organized structure composed of tightly packed osteons (Figure 1.1). The compact architecture of cortical bone contributes to the structural integrity of bone [6]. Blood microvasculature, nerve cells and osteocytes are housed within the osteons along the Haversian canal. Vessel sprouting occurs perpendicular to the Haversian canal through the Volkmann's canal. This intricate vascular network allows for blood and nutrient transport, which is essential for bone remodeling.

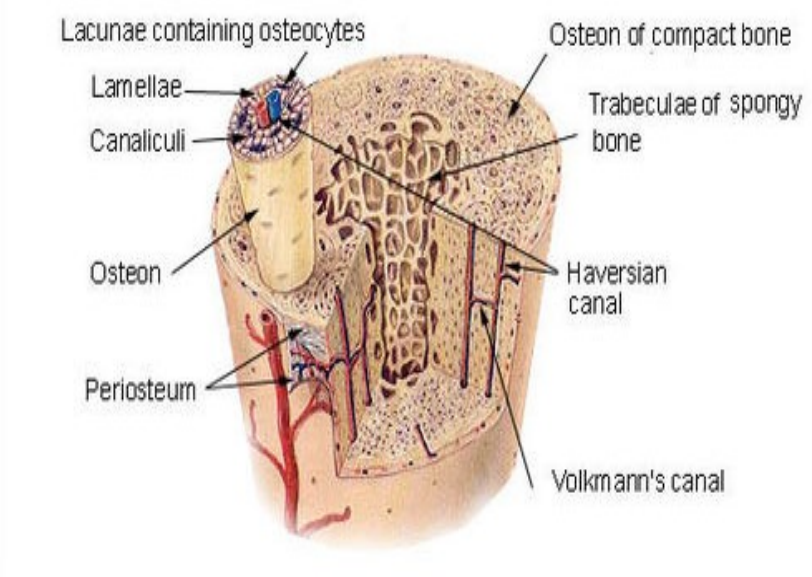

Figure 1.1. Structural organization of the bone tissue, adapted from SEER Training Modules, *Structure of Bone.* US National Institutes of Health, National Cancer Institute.

The highly porous trabecular bone structure is a fibrous meshwork of collagenous tissue filled with bone marrow. Trabecular bone, or spongy bone, is 90% porous with lower mechanical strength than cortical bone [5, 6]. Due to differences in organization, composition and porosity, the mechanical properties of cortical, trabecular, and whole

bone vary, as seen in Table 1.1 [7] .

	Tensile Strength	Young's Modulus
Trabecular Bone	3-9MPa	.01-.9GPa
Cortical Bone	167-215MPa	10-20GPa
Whole Bone	70MPa	1GPa

Table 1.1. Mechanical properties of trabecular, cortical and whole bone [7]

1.2. Current Treatments for Damaged Bone

Naturally, bone regenerates on its own without scar tissue formation [8]. This repairing process is facilitated by the normal function of osteoclasts and osteoblasts as previously mentioned. In the case of bone diseases due to abnormal bone physiology or significant skeletal bone loss, the innate healing process is compromised. As a result, surgical intervention is required to replace the damaged bone and provide structural support while the inherent bone regeneration process takes place. In the U.S, there are approximately 500,000 bone grafting treatments performed annually; leading to a $2.5 billion expenditure and a $1 billion market [9]. The bone grafts and substitutes market is expected to reach $3.5 billion in 2023 due to the 2-3% increase in the average life expectancy [1, 10, 11]. The gold standard orthopedic procedure to replace damaged bone is autografting. Autografting utilizes an autologous bone tissue source usually harvested from the iliac crest. Autografts provide sufficient mechanical strength upon implantation, but disadvantages associated with this procedure include limited supply, donor site

morbidity, and increased pain and insurance expenses due to the multiple surgeries. The second most commonly used biological source for bone grafting are allografts. Allografting requires the use of donated bone tissue from a cadaveric source. The abundant supply of allograft tissue is an advantage, but there is a possible risk of disease transmission or immunogenic reaction. To reduce this risk, allografts undergo harsh decellularization techniques to remove any foreign material. Unfortunately, this process can weaken the graft's mechanics by damaging the collagenous matrix and potentially lead to a 30-60% risk of failure over 10 years *in vivo* [7]. Similar limitations are seen with xenografts from a bovine or porcine source. Alternatives such as metallic implants (used in joint replacement) lack the ability to bond with surrounding bone, whereas bone cements cannot be used exclusively to repair load-bearing bones.

Some of the commercially available bone graft substitutes include derivatives of biological material such as collagen and demineralized bone matrix (DMB), ceramics such as tricalcium phosphate, hydroxyapatite, and calcium phosphate and growth factors or a combination [12-16]. Table 1.2 compares the osteoconductive, osteoinductive, and osteogenic capabilities of biomaterials, biological, ceramic and composite grafts. Osteoconduction is a physical property of a graft to serve as a scaffold for new bone development. Osteoinduction is the ability for a material to promote differentiation of osteoprogenitor cells into osteoblasts and the process of osteoblasts laying down new bone is called osteogenesis. While a majority of the grafts listed are osteoconductive, with highly porous matrices, a small number of them have osteoinductive capacities. Given the drawbacks associated with these current technologies, the field of tissue engineering has emerged to bridge the gap between the need and lack of an ideal bone

graft.

Type	Graft	Osteoconductive	Osteoinductive	Osteogenesis
Bone	Autograft	3	2	2
	Allograft	3	1	0
Biomaterials	Demineralized Bone Matrix	1	2	0
	Collagen	2	0	0
Ceramics	TCP, hydroxyapatite	1	0	0
Composite Grafts	β-TCP/BMA composite	3	3	2
	BMP/synthetic composite	—	3	—

Table 1.2. Comparison of commercially available candidates for bone grafts on a scale of 3 (high) to 0 (low). Adapted and recreated from Hak, D.J., *The use of osteoconductive bone graft substitutes in orthopaedic trauma.* J Am Acad Orthop Surg, 2007. 15(9): p. 525-36. [15].

1.3. Tissue Engineered Graft As a Promising Alternative

The field of tissue engineering (TE) is a rising and promising interdisciplinary field that combines the use of cells, bioactive molecules, and engineered scaffolds to improve tissue regeneration. TE grafts have advantageous features such as abundant supply and the ability to customize the therapy to the patient. The idea behind tissue engineering is the use of the patient's own cells to regenerate tissue; usually with the addition of a biodegradable scaffold to provide initial structure and support for matrix deposition and tissue formation. The principal of TE is depicted in Figure 1.2. Cells are harvested from

the patient, cultured and expanded in monolayer. The cells are then seeded into a three-dimensional scaffold with the addition of growth factors, nanoparticles, or a secondary cell type to enhance the patient's normal cellular activity. As the cells proliferate, they will deposit factors and will develop into organized tissue. The TE scaffold can then be implanted back into the patient at the site of interest [17].

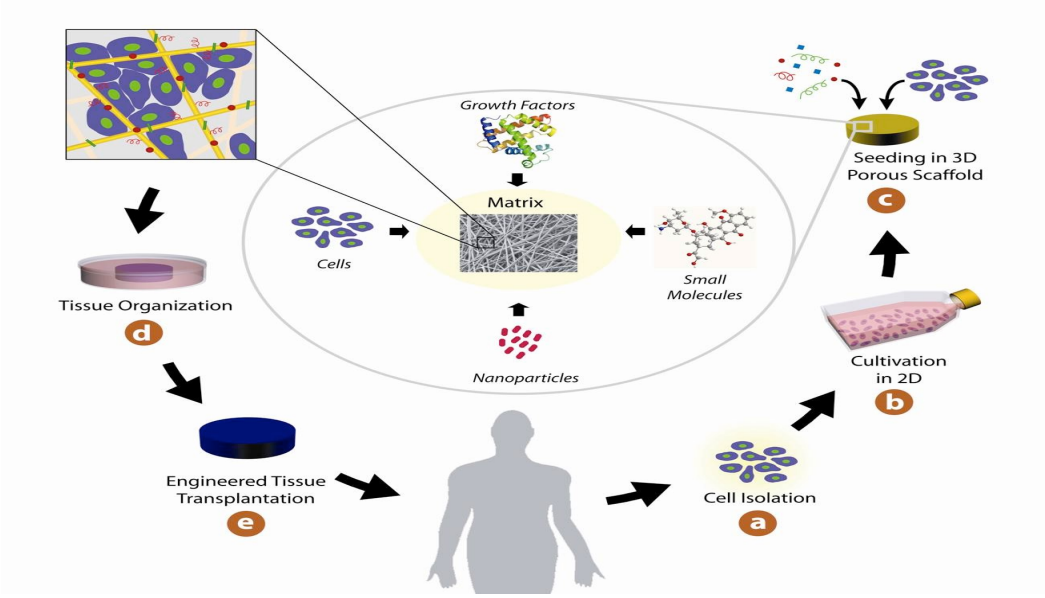

Figure 1.2. Principles of Tissue Engineering (TE) [17]

Ideally the scaffold used in this TE approach should have the ability to promote cellular attachment, proliferation, infiltration and bone matrix deposition by mimicking the extracellular matrix. In order to meet these requirements, the scaffold must be biocompatible, osteoconductive, osteoinductive and osteogenic as previously mentioned. Additionally, the TE scaffold must be porous with favorable degradation rates and mechanical properties comparable to native bone. Most osteoblastic cells desire a matrix for bone grafting with a pore size range of 5-200 microns [3,6,18]. This pore range also

allows for the infiltration of nutrients, and connective soft tissue. The scaffold must serve as a temporary matrix for tissue formation and the degradation rate should be proportional to bone renewal and growth rate. To reduce the risk of mechanical failure *in vivo*, the scaffold should possess mechanical properties that are comparable to the surrounding tissue. Although TE bone replacements have enormous potential, aspects such as cellular infiltration, vascularization, comparable mechanical strength and osteoblastic differentiation limit development of truly viable and functional bone. Many researchers solely focus on developing porous scaffolds that tend to lack the necessary mechanics for load-bearing applications. The calcium phosphate and ceramic-based bioactive TE grafts have enhanced mechanical strength and osteoconduction, but lack osseointegration (ability of a implant to integrate with the surrounding tissue). Furthermore, very few effective strategies exist for stimulating osteoblastic and vascular differentiation simultaneously. The presence of newly forming osteoblastic tissue and vasculature is crucial for long-term mechanics and graft viability. The use of growth factors such as bone morphogenetic proteins (BMP) to induce osteoblastic differentiation *in vivo* can have adverse effects such as an overexpression of bone development and ectopic bone formation. Recent directions to enhance vascularization in bone regeneration are largely aimed at enhancing early vascular support using pre-vascularization of tissue-engineered constructs [18, 19].

1.4. An Osteoinductive Pre-Vascularized Scaffold as a Viable TE Graft

In this thesis project, I discuss an experimental plan that harvests the structure, osteoinduction, and osteoconduction of a mineralized biomimetic trabecular scaffold and vascular tissue inducing cortical structures. I introduce a biomimetic, load bearing,

osteoinductive pre-vascularized synthetic tissue-engineered scaffold composed of a porous trabecular structure bound to a mechanically reinforced, cortical bone-like sheath. The complete scaffold will simultaneously differentiate human bone marrow stromal cells (hMSCs) into osteoblasts and vascular endothelial cells for improved long-term allograft mechanics and viability (Fig. 1.3).

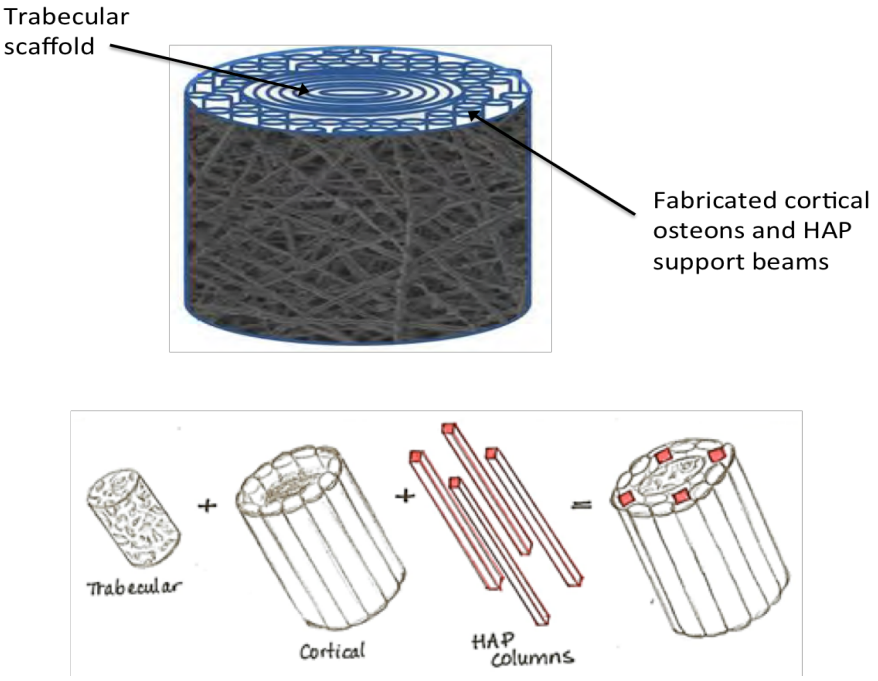

Figure 1.3. Schematic of proposed scaffold

The purpose of the sheath is 3-fold. First, the sheath will increase overall strength using a mineralized architecture and embedded HAp support posts. Second, the sheath will promote the differentiation of hMSCs along the osteoblastic and vasculature lineages in

the designated areas without the use of growth factors. Third, the sheath will promote organized and functional vasculature development by sponsoring vessel growth inside decellularized lumens that mimic native osteons. This cortical structure does not typically exist in commercial allograft blocks. This transformative technology is the first synthetic bone graft to contain both trabecular and cortical bone structures and be designed for vascularized bone growth and load-bearing applications. The sheath will be composed of electrospun synthetic and collagen-based materials (gelatin). Electrospinning is a nanofabrication technique used to create nanofibrous scaffold by creating a voltage gradient that draws a thin solid fiber of polymer out of solution. Figure 1.4 is a schematic of a basic electrospinning set-up [20]. Gelatin is biocompatible, biodegradable, commercially available, non-immunogenic, and promotes cell proliferation [21, 22]. The addition of gelatin will increase mineralization and integration between the mineral and fibrous phases, by providing nucleation sites for calcium phosphate [23, 24].

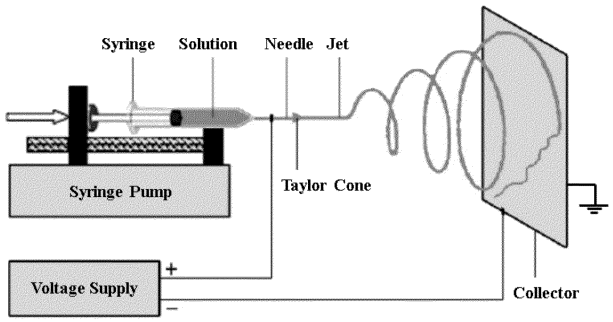

Figure 1.4. Schematic of an electrospinning set-up [20]

The primary materials used to create the base of the proposed TE graft are two FDA approved polyesters poly (α-hydroxy acid) polyesters, poly-l-lactide (PLLA) and poly-d-

lactide (PDLA). PLLA and PDLA were selected based on their favorable materials properties, as shown in Table 1.3. The monomers of PLLA and PDLA have a central carbon atom with terminal carboxyl group (-COOH) and a terminal methyl group (CH_3). PLLA is a semi-crystalline polymer with a higher tensile strength and a slower degradation than PDLA. Both polymers degrade via hydrolytic degradation [25, 26]. PDLA, the less crystalline polymer, was selected as the sintering agent to hold the scaffold layers together when heated up to its glass transition temperature of 54°C. At this temperature, PDLA transitions from a hard solid state to a melted soft rubbery state and acts as the glue to hold the three-dimensional structure together.

	Degradation Rate	**Tensile Strength**	**Tensile Modulus**	**Glass Transition Temperature**
PLLA	> 24 months	60-70MPa	3GPa	60-65°C
PDLA	12-15	40-50MPa	2GPa	44-55°C

Table 1.3. Material properties of PLLA and PDLA [2]

In order to obtain a dual integrated bone scaffold that promotes both osteogenic and organized microvascular tissue, we will use human mesenchymal stromal cells (hMSCs). MSCs have been investigated in the repair of numerous tissues from bone to nervous tissue. Their ability to divide and differentiate into multiple cellular lineages makes them an ideal solution for the repair of damaged and diseased tissues. They have been combined with scaffolds for tissue regeneration and injected into damaged tissues directly [27, 28]. When the stem cells are directed along the appropriate lineage, either *in vitro* before implantation or *in vivo*, they can produce healthy new tissue to replace the damaged or host tissue. A recent long- term investigation of human MSCs (hMSCs)

osteoblastic differentiation over 21 days indicate that hMSCs seeded onto a hydroxyapatite-sprayed scaffold developed a significantly higher level of bone marker alkaline phosphatase activity, as well as a higher matrix biomineralization rate than hMSCs seeded on a non hydroxyapatite sprayed scaffold [29]. Additionally, MSCs have been utilized to promote vascularization *in vivo* when exposed to soluble factors secreted from endothelial cells and growth factors [30, 31] or when placed on a vascular allograft [32, 33].

1.5. Dissertation Summary

The results presented in this dissertation highlight the development and characterization of a novel TE synthetic bone graft with enhanced mechanical strength and vascularization. I hypothesize the joining of a porous trabecular scaffold with the addition of HAp, pre-vascularized cortical bone scaffold and HAp columns will promote differentiation of hMSCs into osteoblasts and vascular endothelial cells in appropriate areas in the scaffolds *in vitro* and *in vivo* and be utilized as viable bone replacement with enhanced long-term strength *in vivo.* This technology is transformative because it will be the first synthetic bone graft to contain both trabecular and cortical bone structures, designed for vascularized bone growth and load-bearing applications. The project objectives for this project as follows:

Objective 1: To evaluate the biomechanical properties of the individual scaffolds and complete scaffold using *in vitro* material testing. We hypothesize that combining a porous trabecular scaffold, mineralized cortical bone scaffolds, and the HAp columns

will produce a full thickness bone scaffold which can be utilized as a bone replacement; resulting in similar mechanical properties to native bone and enhanced long-term strength.

Objective 2: To evaluate the biological properties of the individual scaffolds and complete scaffold using cellular response *in vitro* analysis. We hypothesize that the addition of HAp in the scaffold and the pre-vascularized cortical scaffold will promote osteogenic and angiogenic differentiation of hMSCs in the appropriate areas of the scaffolds.

Objective 3: To determine the biological response of the complete scaffold *in vivo* using a small animal model. We hypothesize that the joining of a pre-vascularized cortical and osteoinductive trabecular three-dimensional bone scaffold will promoted vascular integration and stem cell differentiation *in vivo*.

This dissertation is divided into six chapters. Each chapter focuses on the individual scaffold sections and the corresponding material and biological characterization. Chapter 2 discusses the processing techniques investigated to develop a stable polymeric and gelatin scaffold, which mimics the porous trabecular structure. We concluded that the use of a FDA approved crosslinking agent, microbial transglutaminase (mTG), yielded the most mechanically stable sintered scaffold. Additionally, we demonstrated the ability to successfully incorporate HAp crystals into the electrospun scaffold leading to osteoblastic differentiation of hMSCS *in vitro*. Chapter 3 focuses on the development of the cortical

scaffold and the pre-vascularized matrix necessary to promote angiogenic differentiation. The biomimetic structure stimulated circumferential endothelial cellular growth and a vascularized network. Decellularization methods led to an 86% decrease in cellular viability with a 96% maintained network. This pre-vascularized matrix promoted the secretion of soluble pro-angiogenic growth factors. In Chapter 4, we introduce HAp columns and their use as mechanical reinforcement throughout the complete scaffold. First, varying types of HAp nanopowder and sintering parameters was investigated. The properties of the most mechanical enhanced HAp columns were then used to generate a finite element model to determine the arrangement and total composition of HAp columns to be embedded in the scaffold. Lastly, the trabecular and cortical scaffolds are combined with the HAp columns and compression testing confirmed a statistically significant increase in mechanical properties with the addition of the HAp columns. Chapter 5 focuses on the results from the 8 week subcutaneous study. Qualitatively, there was a fibrotic capsule surrounding the scaffold, which decreased in thickness on the inferior side. New collage formation, cellular infiltration and blood vessels were also observed in the histology images along with scaffold integration up to 4 weeks. Overall conclusions and recommendations for future directions are discussed in Chapter 6.

1.6. References

1. Hing, K.A., *Bone repair in the twenty-first century: biology, chemistry or engineering.* Philos Transact A Math Phys Eng Sci, 2004. **362**(1825): p. 2821-2850.
2. Wang, H., et al., *Biocompatibility and osteogenesis of biomimetic nano-hydroxyapatite/polyamide composite scaffolds for bone tissue engineering.* Biomaterials, 2007. **28**(22): p. 3338-48.

3. Rho, J.Y., L. Kuhn-Spearing, P. Zioupos, *Mechanical Properties and the hierarchical structure of bone.* medical Engineering and Physics, 1998. **20**(2): p. 92-102.
4. Katja M.R Nuss, B.v.R., *Biocompatibilty Issues with Modern Implants in Bone - A Review for Clinical Orthopedics.* Open Orthop J. , 2008. **2**: p. 13.
5. Wang, X., S. Puram, *The toughness of cortical bone and its relationship with age.* Ann Biomed Eng, 2004. **32**(1): p. 123-135.
6. An, Y.H. and R.A. Draughn, *Mechanical testing of bone and the bone-implant interface*. 2000, Boca Raton: CRC Press.
7. Wheeler, D.L., Enneking, W.F., *Allograft bone decreases in strength in vivo over time.* Clin Orthop Relat Res, 2005. **435**: p. 36-42.
8. Frohlich, M.e.a., *Tissue engineered bone grafts: biological requirements, tissue culture and clinical relevance.* . Curr Stem Cell Res Ther, 2008. **3**(4): p. 254-264.
9. CR, P., *Bone repair techniques, bone graft, and bone graft substitutes.* Clin Orthop Relat Res, 1999. **360**: p. 71-86.
10. Greenwald, S., Boden, S.D., Goldber, V.M, Khan, Y., Laurensin, C., Rosier, R.N, *Bone-Graft Substitutes: Facts, Fictions, and Applications.* The Journal of Bone and Joint Surgery, 2001. **83A**: p. 98-103.
11. Research, T.M., *Bone Grafts and Substitutes Market (By Type: Allografts, and Bone Graft Substitutes; By Application: Spinal Fusion, Long Bone, Foot and Ankle, Craniomaxillofacial, Joint Reconstruction, and Dental) - Global Industry Analysis, Size, Share, Growth, Trends and Forecast 2015 - 2023*. 2015.
12. Wagoner Johnson, A.J. and B.A. Herschler, *A review of the mechanical behavior of CaP and CaP/polymer composites for applications in bone replacement and repair.* Acta Biomaterialia, 2011. **7**(1): p. 16-30.
13. Ambrose, C.G. and T.O. Clanton, *Bioabsorbable Implants: Review of Clinical Experience in Orthopedic Surgery.* Annals of Biomedical Engineering, 2004. **32**(1): p. 171-177.
14. Giannoudis, P.V., H. Dinopoulos, and E. Tsiridis, *Bone substitutes: An update.* Injury, 2005. **36**(3): p. S20-S27.
15. Hak, D.J., *The use of osteoconductive bone graft substitutes in orthopaedic trauma.* J Am Acad Orthop Surg, 2007. **15**(9): p. 525-536.
16. Gazdag, A.R.e.a., *Alternatives to Autogeneous Bone Graft: Efficacy and Indications.* J Am Acad Orthop Surg, 1995. **3**(1): p. 1-8.
17. Dvir,Tal, etal. *Nanotechnological strategies for engineering complex.* Nature Nanotechnology, 2001. **6**: p. 13-22.
18. Novosel, E.C., C. Kleinhans, and K. P.J., *Vascularization is the key challenge in tissue engineering.* Adv Drug Deliv Rev, 2011. **63**(4-5): p. 300-311.
19. Krishnan, L., N.J. Willett, and R.E. Guldberg, *Vascularization strategies for bone regeneration.* Annals of biomedical engineering, 2014. **42**(2): p. 432-44.
20. Thomas, S., Y. Pais, and N. Alcantar, *Electrospun cactus mucilage nanofibers*, in *Application*, USPTO, Editor. 2013, University of South Florida: U.S.
21. Sell, S.A.e.a., *Electrospinning of collagen/biopolymers for regenerative medicine and cardiovascular tissue engineering.* Adv Drug Deliv Rev, 2009. **61**(12): p. 1007-1019.

22. Sisson, K.e.a., *Evaluation of Cross-Linking Methods for Electrospun Gelatin on Cell Growth and Viability.* Biomacromolecules, 2009. **10**(7): p. 1675-1680.
23. Landis, W.J. *The strength of a calcified tissue depends in part on the molecular structure and organization of its constituent mineral crystals in their organic matrix.* Bone, 1995. **16**(5): p. 533-544.
24. Andric T, W.L., Freeman JW, *Rapid Mineralization of Electrospun Scaffolds for Bone Tissue Engineering.* Journal of Biomaterials Science, Polymer Edition, 2011. **22**(11): p. 1535-50.
25. Middleton, J.C. and A.J. Tipton, *Synthetic biodegradable polymers as orthopedic devices.* Biomaterials, 2000. **21**(23): p. 2335-2346.
26. Balasundaram, G. and T.J. Webster, *An overview of nano-polymers for orthopedic applications.* Macromolecular bioscience, 2007. **7**(5): p. 635-642.
27. Watanabe, N., et al., *Fate of Donor Bone Marrow Cells in Medial Collateral Ligament After Simulated Autologous Transplantation.* Microscopy Research and Technique, 2002. **58**(1): p. 39-44.
28. Gafni, Y., et al., *Stem cells as vehicles for orthopedic gene therapy.* Gene Therapy, 2004. **11**(4): p. 417-426.
29. Ramier, J., et al., *From design of bio-based biocomposite electrospun scaffolds to osteogenic differentiation of human mesenchymal stromal cells.* Journal of materials science. Materials in medicine, 2014.
30. McFadden, T.M., et al., *The delayed addition of human mesenchymal stem cells to pre-formed endothelial cell networks results in functional vascularization of a collagen-glycosaminoglycan scaffold in vivo.* Acta biomaterialia, 2013. **9**(12): p. 9303-16.
31. Aguirre, A., A. Planell, and E. E, *Dynamics of bone marrow-derived endothelial progenitor cell/mesenchymal stem cell interation in co-culture and its implications in angiogenesis.* Biochemical and biophysical research communications, 2010. **400**(2): p. 284-291.
32. Quint, C., et al., *Decellularized tissue-engineered blood vessel as an aterial conduit.* PNSA, 2011. **108**(22): p. 9214-9219.
33. Zhao, Y.e.a., *The development of a tissue-engineered artery using decellularized scaffold and autologous ovine mesenchymal stem cells.* Biomaterials, 2010. **31**(2): p. 296-307.

CHAPTER 2: THE DEVELOPMENT AND *IN VITRO* EVALUATION OF A POROUS OSTEOINDUCTIVE TRABECULAR BONE SCAFFOLD

Note: Excerpts from this chapter have been previously published and are the original work of the PhD Candidate, Brittany Taylor.

Taylor, B.L., Limaye, A.N., Yarborough, J.A., Freeman, J.W. *Investigating Various Processing Techniques for a Bovine Gelatin Scaffold for Bone Tissue Regeneration*. Journal for Biomedical Research: Part B (Recently Accepted for Publication)

2.1. Introduction

Bone is a complex hard tissue with a heterogeneous composition and structure. The main components of bone are an organic matrix (collagen type I), inorganic mineral crystals, and water [1-3]. Each component plays a role in bone's overall mechanical properties. The organic matrix, mainly type I collagen, contributes to the toughness of bone. The hydrated inorganic mineral phase composed of hydroxyapatite (HAp) and water are responsible for the stiffness and viscoelastic behavior of bone, respectively. Injured and damaged bone has the ability to heal naturally unless there is significant bone loss. In this case, surgical implantation of a biological, metallic, or ceramic graft is required at the defect site. Autografts and allografts have the potential to result in donor site morbidity and a 30-60% risk of failure over 10 years due to the decrease of mechanical properties *in vivo* [4, 5]. Metallic implants, used in joint replacement, lack the ability to bond with surrounding bone, whereas bone cements cannot be used exclusively to repair load-bearing bone defects due to its low mechanical strength. Given the

drawbacks associated with the use of biological grafts, metallic implants, and cements, there is a need for a tissue engineered (TE) bone graft to improve tissue regeneration [6].

Structurally, bone is divided into a highly dense cortical (compact) bone region and a porous trabecular (spongy) bone region. Trabecular bone is approximately 90% porous and has lower mechanical strength than cortical bone. In this chapter, I discuss the development and analysis of a mineralized biomimetic osteoinductive trabecular scaffold. Materials used to develop a TE scaffold should be biocompatible, biodegradable as well as have the ability to promote cellular attachment, proliferation and mimic the extracellular matrix [7-9]. Pure collagen from bovine or porcine sources has emerged as an ideal material choice given its enzymatic method of degradation and high abundance in native bone. However, the cost of pure bulk collagen and possible immunogenic response are unfavorable characteristics [10, 11]. As a result, research is now focused on utilizing gelatin, the denatured form of pure collagen, as an inexpensive alternative. Gelatin is biocompatible, biodegradable, commercially available, non-immunogenic, promotes cell proliferation and has the same desirable characteristics as collagen [12-14]. Gelatin also has exposed carboxyl groups that act as nucleation sites for ions and promote the precipitation of mineral content [15, 16]. Nonetheless, a limitation of gelatin is its hydrophilic behavior and therefore requires crosslinking in order to retain its structure in aqueous environments. I hypothesize the addition of stable crosslinked gelatin will increase mineralization and integration between the mineral and fibrous phases of a biomimetic trabecular scaffold. To validate this hypothesis, I investigated various processing techniques, crosslinking agents, and mineralization techniques. The end goal of the work presented in this chapter is to develop a mechanically enhanced porous

osteogenic scaffold by mimicking the structure and composition of native trabecular bone.

The scaffold is composed of two poly (α-hydroxy acid) polyesters, poly-l-lactide (PLLA) and poly-d-lactide (PDLA) due to their favorable material and mechanical properties. Both PLLA and PDLA are FDA approved materials that degrade via hydrolytic degradation and are widely utilized for tissue engineering applications [17, 18]. Additionally, the blend of the two polymers enables the control of crystallinity, morphology and degradation [10]. PDLA is used to maintain the integrity of the three-dimensional scaffold by sintering the multiple layers together. The gelatin crosslinking agents investigated were glutaraldehyde, 1-Ethyl-3-(19) Carbodiimide Hydrochloride (EDC), and Microbial transglutaminase (mTG). Glutaraldehyde and EDC are commonly used crosslinking biomedical agents. Glutaraldehyde has demonstrated the ability to increase structural stability of gelatin bonds when crosslinked. Nonetheless, high concentrations of glutaraldehyde has been shown to have detrimental effects on cells *in vitro* and may leach in the body *in vivo* during gelatin degradation [19]. As a result, I selected low concentrations of glutaraldehyde in combination with additional less toxic crosslinkers. EDC works by activating carboxyl groups for direct reaction with primary amines via amide bond formation [20]. This reaction enables the scaffold to retain its original composition by specifically maintaining fibrous structure [10]. mTG, derived from *Streptoverticillium* species, has been used widely in the food processing industry and recently utilized for various biomedical applications, such as drug delivery, injectable cell delivery and scaffold fabrication [21, 22]. Specifically, mTG has demonstrated the ability to crosslink highly resistant polymers for scaffold generation while also enabling a

decrease in cytotoxicity whereby increasing biocompatibility [22]. Overall, several studies have demonstrated that crosslinking exhibits mechanical stability of the scaffolds over time when compared to scaffolds that have not been crosslinked [10].

Porosity is critical in tissue engineering. To mimic the intricate porous structure seen in trabecular bone, I used sodium chloride (NaCl) crystals. The NaCl crystal acted as porogens that were leached out later. The nanofibrous scaffold has inherent nanopores but the addition of the porogens creates micro- and macropores. Stable pores are crucial for cellular movement, tissue infiltration, and nutrient transport and can be achieved with the additional processing steps. We also aim to promote the differentiation of human bone marrow derived stromal cells (hMSCs) along the osteoblastic lineage by incorporating inorganic bone minerals, hydroxyapatite (HAp) and calcium, into the scaffold.

2.2. Materials sand Methods

PLLA (MW = 152,000) was purchased from Sigma Aldrich (St. Louis, MO, USA). PDLA (MW=124,000) was purchased from Evonik Birmingham Laboratories (Birmingham, AL, USA). Solvents dichloromethane (DCM), dimethylformamide (DMF), and tetrahydrofuran (THF) were purchased from Fisher Scientific (Pittsburgh, PA, USA). Gelatin, from porcine skin, was purchased from Sigma Aldrich (St. Louis, MO, USA). The solutes used in the simulated body fluid (SBF), sodium chloride (NaCl), potassium chloride (KCl), calcium chloride dihydrate ($CaCl•H_20$), magnesium chloride heptahydrate ($MgCl_2•H_20$), sodium bicarbonate ($NaHCO_3$), and sodium phosphate monobasic (NaH_2PO_4) were purchased from Fisher Scientific (Pittsburgh, PA, USA). Synthetic

nanopowder HAp (<200 nm) was purchased from Sigma-Aldrich (Atlanta, GA, USA).

2.2.1. Gelatin Crosslinking Study I

Porcine gelatin powder (12%w/v) was mixed with dI H_20 in petri dishes and placed in a desiccator overnight. The solidified gelatin was then cut into 2.5 x 10cm strips. The samples were exposed to 25mM glutaraldehyde (Glut_CL) and crosslinked for 2 hours via vapor crosslinking in a closed container at 37°C. The samples in the EDC group (EDC_CL) were submerged in EDC for 2 hours while the mTG crosslinked samples (mTG_CL) were submerged in 12% mTG dissolved in phosphate buffer saline (PBS) for 5 hours, both at 37°C. The rationale for varying the crosslinking times for each process was based on similar studies, which concluded the optimal times and concentrations for effective crosslinking of gelatin substrates [23, 24].

The scaffolds (n=6) were mechanically tested in tension at a rate of 10%strain/min until failure using an Instron 5869 with Bioplus Bath (Norwood, MA, USA) under physiological conditions in phosphate buffer saline (PBS) (pH 7.4). The ultimate tensile strengths, tensile moduli and tensile yield strengths were compared to determine which crosslinking agent to use for the electrospun polymeric-gelatin scaffold to prevent gelatin leaching.

2.2.2. Scaffold Fabrication using Electrospinning

Electrospinning is broadly used to create nanofibrous scaffolds using electrical forces to produce thin fibers of polymer [25]. The base electrospinning solutions were prepared by dissolving PLLA (7% w/v) in DCM and DMF with 10% gelatin and PDLA (22w/v%) in

THF and DMF at a 3:1 ratio. Additional agents were added into the solution depending on the study and rationale. A 5ml syringe with an 18-gauge blunt needle attachment was used for all the electrospinning experiments. Electrospinning was performed with a working distance of 15cm for the PDLA solutions and 10cm for the PLLA/10%Gel solutions. The polymer solutions were extruded at 5ml/hr onto an 8cm diameter rotating aluminum mandrel (~ 2000 RPM). The voltages were set to +15kV/-10kV for PLLA/10%gel and +10kV/-5kV for the PDLA solution. These parameters were evaluated and optimized in previous studies [16, 26, 27].

First, 1.5mL of PDLA solution was electrospun onto the mandrel to create a nanofibrous layer. Next, 5ml of the PLLA/10%Gel solution was electrospun on top of the PDLA layer. NaCl crystals were released from a container vertical to the mandrel during electrospinning. This process of using salt particles to develop pores is further discussed in previous work [26, 27]. A second 1.5ml layer of PDLA depending on the experiment was then electrospun onto the PLLA/10%Gel with salt layer. PDLA was used as the top and bottom layer so that the electrospun scaffolds could be stacked and sintered to create a three-dimensional structure. The electrospun PLLA_10%Gel_PDLA scaffolds were placed into a desiccator overnight to remove any residual solvents.

2.2.3. Varying Scaffold Fiber Angle

PLLA/10%Gel_PDLA electrospun scaffolds were vapor crosslinked with 25mM glutaraldehyde for two hours and cut into 1cm wide strips. Strips were cut at an angle where the majority of the nanofibers were arranged at 0°, 15°, 30°, 45° and 90° angles from the top right corner of the scaffold, Figure 2.1. This was based on the assumption that the nanofibers were aligned after formation. The strips were then

wrapped around an 18-gauge blunt needle tip and heat sintered at 54°C for 45 minutes to create three-dimensional electrospun columns with average diameters of .5 mm and 1 mm in height (2:1 height to diameter ratio).

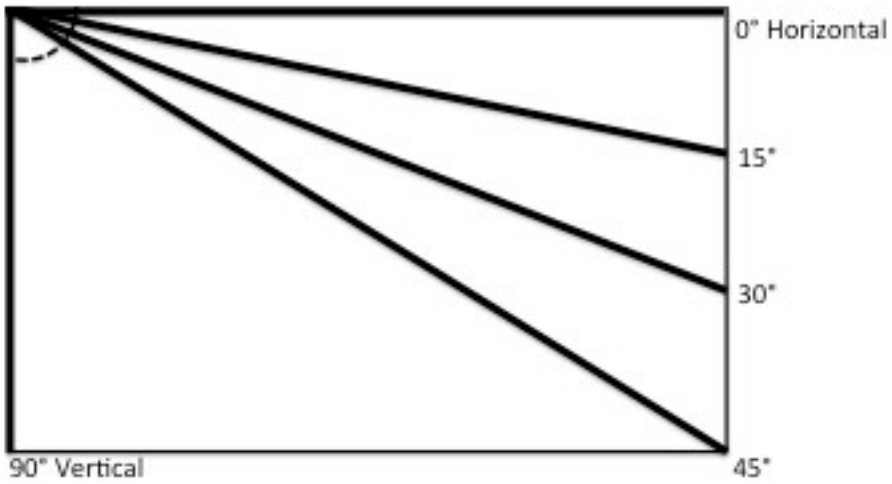

Figure 2.1. Diagram of fiber angles (0°, 15°, 30°, 45° and 90°) at which the scaffolds were cut.

The scaffolds were mechanically tested in compression at a 1mm/min (10% strain/min) rate using an Instron 5869 (n=6). The samples were vacuum soaked in PBS for approximately 30 minutes prior to testing. The compressive moduli, compressive yield strengths, and ultimate compressive strengths were calculated and compared to determine the fiber angle at which the scaffolds should be cut to yield the highest mechanical properties.

2.2.4. Incorporating HAp into the Electrospun Scaffolds

Hydroxyapatite ($Ca_5(PO_4)_3(OH)$) is a form of hydrated calcium phosphate. Ceramics such as HAp have been showed to promoted osteoblastic differentiation of stem cells [28] . Previous work aimed to incorporate synthetic HAp powder into the

polymeric scaffold by spreading the powder on the scaffold and allowing it to infiltrate the nanofibrous material. SEM images of the scaffold with HAp showed a non-uniform distribution of the HAp powder and low yield. As a result, we electrospun the HAp directly into the scaffold. A PDLA with 10% HAp solution was created by first dissolving PDLA (22w/v%) in DMF and THF. Prior to electrospinning, the HAp powder was added into the PDLA solution and vortexed for 15 minutes. HAp was only added into the PDLA layers. Scanning electron microscopy (SEM) and energy-dispersive x-ray fluorescence (ED-XRF) was performed on the PDLA/10%HAp scaffolds to qualitatively and quantitatively evaluate the presence of HAp in the scaffold. Samples (n=3) were dried overnight and sputter coated with gold and palladium for SEM imaging.

2.2.5. Gelatin Crosslinking Study II

In this study, we investigated various combinatorial crosslinking methods. The groups for two separate studies are outlined in Table 2.1. Crosslinking using glutaraldehyde alone was included in this study as a comparison to the scaffolds crosslinked in previous work [16, 26, 27]. Additionally, glutaraldehyde crosslinking was included in the methods along with mTG crosslinking to determine the effect of a combined crosslinking approach. These groups vary from the groups in the previously mentioned crosslinking study by including a series of vapor and submersion crosslinking steps. The base scaffold for each group was electrospun PLLA/10%Gel_PDLA scaffolds. For the scaffolds electrospun with mTG, mTG powder was added into the PLLA/10%Gel solution and vortexed for 30 minutes prior to electrospinning. mTG was added directly into the polymer solution based on findings that 0.5gm of mTG per mL of distilled water reaches an enzyme activity level of 15 U/gm-gelatin [29, 30]. This level of enzymatic activity has been

shown to promote crosslinking of gelatin. Fiber morphology was qualitatively evaluated with SEM.

Scaffolds from each group were cut into 1cm wide strips, rolled around an 18-gauge needle to a diameter of 0.5cm, secured with tape and sintered at 54°C for 45 minutes. Samples (n=6) from each group were mechanically tested in compression using an Intron 5869 at 10%/min strain rate until failure. All the samples were vacuum soaked in PBS prior to testing. The SEM images, ultimate compressive strengths, compressive moduli and compressive yield strengths were compared to determine the optimal method of adding the mTG crosslinking agent into the scaffold in terms of mechanical strength and integrity.

Group Name	Electrospun with mTG	Vapor crosslinked w/ 25mM Glut. 37°C for 2hrs	Soaked in 10M mTG at 37°C for 5hrs	Crosslinked at 37°C for 18hrs w/ 10M mTG vapor
Control				
Vap_mTG				✔
mtG_Glut	✔			
mTG_Vap_mTG	✔			✔
mTG_Soak_mTG	✔		✔	
mTG_Glut	✔	✔		
mTG_Glut_mTg	✔	✔	✔	

Table 2.1. Groups for Gelatin Crosslinking Study II

2.2.6. Investigating Sintering and Leaching Techniques

Previous work with the trabecular scaffold utilized a wrapping method to create the cylindrical structure [31]. Unfortunately, this scaffold fabrication method led to inconsistent mechanical properties due to non-uniformed wrapping tightness. To overcome this, we stacked .5cm die cut PDLA/15%HAp_PLLA/10%gel electrospun scaffold circles to a height of 1cm. The experimental groups for this study were scaffolds that were sintered then leached (S_L) and scaffolds that were leached then sintered (L_S). The rationale for this study was to determine which processing method would form the most stable porous structure. The S_L samples were from scaffolds that were leached in dI H_20 for 3 hours and then dried in a vacuum overnight. The samples were then cut into 1.5cm width strips, wrapped around 3x4cm cardboard pieces, secured with tape, and sintered at 54°C for 45mins. The sintered samples were then cut off the cardboard, stacked to a height of 10 mm and sintered at 54°C for 45mins for a second time with a 30g weight on top. After the second sintering step, the samples were die punched into .5cm diameter circles.

The L_S samples were cut into 1.5cm wide strips, wrapped about the cardboard pieces, secured with tape, and sintered at 54°C for 45minutes. The sintered samples were leached in dI H_20 for 3 hours and then dried in a vacuum overnight. Once dried, the samples were stacked to a height of 1cm, sintered for a second time at 54°C for 45 minutes with a 30g weight on top and then punched into 0.5cm diameter circles using a die punch. Samples (n=3) were dried overnight and sputter coated with gold and palladium for SEM imaging.

2.2.7. Comparing Mineralization Techniques (Flow, Static, Electrodeposition)

Mineralization is the process of allowing calcium ions from a simulated body solution (SBF) to attach to the exposed nucleation sites within the scaffold. SBF has a calcium concentration similar to blood plasma. The addition of this inorganic content contributes to the scaffold's structural integrity and osteoblastic differentiation capabilities. In this study, we exposed the scaffolds to 10X SBF under static, dynamic and active conditions. Namely, these conditions are defined as static mineralization, flow mineralization, and electrodeposition mineralization.

Static mineralization is the most commonly used mineralization technique. In static mineralization, the scaffolds were submerged in the SBF solution without any active flow. However, static mineralization is time consuming because the solution has to be changed every 2 hours and yields non-uniform mineralization throughout the scaffold [32, 33]. Flow mineralization on the other hand, utilizes a pump to actively flow the SBF solution through a chamber in which the scaffolds are housed. Bancroft et al. concluded a fluid flow of ions through a 3D perfusion culture system increase mineralized matrix deposition [34]. The advantages of using flow mineralization include a rapid and constant replacement of the SBF solution. Electrodeposition is the process of using cathodes to promote directional ionic flow and actively force the SBF through a substrate. This process has been proven to be rapid and effective method to generate apatite coatings on metallic substrates [35-37].

PDLA_PLLA/10%Gel scaffolds were used for this study and prepared using the sintering then leaching techniques described in Section 2.2.6. The SBF was prepared according to Jalota et al. [38, 39]. Scaffolds mineralized via static mineralization were

completely submerged in 40mL of SBF. The SBF was changed every hour. In the electrodeposition set-up a platinum wire was placed through the center of a cylindrical scaffold and a silicon electrode was placed around the scaffold in an U-shape, as shown in Figure 2.2. The scaffold was placed in 40mL of SBF with a pH of 4.4. The positive (working) lead was attached to the silicon electrode and the negative lead was attached to the platinum wire. The scaffold was mineralized for 1 hour at 5V, 10V, or 15V. The current was maintained around .03 Amps . After 1 hour of mineralization, the positive and negative leads were switched to change the direction of the gradient and force the minerals towards the outside of the scaffold. Samples from both groups were mineralized for a total of 2 hours.

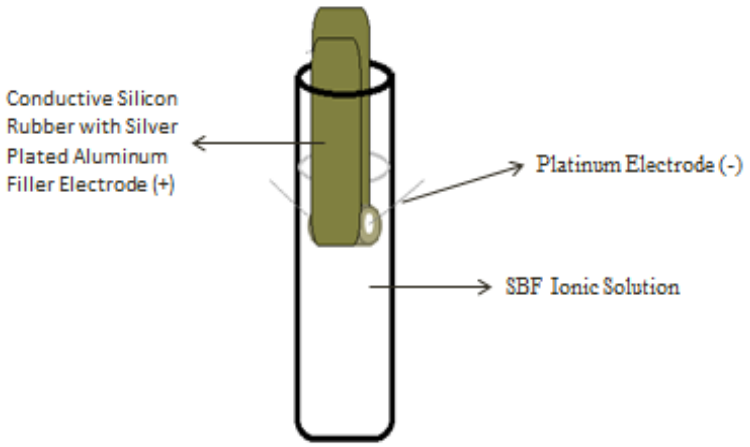

Figure 2.2. Schematic of the electrodeposition mineralization set up

The mineral content deposited on the scaffolds after each mineralization process was evaluated quantitatively using an alizarin red stain as an indirect measure of calcium content (n=3). The scaffolds were manually sliced into 100 µm thick cross-sectional slices and stained with the alizarin red dye (pH=4.23). Cetylpyridinium chloride (CPC)

(pH of 7.0) was used to extract the alizarin red stain from the samples and read at 540 nm on a spectrophotometer. Ash weight (% mineral content) analysis was also performed by placing the scaffolds in a furnace set at 700°C for 24 hours. All organic material is burned off at this temperature, leaving behind only the inorganic mineral.

We also performed a study using the electrodeposition mineralization technique. We mineralized the scaffold for 6 hours (switching the leads every 2 hours) at 4V. The samples from this group were evaluated using ash weight characterization and compression mechanical testing (1mm/min).

2.2.8. Investigating a Novel Co-Electrospinning Technique

Gelatin provides exposed carboxyl groups for the ions from the 10X SBF solution to attach to and form calcium phosphate. Therefore, I hypothesized the increase in overall gelatin concentration in the scaffold would lead to an increase in mineral content. The aim of this study was to develop an electrospinning technique to include additional gelatin into the trabecular scaffold. Porcine gelatin was mixed with acetic acid, ethyl acetate, and dI H_2O to yield a 15% gelatin solution for electrospinning. This solution was maintained in a 37°C water bath and sonicated on ice for approximately 30 minutes prior to electrospinning. A co-electrospinning set-up was developed using two syringes, one with a PLLA/10%Gel solution and the other with the 15% Gel solution. The solutions were pumped at different speed and ejected through a single charged needle (Figure 2.3).

First, a layer of PDLA was electrospun as previously described followed by a layer of PLLA/10%Gel_15%Gel. The PLLA/10%Gel solution was ejected from one syringe at a rate of 5ml/hr while the gelatin solution was pumped from the second syringe at 0.08ml/hr. The working distances remained at 10cm. The gelatin solution was pumped

at a different speed due to the solution's viscosity. The scaffolds were then dried in a desiccator and crosslinked using 25mM glutaraldehyde via vapor. Glutaraldehyde was used in this study to compare to scaffolds developed in previous studies. SEM analysis was performed to characterize the scaffolds (n=3). Fiber diameters were measured using ImageJ software and compared. Scaffolds (n=6) were mineralized using static mineralization for 7 days. Compressive mechanical tests were performed to compare mineralized and non-mineralized scaffolds (n=6). The compression rate was 1mm/min and samples were vacuum soaked in PBS prior to testing.

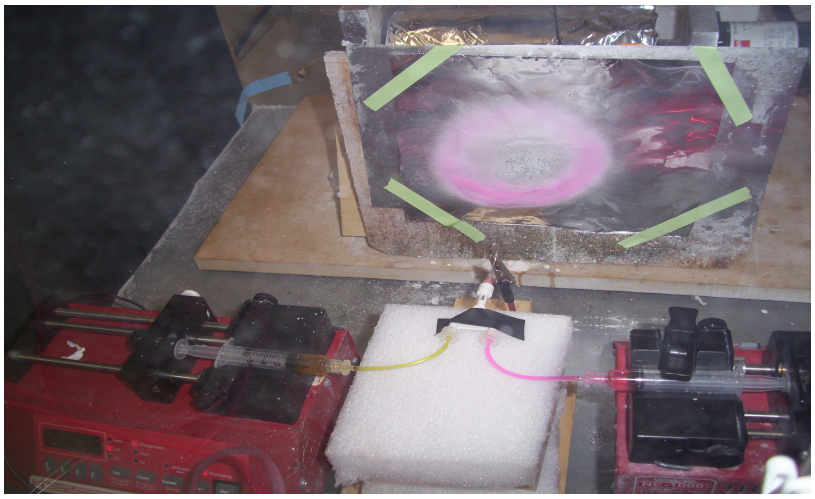

Figure 2.3. Co-electrospinning set-up. The left syringe is the 15%Gel solution with yellow dye. The right syringe is the PLLA/10% Gel solution with pink dye.

2.2.9. *In Vitro* Analysis of hMSCs on Trabecular Scaffold (Study I)

We performed a biocompatibility and differentiation *in vitro* cell study to evaluate the performance of human bone marrow derived stromal cells (hMSCs) on the scaffold. The cells were gifted from Dr. Ronke Olabisi's laboratory at Rutgers

University. The hMSCs were harvested from human fetal long bone and filtered and expanded by Samineni et al [40]. The hMSCs (passage 8) were maintained and expanded in Alpha-Modified Minimum Essential Media (α-MEM) supplemented with 10% fetal bovine serum (FBS) and 1% penicillin streptomycin for one week prior to the start of the cell study. The groups for this study are outlined in Table 2.2. The rationale for these groups was to compare the effect of HAp and amount of mineral content on cellular behavior. The hMSCs were seeded onto the appropriate substrate at 10,000 cells per substrate. Scaffolds were prepared as previously mentioned (PDLA_PLLA/10%Gel with and without 10% HAp depending on the group). All substrates were glued to well plate with sterile silicon adhesive and sterilized using 70% ethanol soak for 30 minutes, followed by UV radiation for 30 minutes per side. Substrates were also pre-conditioned with media for 24 hours prior to cell seeding. All mineralized scaffolds were mineralized via static mineralization for 12 hours.

Group	**Mineralized**	**HAp in scaffold**	**Salt Leached Pores**
TCP (Control)			
NoMin_NoHAp_NoSalt			
NoMin_NoHAp_SL			✔
NoMin_HAp_SL		✔	✔
Min3days_HAp_SL	3 days	✔	✔
Min7days_NoHAp_SL	7 days	X	✔
Min7days_HAp_SL	7 days	✔	✔

Table 2.2. Experimental design for trabecular scaffold *in vitro* study

Cells were allowed to attach to the substrate and proliferate in α-MEM. Media was switched to osteogenic media seven days after seeding. The osteogenic media was α-

MEM supplemented with .1M ascorbic acid, 0.01M dexamethasone and 0.01M Beta-glycerophosphate. PrestoBlue® assay was performed as an indirect measurement of cellular viability by quantifying the cellular metabolic activity. Alizarin red stain was performed to determine the amount of calcium deposited from the cells in response to the scaffold's composition. The groups were compared to evaluate the scaffold's biocompatibility and osteogenesis capabilities over a 28-day timespan.

2.2.10. *In Vitro* Analysis of hMSCs on Trabecular Scaffold (Study II)

In a follow up study, we further evaluated the osteogenic potential of the PDLA/PLLA_10%Gel/10% HAp scaffold over 10 days. The purpose of incorporating HAp into the scaffold was to act as an inducer for stem cell osteogenic inducer. Human Marrow Stromal Cells (hMSCs) at passage 1 were obtained from Texas A&M Health Science Center. The cells, donated from a male age 22 y/o, were maintained in α-MEM without supplemented with 10% fetal bovine serum (FBS), 1% penicillin and 1% 2mM L-glutamine. The cells were seeded at 50,000 cells/substrate onto TCP (control), a scaffold without HAp (PDLA/PLLA_10%Gel) and a scaffold with HAp (PDLA/PLA_10%Gel/10%HAp). Scaffolds from both experimental groups were mineralized via static mineralization for 6 hours. Cellular viability was assessed using PrestoBlue® assay. The cellular activity was normalized to cell number. The cell supernatant from each group was collected at time points 0, 3, 7, and 10 days and evaluated for osteogenic protein secretion using a quantitative ELISA for intact human osteocalcin (OC). Serum OC is a noncollagenous protein marker for osteoblast activity [41]. Analysis was performed using a novex by Life Technologies Osteocalcin ELISA kit. For further evaluation, alkaline phosphatase (ALP), an early marker of osteogenesis,

was detected using an Alkaline Phosphatase Staining Kit II from Stemgent Inc (USA). The assay was performed according to the kit's protocol. Images were taken at 3, 7 and 10days with a colored light microscope for qualitative analysis. To quantify the ALP activity using ImageJ, three images from each group were taken and converted to grayscale. The images were then segmented to isolate the red-stained areas using a set threshold (Figure 2.4). The thresholded areas were then measured and compared to quantitatively evaluate the ALP activity between groups in terms of area and percent area.

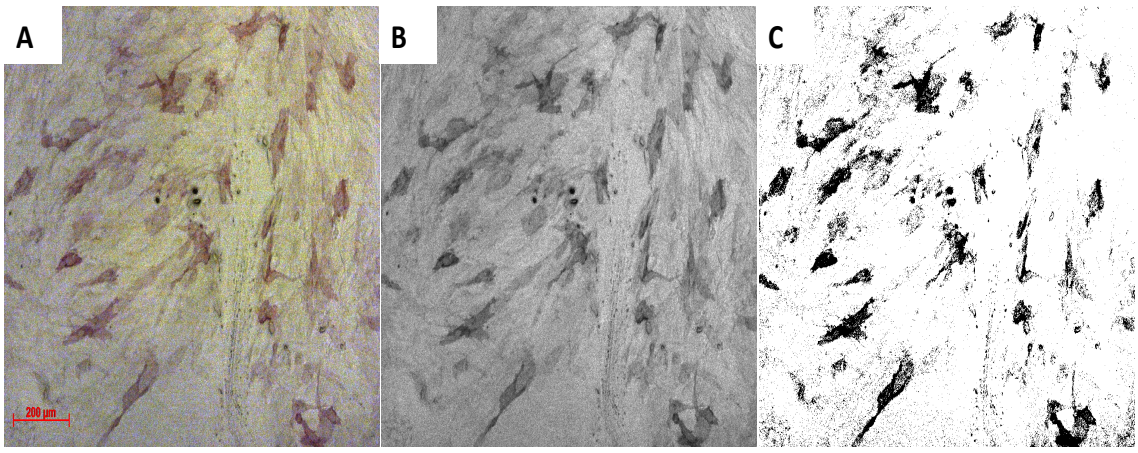

Figure 2.4. A) ALP stained images (10X) were processed in ImageJ to calculate area and percent area of ALP secretion. The images were converted to grayscale (B) and then segmented to isolate the red-stained areas (C). Area size and percent area was computed and compared between groups. Scale bar = 200μm.

2.2.11. Statistical Analysis

Statistical analysis was performed using KaleidaGraph Synergy Software. All data was subjected to an one-way analysis of variance (ANOVA) with post-hoc

analysis (Tukey test) to determine the statistical significance of differences between groups, $p < 0.05$.

2.3. Results

2.3.1. Gelatin Crosslinking Study I (Tensile Testing)

The tensile behaviors of gelatin strips crosslinked with mTG and EDC are shown in Figure 2.5. The gelatin strips crosslinked with glutaraldehyde did not maintain their structure and therefore were not able to be mechanically tested. This could be due to the inability of the glutaraldehyde vapor to penetrate the thick gelatin strips and create crosslinked bonds. There was no significant difference in the ultimate tensile strengths and moduli between the mTG and EDC methods. The tensile yield strength of the gelatin strips crosslinked with mTG was significantly greater than the gelatin strips crosslinked with EDC. Transglutaminase enzymes, such as mTG, crosslink proteins by catalyzing formation of covalent glutamine and lysine amine bonds between gelatin strips [42-44]. This forms a more stable, permanent network of polypeptides [24, 45]. The increase in polypeptide chain lengths leads to improved tensile strength, a desirable feature for gelatin retention in a TE scaffold.

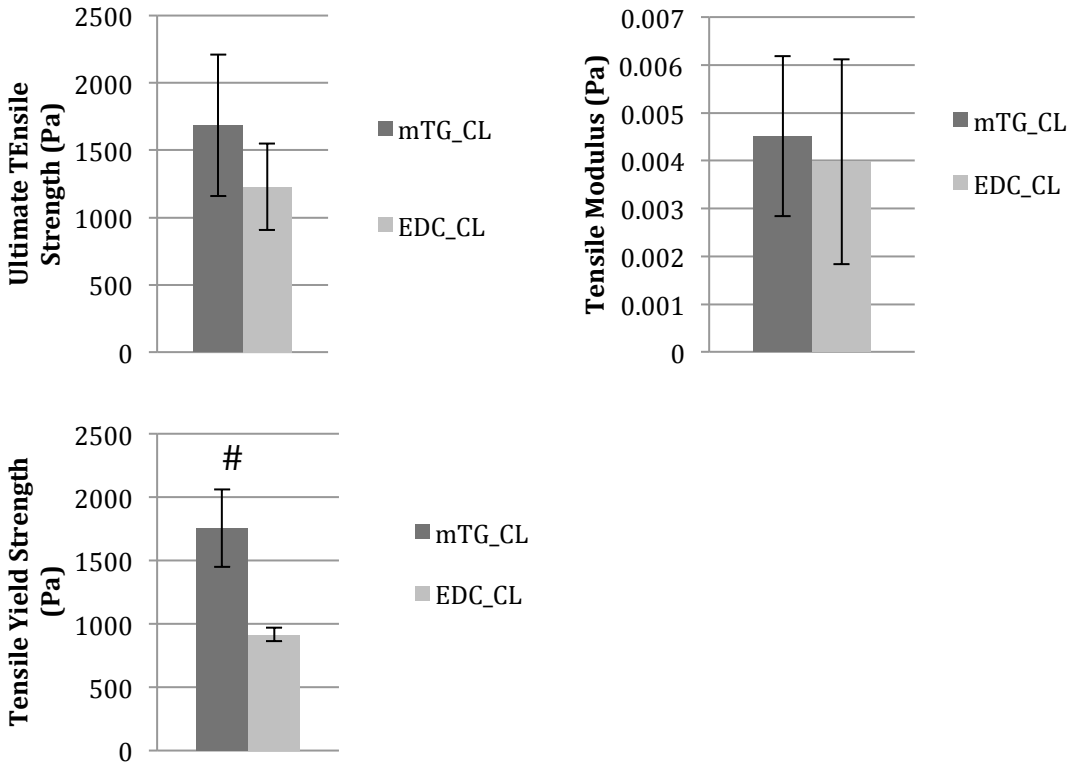

Figure 2.5. Tensile mechanical testing (10% strain/min) results for samples of gelatin crosslinked with mTG and EDC. mTG crosslinking proved to be the better crosslinking method in terms of mechanical properties due to the ability to create more stable bonds. Statistical analysis: # denotes ANOVA Tukey Test (post- hoc) $p<0.05$.

2.3.2. Varying Fiber Angle (Mechanical Testing)

The purpose of this study was to determine a nanofiber angle within the scaffold that would yield the highest tensile mechanical properties. The electrospun scaffolds were cut into strips and rolled at varying angles into 1cm by .5cm cylindrical columns. Figure 2.6 shows the tensile moduli and tensile yield stresses for the scaffolds with fibers angles at 0°, 15°, 30°, 45°, and 90°. The samples with 0° and 90° angled fibers had the lowest yield stresses and Young's moduli whereas the samples with the angled

fibers at 15°, 30° and 45°, displayed higher tensile properties. Also, there appears to be an indirect correlation between the fiber angles and the tensile properties. As the fiber angles increased from 15° to 45°, the tensile moduli and tensile yield strengths decreased.

The differences in mechanical behavior as a result of varying the fiber angle can be explained using the force polygon shown in Figure 2.7A. The force polygon depicts the forces acting internally within each column [46]. The angle from the upright origin (β) is the corresponding angle at which the strips were cut: 0°, 15°, 30°, 45° and 90°. The total forces, horizontal, vertical and an inclined internal, collectively add to the increased yield strength and young's modulus of the columns. This is evident in the decreased mechanical properties of the columns with 0° and 90° angled fibers. The columns with the 0° angled fibers do not have a horizontal force, therefore decreasing the overall total force. The columns with the 90° angled fibers lack a horizontal or internal inclined force and therefore yielded the lowest total forces of all the fibers ($\cos 0° = \tan 0° = 0$) and hence, the lowest compressive mechanical properties.

The axial forces within the columns defined as the inclined forces, N, are equal to the combination of a vertical (gravity loads) and horizontal component. The horizontal component is a result of the angle and inclined internal force and the vertical component is the known yield strength exerted by the column. From the force polygon, the relationship between the inclined internal force, the vertical force and horizontal force are shown in the equations in Figure 2.7B. The mechanical properties of the columns correspond to the fibers acting as individual forces, which oppose the applied

compressive load. As a results, the angled fibers at 15°, 30°, and 45° had greater total forces, vertical, horizontal, and inclined internal forces, acting against compression, thus yielding higher mechanical strength.

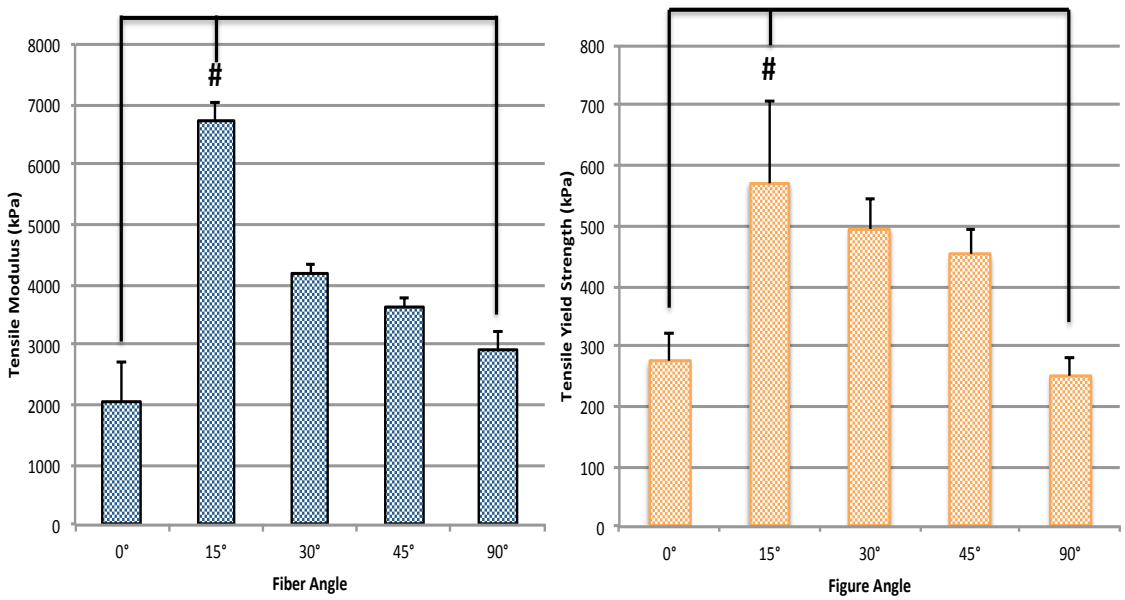

Figure 2.6. Tensile moduli and tensile yield strengths of the scaffolds with varying fiber angles. Columns with fibers angled at 15° were significantly greater than the columns with 0° and 90° angled fibers. Statistical analysis: # denotes ANOVA Tukey Test (post-hoc) $p<0.05$.

A

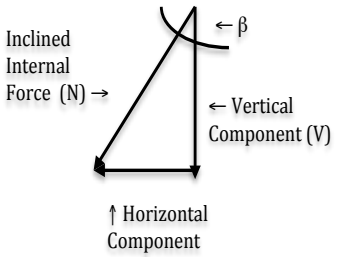

B

$$\frac{V}{N} = \cos\beta \rightarrow \qquad N = \frac{V}{\cos\beta}$$

$$\frac{H}{V} = \tan\beta \rightarrow \qquad H = V\tan\beta$$

Figure 2.7. A) Force polygon, B) Force polygon equations

2.3.3. Incorporating HAp into Scaffold (SEM Images & ED-XRF Analysis)

Figure 2.8 is the SEM image of the PDLA/10%HAp scaffold. The image shows congregates of HAp nanopowder embedded throughout the PDLA scaffold. The presence of the HAp in the scaffold was validated using ED-XRF, Figure 2.9. HAp, $Ca_5(PO_4)_3(OH)$, is a naturally occurring mineral form of calcium apatite. Calcium and phosphorus, the two elements in HAp, expressed a statistically significant higher intensity in the PDLA/10%HAp scaffold in comparison to the control PDLA electrospun scaffold. The intensity reading of the phosphorus and calcium in the control scaffold can be contributed to artifacts or detection of the PDLA compounds.

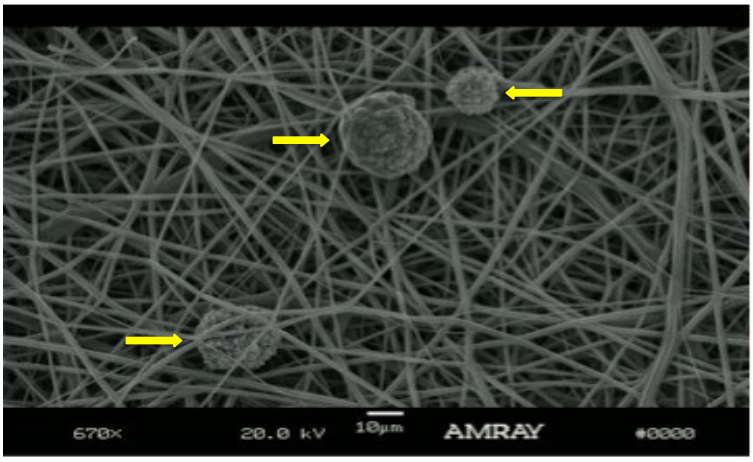

Figure 2.8. SEM image of the PDLA/10%HAp electrospun scaffold. The yellow arrows indicate the HAp congregates. (Scale bar = 10µm)

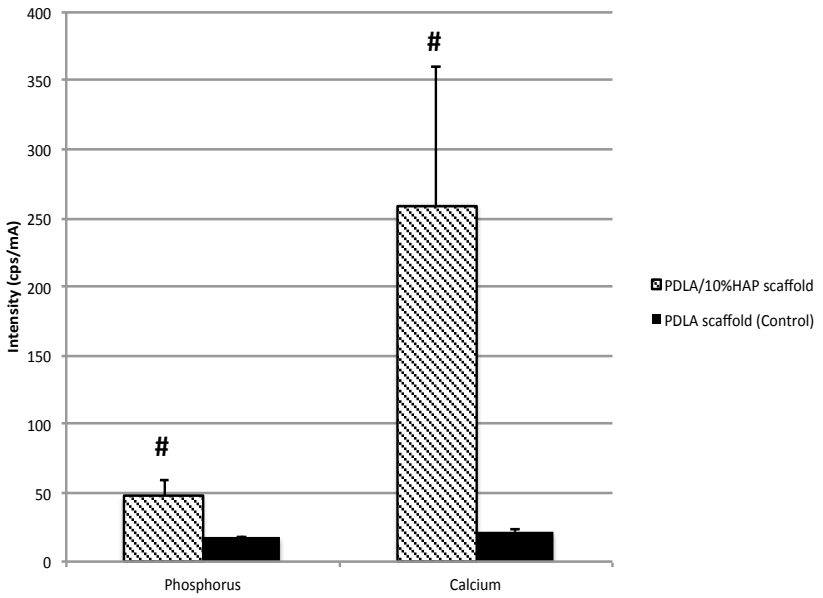

Figure 2.9. Energy dispersive-X-ray fraction results of PDLA scaffold with (PDLA/10%HAp) and without HAp (PDLA Scaffold). There was a statistically significant detection of phosphorous and calcium, the two primary elements in HAp, in the PDLA/10% HAp scaffold in comparison to the control PDLA scaffold. Statistical analysis: # denotes ANOVA Tukey Test (post-hoc) $p<0.05$.

Qualitative and quantitative analysis show the ability to successfully incorporate HAp crystals into the synthetic polymeric scaffold. The HAp particles are also embedded and retained in the scaffold. This is desirable because the HAp particles are least likely to be leached from the scaffold prematurely. Additionally, this method retains more HAp powder than the spreading method that was previously investigated.

2.3.4. Gelatin Crosslinking Study II (SEM Images & Mechanical Testing)

SEM images of PDLA_PLLA/10%Gel crosslinked with varying techniques are shown in Figure 2.10 and Figure 2.11. The purpose of this study was to evaluate the effect of varying crosslinking techniques on fiber morphology. Figure 2.10A shows the control scaffold that did not undergo crosslinking. The fibers are uniformed with pores throughout the fibrous network. Figure 2.10B represents the scaffold crosslinked with 25mM glutaraldehyde. The fibers in this scaffold appeared fused with a less porous structure than shown in Figure 2.10A. Large collections of crosslinked gelatin beads are seen in the SEM images of the scaffold electrospun with mTG and crosslinked with vapor mTG (Figure 2.10C). Figure 2.10D is an SEM image of the scaffold that was soaked in mTG. Beads of gelatin are also evident in these images.

Figure 2.11A is the control scaffold that was not crosslinked for comparison. Figure 2.11B is of SEM images of a scaffold that was electrospun with the crosslinker mTG in the solution. The fiber morphology in Figure 2.11B is very similar to the morphology in Figure 2.10A. The scaffolds in Figure 2.11C and Figure 2.11D were exposed to vapor 25mM glutaraldehyde. The fibers in these scaffolds appear swollen and fused together. Additionally, soaking the electrospun PDLA_PLLA/10%Gel scaffold in mTG as a final crosslinking step appears to cause a significant swelling of the fibers, as shown in Figure 2.10C. This fiber swelling can lead to a decrease in porosity, fiber integrity and scaffold strength

Compressive mechanical testing using an Instron 5869 was performed on the scaffolds at a 1mm/min rate. Figure 2.12 compares the compressive moduli, ultimate compressive strengths, and yield strengths of the scaffolds from each group. All of the

compressive properties of the PDLA_PLLA/10%Gel scaffold electrospun with mTG were statistically greater than the other groups, including the control sample. The samples that were soaked in the mTG crosslinking solution yielded lower mechanical properties than the samples that were not soaked in the mTG solution. There was also a decrease in mechanical properties when the scaffolds with mTG were also crosslinked with 25mM glutaraldehyde. The swelling seen with the fibers exposed to solely glutaraldehyde crosslinking in the previous study, may have contributed to the decrease in mechanical properties in comparison to the mTG crosslinked samples. The mechanical data also suggests that the additional mTG soak had adverse effects of the scaffold's overall mechanical properties. From the mechanical data, we can conclude that mTG included in the electrospinning solution yields a more mechanically enhanced scaffold.

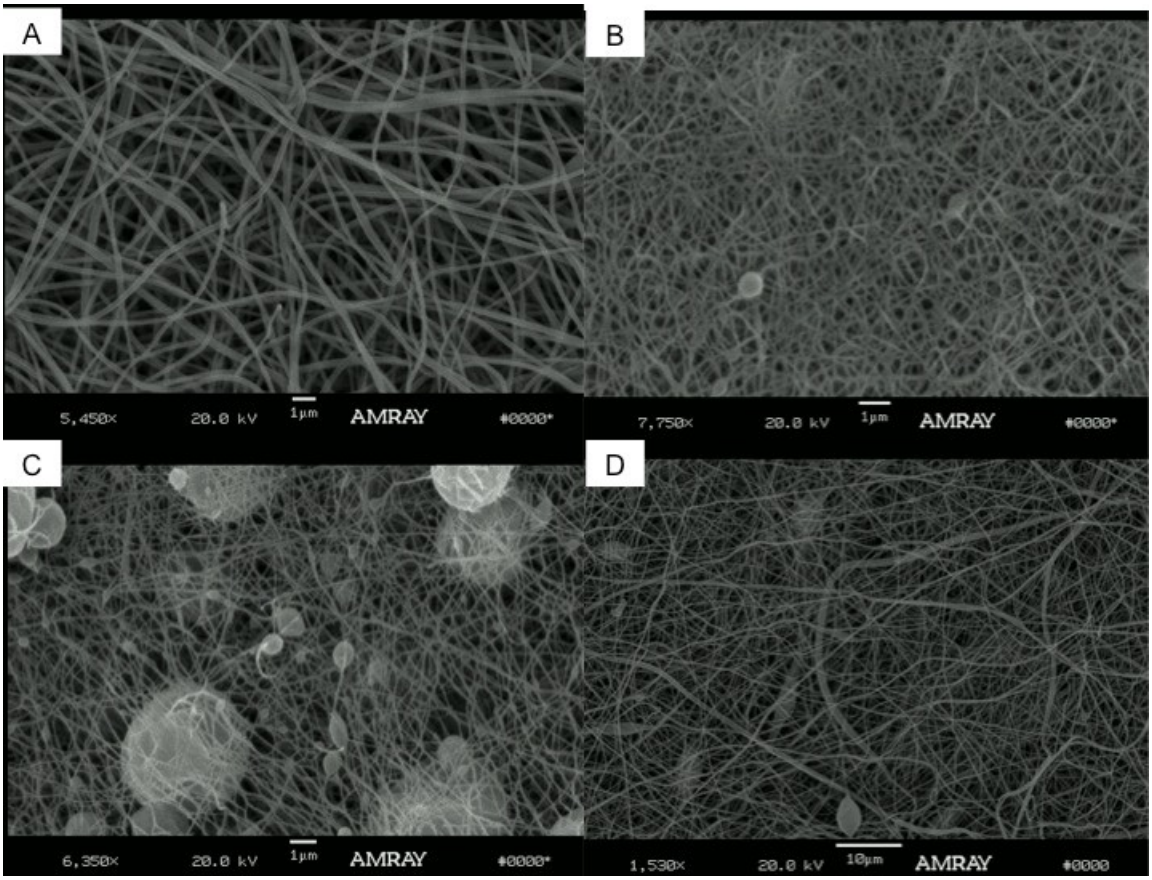

Figure 2.10. Scanning electron microscopy (SEM) images of the electrospun scaffolds with varying crosslinking techniques: A = Control, B = Glut, C = mTG_Vap_mTG, and D = mTG. Scale bar = 1µm for Image A, B, and C and 10µm for image D.

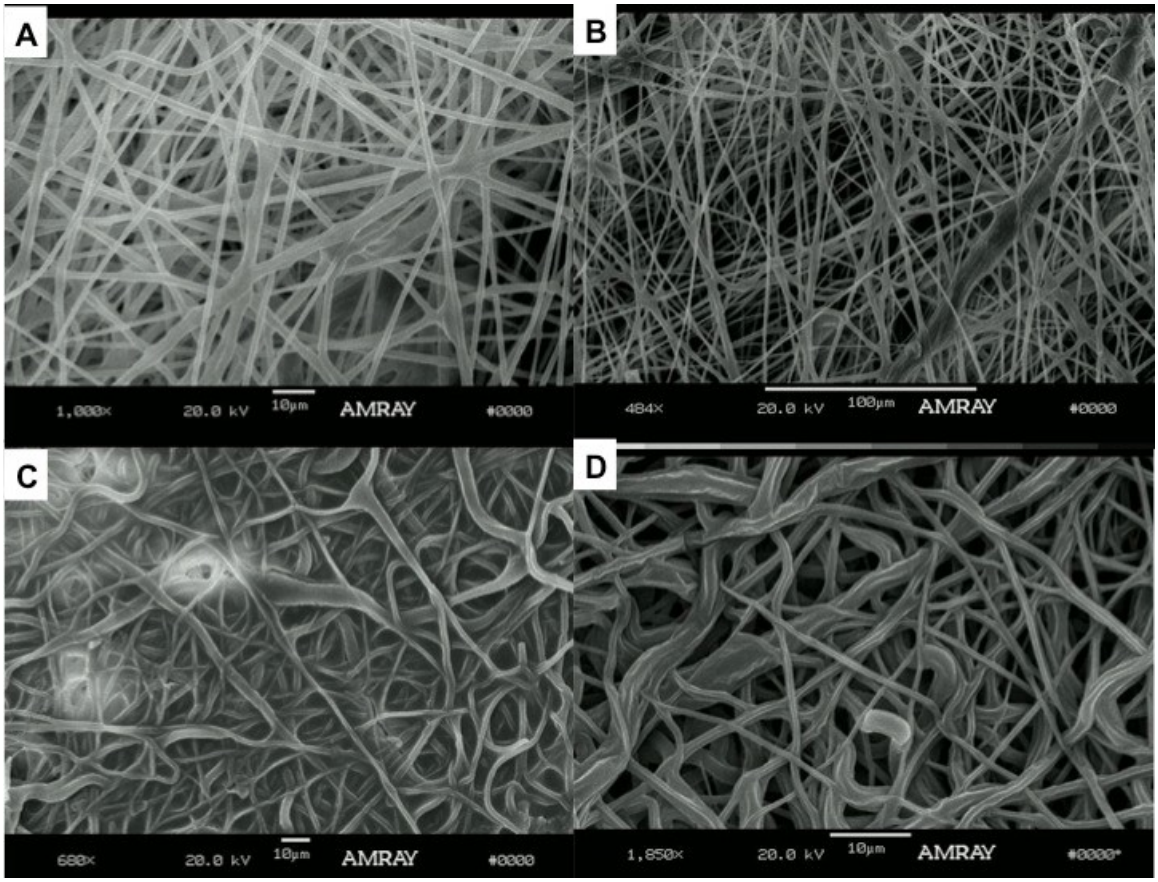

Figure 2.11. Scanning electron microscopy (SEM) images of the electrospun scaffolds with varying crosslinking techniques: A = Control, B = mTG, C = mTG_Glut_Soak_mTG, D = mtG_Glut. Scale bar =10µm images A, C, and D and 100µm for image B.

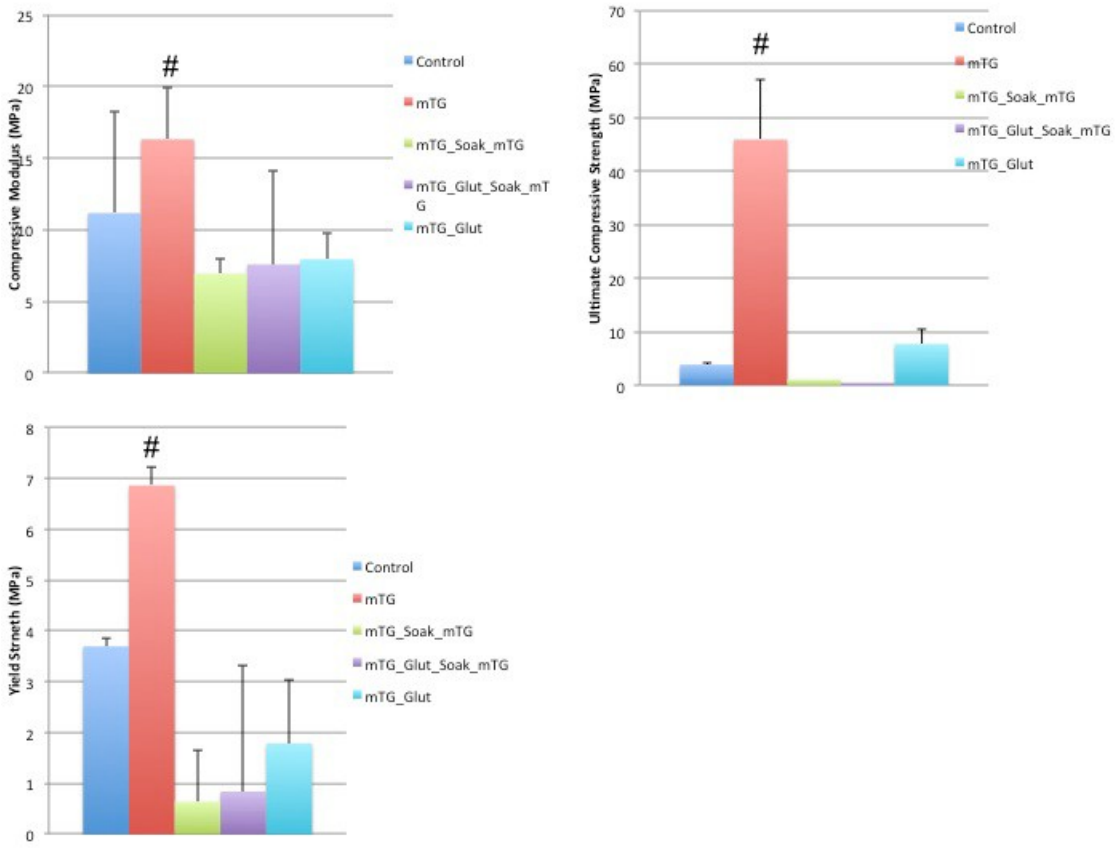

Figure 2.12. Compressive mechanical testing results for PDLA/PLLA_10%Gel electrospun scaffold exposed to varying crosslinking techniques. The scaffold with mTG incorporated during electrospinning yielded statistically higher compressive properties. Statistical analysis: # denotes ANOVA Tukey Test (post-hoc) $p<0.05$ from the other groups.

2.3.5. Investigating Sintering and Leaching Techniques (SEM & Mechanical Testing)

SEM images of the scaffolds from the sintering leaching study are shown in Figure 13. Figure 2.13A shows the ability to retain salt crystals in the scaffold during

electrospinning. The SEM image in Figure 2.13B is of a scaffold sintered prior to salt leaching. Figures 2.13 (B-D) also validate the leaching process. Figures 2.13C and 2.13D are scaffolds that were leached before being sintered. The pores in these scaffolds appear to be less structured than the pores in Figure 2.13B.

Overall, the SEM images suggest the need for sinterin prior to leaching g to create a stable structure around the NaCl crystals, which were maintained after salt leaching. This allows for enhanced porosity in the scaffold. The L_S samples displayed smaller pores. This could be due to the pores elongating and crushing during the stacking and sintering process. The results from the study conclude the need to sinter the scaffolds prior to salt leaching in order to yield uniform pores. Stable pores are necessary for cellular infiltration and nutrient transport.

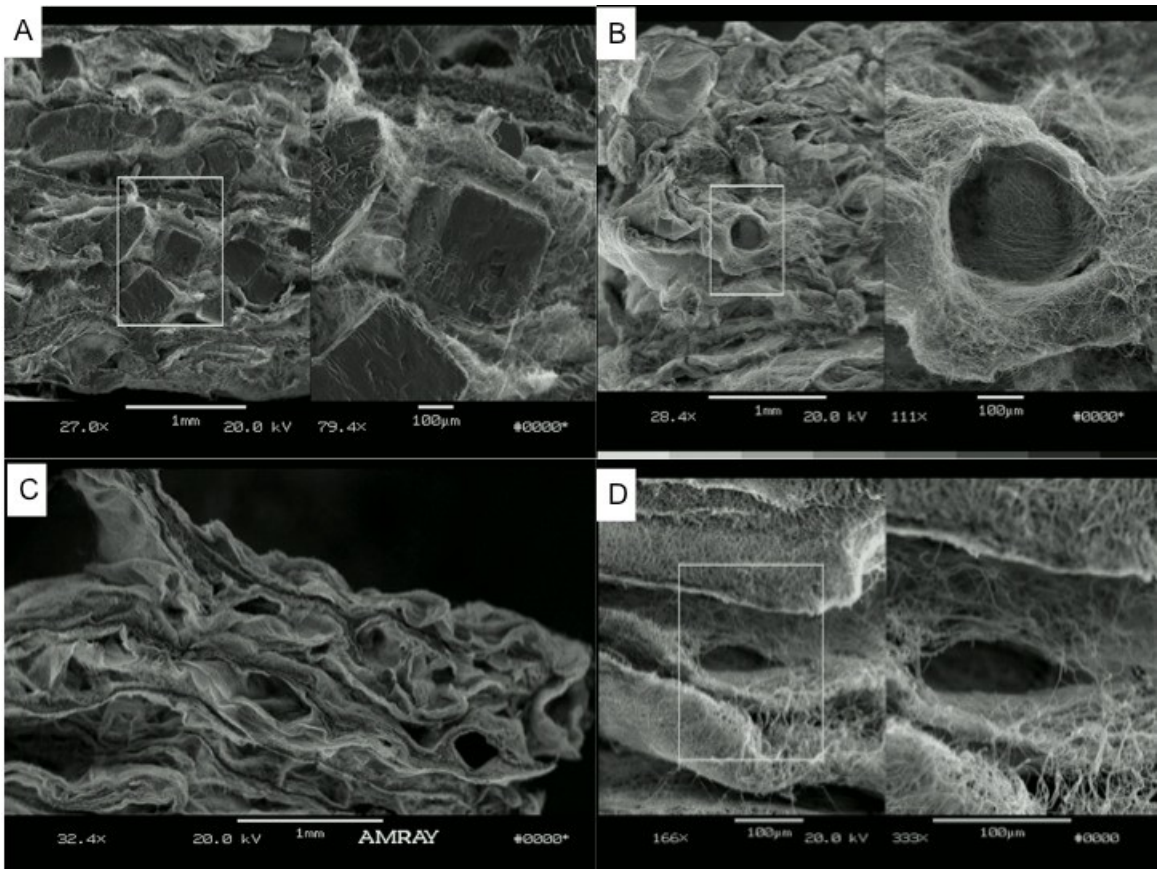

Figure 2.13. SEM images of A.) PLLA/10%Gel_PDLA scaffold with NaCl crystals, B.) PLLA/10%Gel_PDLA scaffold after sintering then leaching (S_L), C & D.) PLLA/10%Gel_PDLA scaffold after leaching then sintering (L_S). Scale bars = 1mm for image A (left), B (left) and C, 100µm for image A (right), B (right) and D.

2.3.6. Various Mineralization Techniques (Mechanical Testing & Alizarin Red)

Static, flow and electrodeposition mineralization were investigated in this study as techniques to enhance the calcium deposition and overall mineral content process. Figure 2.14 shows the compressive properties of co-electrospun scaffolds that were mineralized via flow mineralization up to Day 14. There is an apparent decrease in mechanical properties from Day 7 to Day 14. This may be due to the over accumulation

of mineral ions at the nucleation site, blocking the attachment of additional mineral. Also, the flow mineralization may be too forceful causing scaffold degradation, therefore decreasing the scaffold's integrity.

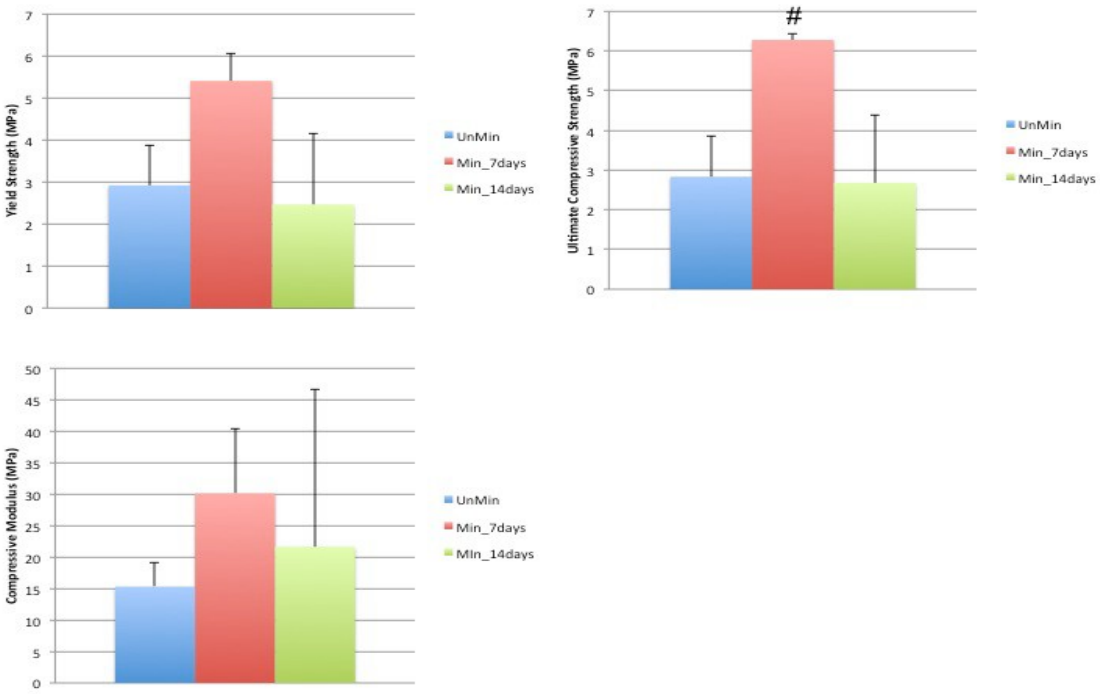

Figure 2.14. Compressive properties (1mm/min) of co-electrospun PDLA_PLLA/10%Gel_15%Gel scaffolds mineralized via flow mineralization up to 14 days. Scaffolds mineralized for 7 days yielded higher compressive properties than the unmineralized (UnMin) and scaffolds mineralized for 14 days (Min_14days). Statistical analysis: # denotes ANOVA Tukey Test (post-hoc) $p<0.05$.

In the second mineralization study, electrodeposition mineralization and static mineralization was performed for 2 hours with the simulated body fluid solution switched after one hour. The average for the samples mineralized via static

mineralization is 2.91±1.54%. The average percent mineralization for scaffolds mineralized by electrodeposition at 5V, 10V, and 15V are 8.51±4.20%, 4.37±2.15%, and 7.63±1.60%, respectively, Fig.2.15.

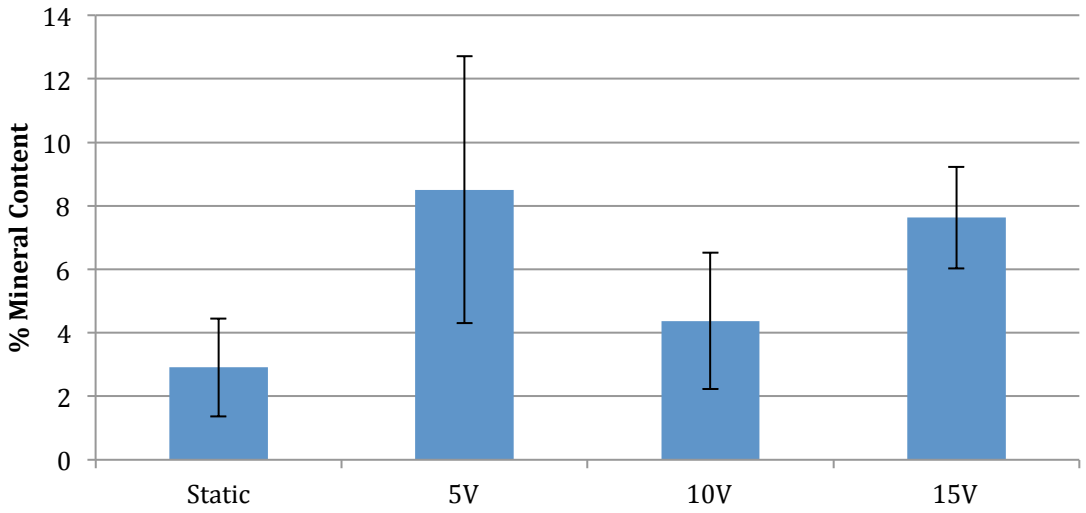

Figure 2.15. Ash weight analysis of scaffold mineralized via electrodeposition mineralization.

The scaffold mineralized via electrodeposition mineralization at 5V had a higher mineral content than samples mineralized via static and electrodeposition at 10V and 15V. Samples mineralized via electrodeposition at 5V, 10V, and 15V displayed a higher percent of mineral content than static mineralization. This could be due to the silicone rubber losing conductivity at higher voltages, therefore decreasing the current flowing through the electrode. The decrease in current created a weaker gradient of minerals forced through the scaffold. The first electrodeposition samples were mineralized at 5V, but the silicone electrode was not as conductive when samples were mineralized at 10V or 15V. In a preliminary study, the trabecular scaffold was mineralized for 6 hours via

electrodeposition mineralization with the leads and solution switched every hour. Ash weight study yielded 61% of the scaffold's overall weight was mineral content. Based on the results from the three methods, we concluded electrodeposition mineralization at 5V is the optimal mineralization technique by actively forcing ions through the scaffold.

2.3.7. Characterization of Co-Electrospinning Technique (SEM & Mechanical Testing)

Gelatin was co-electrospun with the PLLA/10%Gel solution. The objective of this study was to incorporate additional gelatin into the scaffold to enhance cellular attachment and mineralization enhancement. The images in Figure 2.16 are SEM images of a gelatin electrospun scaffold (Gel), a PLLA/10%Gel scaffold and a PLLA/10%Gel_15%Gel co-electrospun scaffold. The distinct two electrospun fiber types are evident in Figure 2.16C. The mean fiber diameters for the Gel, PLLA/10%Gel, and PLLA/10%Gel_15%Gel co-electrospun scaffold were 0.35±.02, 1.32±.05, and 0.88±.02 microns, respectively. The decrease in average fiber diameters from the scaffold in Figure 2.16B to the scaffold in Figure 2.16C is due to the additional thinner gelatin fibers. Qualitatively, the images prove the ability to incorporate electrospun gelatin fibers into the PLLA scaffold.

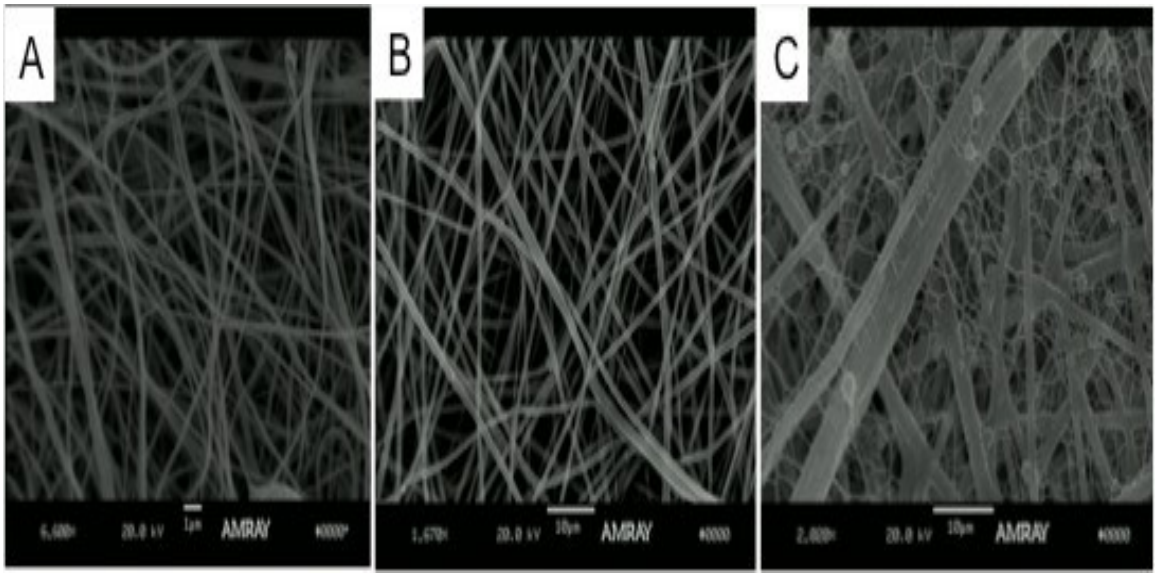

Figure 2.16. SEM images of A.) 100% Gelatin scaffold, B.) PLLA/10%Gel scaffold, C.) PLLA/10%Gel_15%Gel co-electrospun scaffold. (Scale bar for image A = 1μm and for images B and C = 10μm)

Figure 2.17 shows the significant increase in compressive yield strength and ultimate compressive strength with the addition of the gelatin in the co-electrospun scaffold after 7 days of flow mineralization in comparison to the control, PLLA/10%Gel scaffold. Gelatin has exposed carboxyl groups acting as nucleation sites for mineral attachment. As evident from the mechanical analysis, this increase in mineral content led to an increase in mechanical strength. The compressive properties of non-mineralized scaffolds, scaffolds mineralized for 7 days and native trabecular bone are outlined in Table 2.3 for comparison. The compressive modulus of the co-electrospun mineralized scaffold (about 30MPa) is comparable to the compressive modulus of native trabecular bone, 50MPa. The data suggests the addition of the gelatin using co-electrospinning enhances the scaffold's overall mechanical strength by increasing the mineral content.

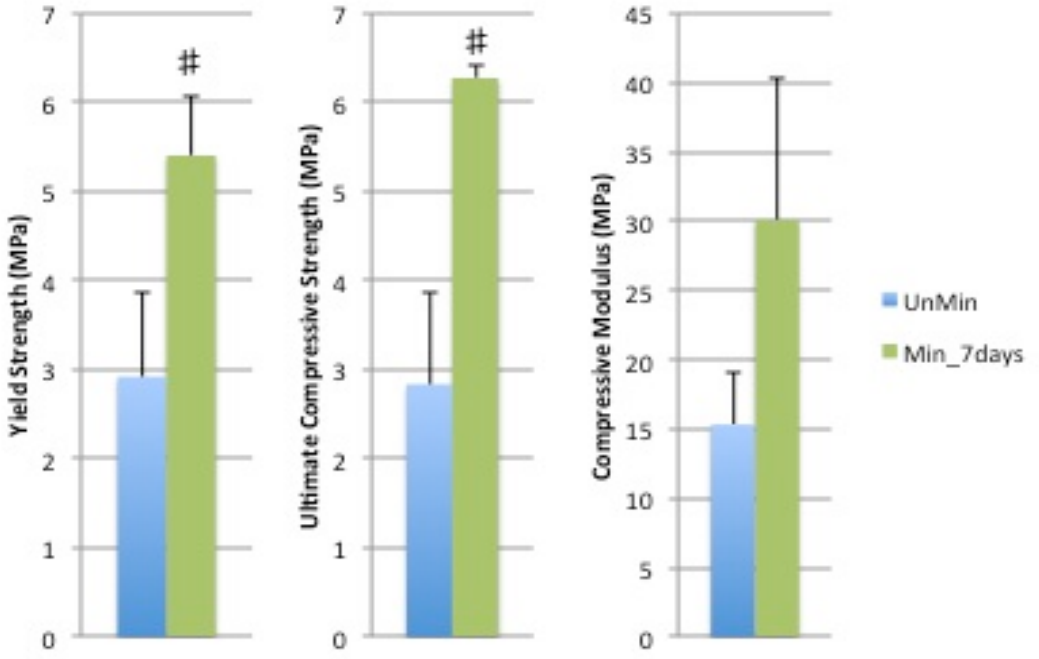

Figure 2.17. Compressive mechanical analysis of non-mineralized and mineralized (7 days) co-electrospun PDLA_PLLA/10%Gel_15%Gel scaffolds. The additional gelatin fibers lead to an increase in mechanical strength by creating more nucleation sites for mineral content. Statistical analysis: # denotes ANOVA Tukey Test (post-hoc) $p<0.05$

	Compressive Modulus (MPa)	Yield Strength (MPa)	Ultimate Compressive Strength (MPa)
UnMin/Min_7day	15.32±3.82 30.13±10.20	2.92±.94 5.41±.67	2.84±1.03 6.28±.15
Native Trabecular Bone	50-500 MPa	7-10 MPa	10-20 MPa

Table 2.3. Calculated compressive properties of non-mineralized and mineralized (7 days) co-electrospun PDLA_PLLA/10%Gel_15%Gel in comparison to native trabecular bone. The mechanical properties of the co-electrospun scaffold mineralized for 7 days exhibits strength comparable to trabecular bone.

2.3.8. *In Vitro* Analysis of hMSCs on Trabecular Scaffold (Cellular Viability and Calcium Deposition)

Metabolic activity was measured using PrestoBlue® assay as an indirect measurement of cellular viability. Figure 2.18 shows the relative florescence units (RFU) of each group over a 28- day timespan. There was no significant decrease in cellular viability in the experimental groups between Day 7 to Day 28. The difference in cellular viability between the control and experimental samples was expected when seeding cells on nanofibrous scaffolds. Decreased cellular viability was seen in all the groups except Min3Days_HAP_Salt group and could be due to high confluence, which inhibits cellular function and causes a decrease in proliferation.

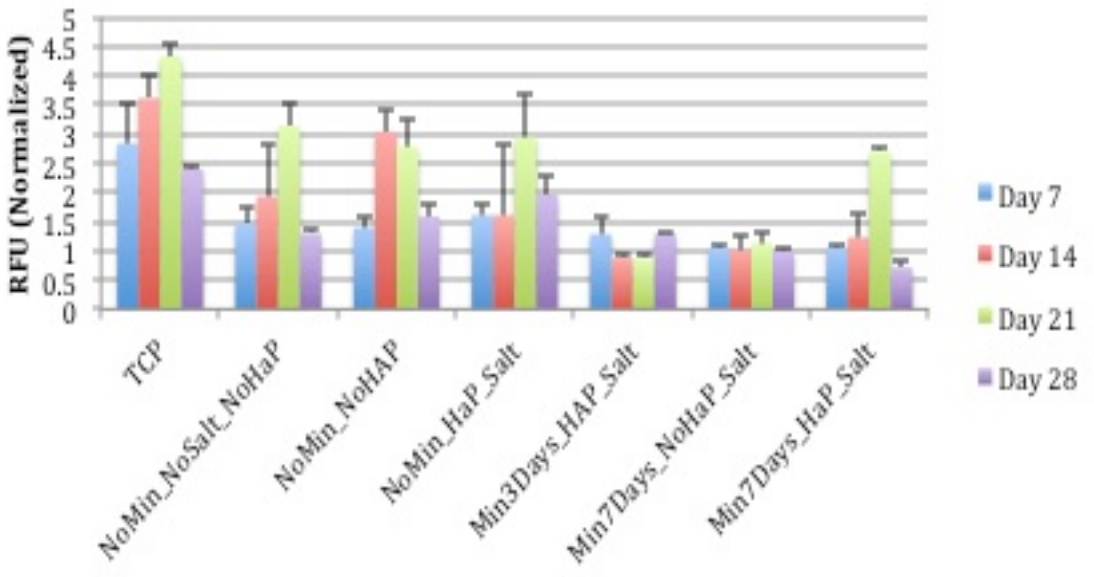

Figure 2.18. Cell viability analysis of hMSCs on TCP and scaffold (y-axis is in relative fluorescence units).

Figure 2.19 is the absorbance readings of the alizarin red stain. The absorbance reading of the associated substrate without cells was subtracted from the absorbance reading of the substrate with the cells. The absorbance reading is directly proportional to the amount of calcium deposited by the hMSCs in response to the scaffold's composition. The groups of interest are outlined in black boxes. Cells seeded on the scaffolds with HAp deposited more calcium than the hMSCs seeded on the scaffold without HAp. Also, the increase in mineralization time was directly related to an increase in absorbance reading for alizarin red, as seen in the graph. The similar trend of decrease in all groups on Day 28 as seen in Figure 2.18 is also seen in Figure 2.19. This further suggests a cellular growth decrease leading to a decrease in cellular calcium

deposition. There is also a significant increase from Day 7 to Day 14 in calcium deposition seen with the Min3Days_HAp_Salt group. We expect this is due to the change to osteogenic media at Day 7.

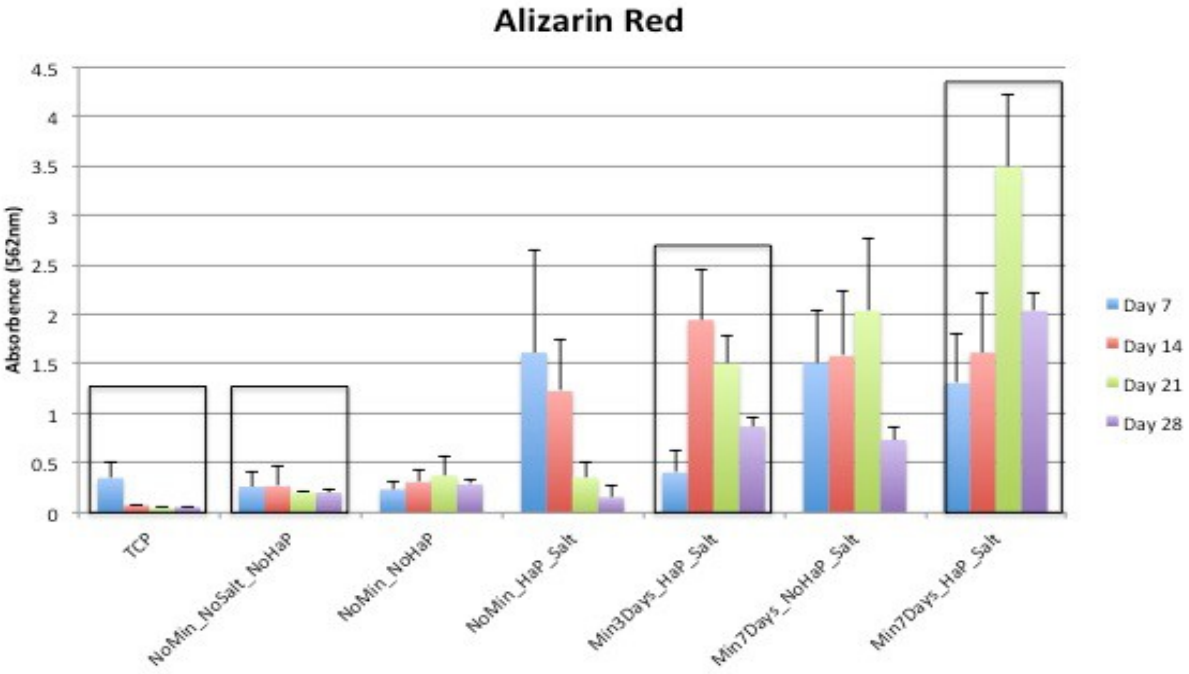

Figure 2.19. Cellular calcium deposition evaluated using alizarin red stain.

2.3.9. *In Vitro* Analysis of Osteogenic Potential of HAp Trabecular Scaffold

The metabolic activity of the hMSCs seeded on TCP and a PDLA scaffold with HAp (PDLA-HAp _hMSCs) and without HAp (PDLA_hMSCs) was assessed to further evaluate the scaffold's biocompatibility. There were no statistically significant differences in the cell's metabolic activity over ten days, as shown in Figure 2.20. This suggests the scaffold is biocompatible and the cells attached to the scaffold similarly to the cells seeded on the TCP. The decrease in cellular viability on Day 10 seen with the hMSCs seeded on the TCP (control) could be due to a high confluency of the cells in 2D, whereas the hMSCS seeded on the 3D scaffold have more surface area for proliferation

and migration.

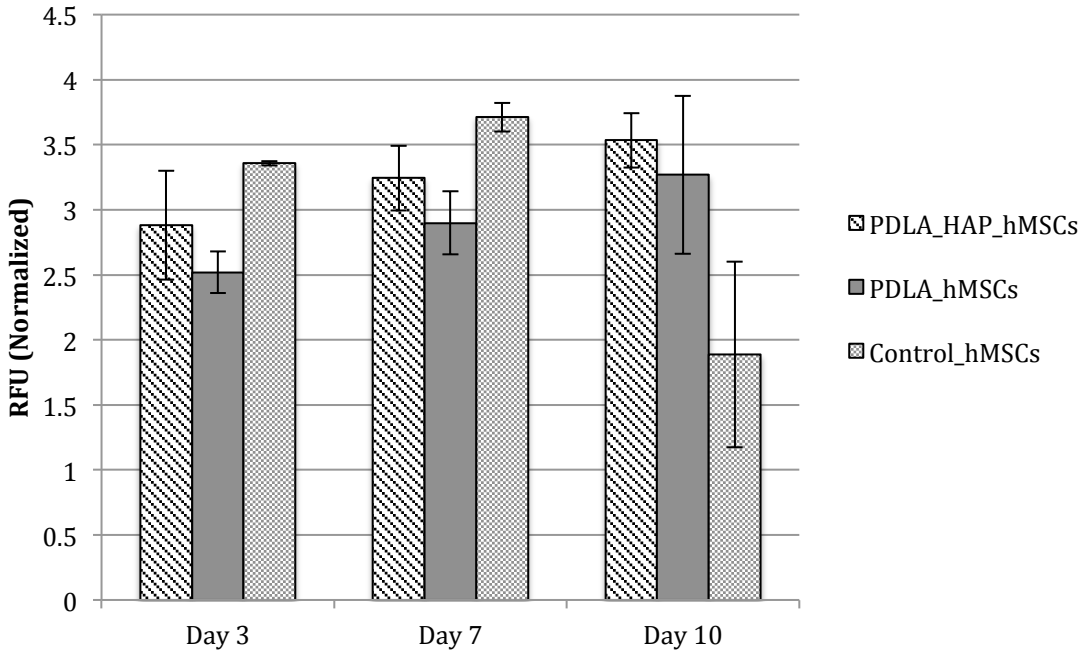

Figure 2.20. Metabolic activity indicates no statistically significant differences in cellular activity between groups up to 10 days.

To evaluate the scaffold's osteogenic potential over a shorter timespan than the previous study, the osteocalcin protein secretion was measured quantitatively using an ELISA kit. MC3T3-E1s were included as a group in this study as a comparison to normal osteoblastic behaviors. Media was also collected from a negative control scaffold (scaffold without cells) to verify the osteocalcin being measured was secreted from the cells and not artifacts of leached HAp. As seen in Figure 2.21, there was an increase in osteocalcin secretion from the hMSCs that were seeded on the control scaffold without HAp and the scaffold with HAp. The unexpected increase in the OC activity for the hMSCs seeded on the control scaffold may be due mechanotransduction in response to

the scaffold's stiffness and the mineral content deposited during the mineralization process. Furthermore, the addition of HAp in the scaffold led to a statistically significant increase in OC secretion from the hMSCs seeded on the scaffold with HAp at Day 10 in comparison to the cells seeded on the control scaffold. Many researchers have concluded OC binds to HAp crystal through gamma-carboxylation of three residues and has a high affinity for hydroxyapatite [41]. Therefore the cells responded to the HAp present in the scaffold, and began to secret an osteogenic protein.

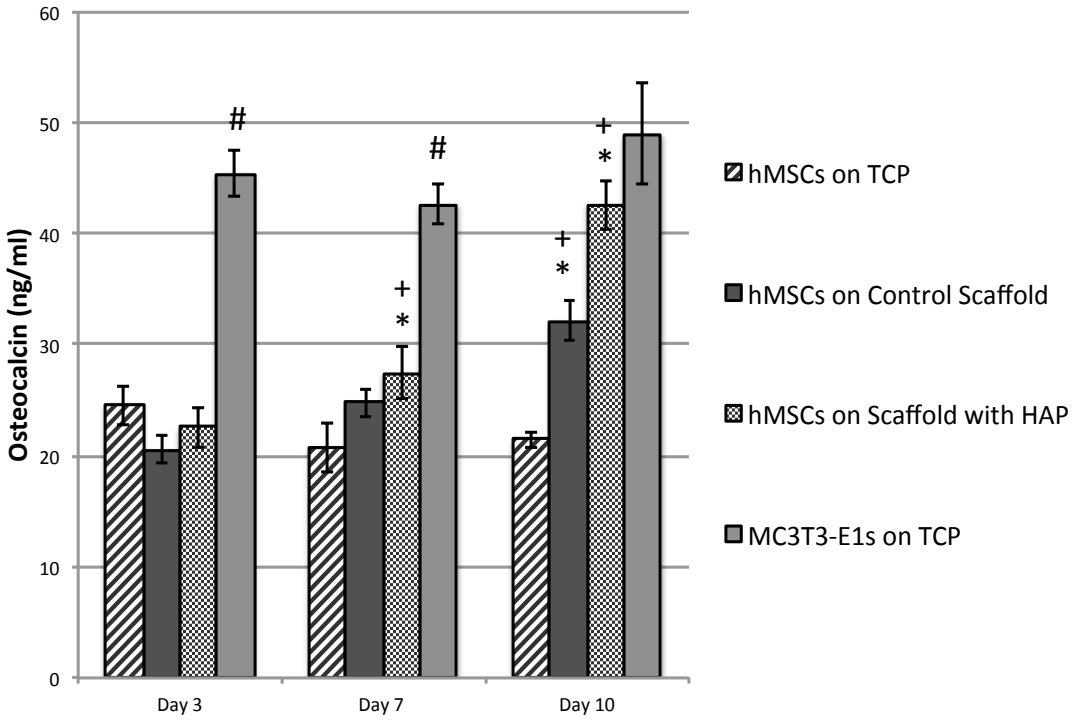

Figure 2.21. Osteocalcin secretion in serum measured at Day 3, 7, and 10 (N=6) . # $p<0.01$ compared to all other samples within the same time point. Statistical analysis via ANOVA Tukey Test (post-hoc): # $p<0.05$ compared samples from other groups at the same timepoint, * $p<0.05$ compared to hMSCs on TCP within the same time point, + $p<0.05$ compared to sample from the same group at a different time point.

Cells from each group were stained for ALP activity. Figure 2.22 qualitatively compares the red-stain indicating ALP at Day 3, 7 and 10. The intensity of the red color indicates an increase in ALP activity. As seen in the image, there is an increase in the ALP activity from the cells seeded on the PDLA_HAp scaffold on Day 3. The pink color expressed indicates differentiation of the hMSCs.

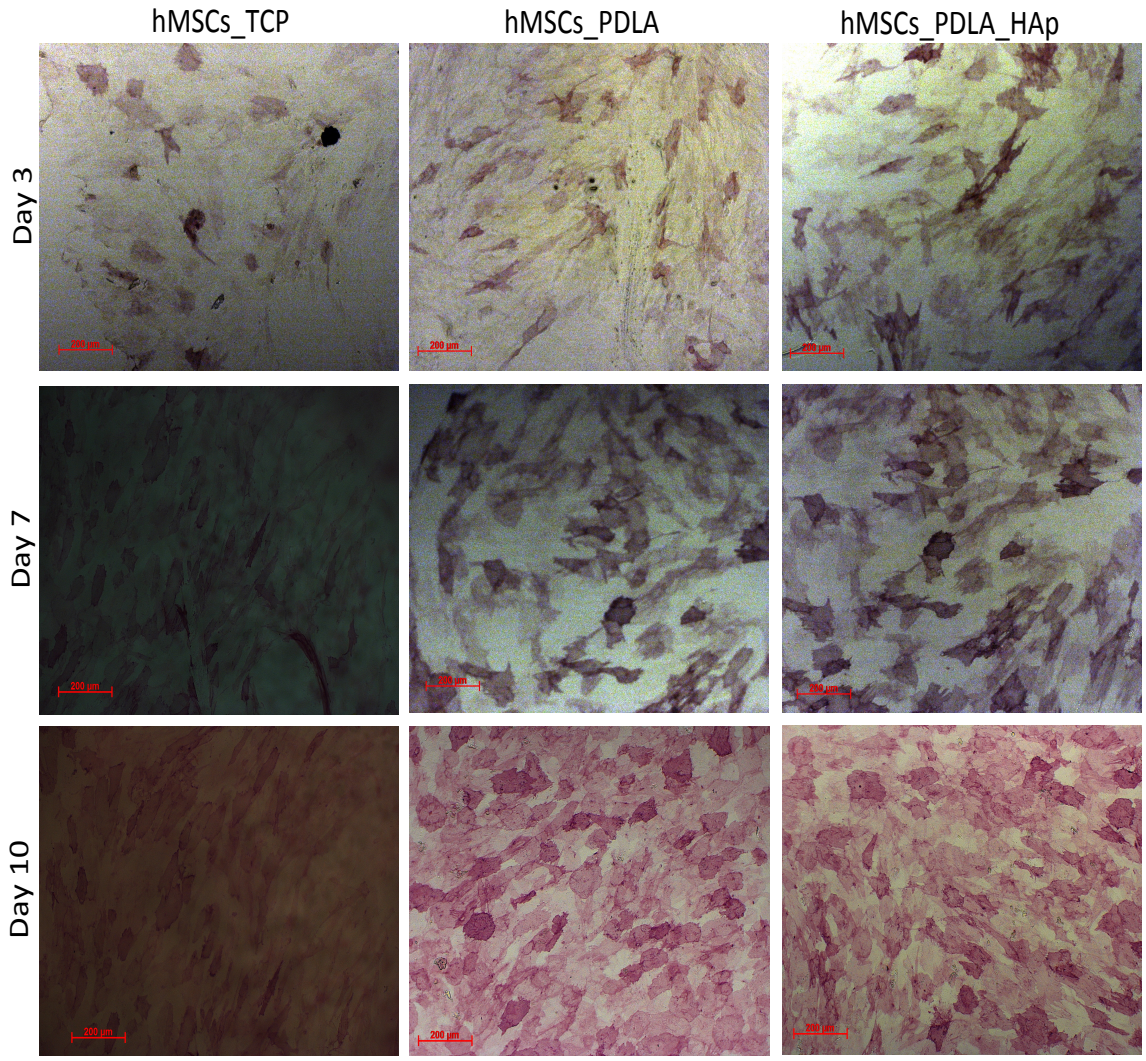

Figure 2.22. Representative images of ALP stain (red) of hMSCS seeded on TCP (hMSCs_TCP), PDLA scaffold without HAp (hMSCS_PDLA) and PDLA with HAp (hMSCs_PDLA_HAp). Scale bar = 200µm

The increase in ALP was verified quantitatively (Figure 23). There was no significant difference in the ALP activity between the two scaffold groups, but a statistically significant difference in ALP activity between the hMSCs seeded on the scaffolds and seeded on TCP. This could be due to the mineral content deposited on the PDLA and

PDLA_HAp scaffold also contributing to the scaffold's osteogenic potential. Additionally, ALP is an early marker for osteogenesis usually highly expressed within 3-7 days *in vitro* from cells seeded on ceramic-based substrates [28, 47]. Therefore, there is a slight decrease in ALP activity on Day 10, as seen in the normalized area and percent area of the ALP stain (Figure 2.23).

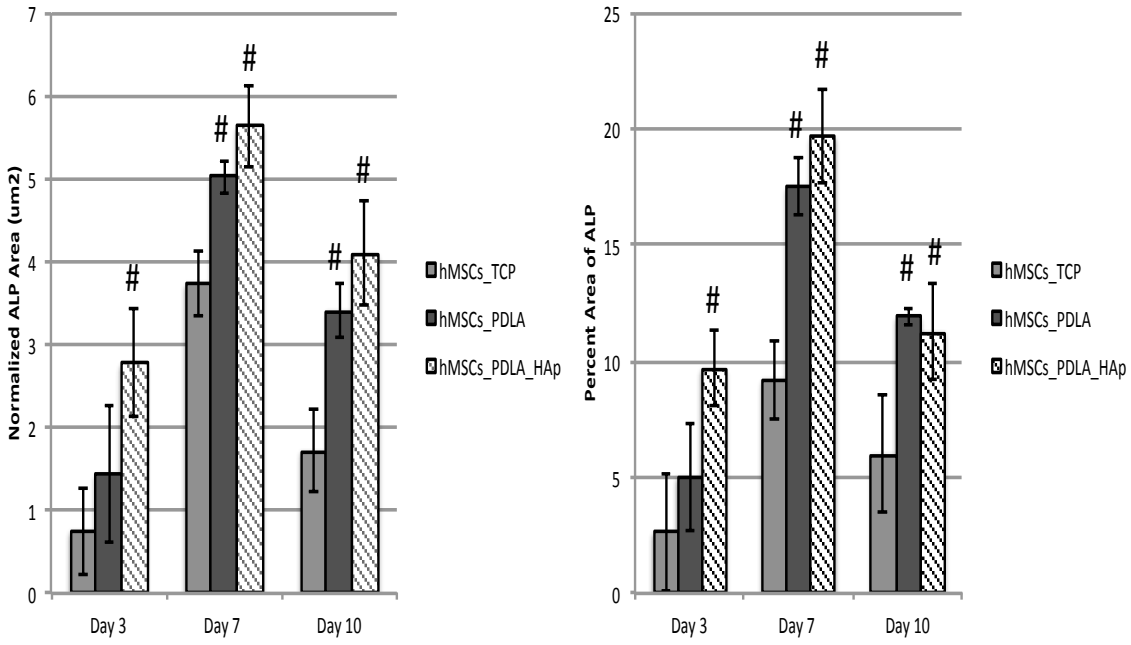

Figure 2.23. Normalized ALP Area (um^2 per substrate) and percent area of ALP. There was a statistically significant increase in ALP from the hMSCs seeded on the scaffold groups, hMSCs_PDLA and hMSCs_PDLA_HAp at Day 7 and Day 10 in comparison to the control. Statistical analysis: # denotes ANOVA Tukey Test (post-hoc) $p<0.05$ from the control (hMSCs_TCP).

2.4. Conclusion

The overall objective of the studies mentioned in this chapter was to develop and characterize a gelatin-synthetic porous osteoinductive scaffold for trabecular bone regeneration. Various processing techniques, crosslinking agents, and mineralization techniques were investigated to enhance the scaffold's mechanical strength and mineral content. We first investigated FDA approved crosslinking agents, glutaraldehyde, EDC, and mTG and their effect on mechanical properties of gelatin strips and electrospun scaffolds. mTG proved to be an optimal crosslinking technique in relation to mechanical behavior. Additionally, many researchers have demonstrated crosslinking with mTG to be a noncytotoxic and suitable process for *in vitro* purposes [48]. Qualitative and quantitative analysis proved successful incorporation of HAp nanopowder into the scaffold during electrospinning. Using a sintering, wrapping then leaching technique, we were able to maintain stable porous structures (5-200um). Developed pores are essential for cellular infiltration and nutrient transport. Electrodeposition mineralization resulted in mineral content three times greater than static mineralization. Incorporating additional gelatin into the scaffold using a novel co-electrospinning process also enhanced mineralization and mechanical strength. Furthermore, we concluded that scaffolds with angled fibers ranging from 15° to 45° exhibited greater mechanical strength. The angled fibers act as opposing vertical, horizontal, and inclined internal forces, which sum up to a higher total force being exert by the scaffold columns than the scaffolds with only vertical (90°) or horizontal fibers (0°). The processing techniques discussed in this work will be employed to develop TE scaffolds that mimic the porous mineralized structure seen with native trabecular bone.

Furthermore, the osteogenic potential of the scaffold with HAp was evaluated quantitatively and qualitatively by detecting the secretion and presence of non-collagenous bone matrix proteins, alkaline phosphate, calcium, and osteocalcin. The overall goal of this work is to develop a porous mineralized trabecular scaffold, which will be combined with a mechanically enhanced pre-vascularized cortical bone scaffold.

2.5. References

1. Hing, K.A., *Bone repair in the twenty-first century: biology, chemistry or engineering.* Philos Transact A Math Phys Eng Sci, 2004. **362**(1825): p. 2821-2850.
2. Wang, H., et al., *Biocompatibility and osteogenesis of biomimetic nano-hydroxyapatite/polyamide composite scaffolds for bone tissue engineering.* Biomaterials, 2007. **28**(22): p. 3338-48.
3. Rho, J.Y., L. Kuhn-Spearing, P. Zioupos, *Mechanical Properties and the hierachial structure of bone.* Medical Engineering and Physics, 1998. **20**(2): p. 12.
4. Wheeler, D.L., Enneking, W.F., *Allograft bone decreases in strength in vivo over time.* Clin Orthop Relat Res, 2005. **435**: p. 36-42.
5. Liu Y, W.G., de Groot K, *Biomimetic coatings for bone tissue engineering of critical-sized defects.* J R Soc Interface, 2010. **7**: p. S631-S647.
6. Taylor, B.L., Andric, T., Freeman, J.W., *Recent Advances in Bone Graft Technologies.* Recent Patents on Biomedical Engineering 2013. **6**(1): p. 1-7.
7. Bose, S., M. Roy, and A. Bandyopadhyay, *Recent advances in bone tissue engineering scaffolds.* Trends in biotechnology, 2012. **30**(10): p. 546-54.
8. Laurencin, C.T., Khan, Y et al, El-Amin, S.F., *Bone graft substitutes.* Expert Rev Med Devices, 2006. **3**(1): p. 49-57.
9. Orban, J.M., K.G. Marra, and J.O. Hollinger, *Composition Options for Tissue-Engineered Bone.* Tissue Engineering, 2002. **8**(4): p. 529-539.
10. Sell, S.A., et al., *The Use of Natural Polymers in Tissue Engineering: A Focus on Electrospun Extracellular Matrix Analogues.* Polymers, 2010. **2**(4): p. 522-553.
11. Song, J.H., H.E. Kim, and H.W. Kim, *Production of electrospun gelatin nanofiber by water-based co-solvent approach.* Journal of materials science. Materials in medicine, 2008. **19**(1): p. 95-102.
12. Sell, S.A., et al., *Electrospinning of collagen/biopolymers for regenerative medicine and cardiovascular tissue engineering.* Advanced Drug Delivery Reviews, 2009. **61**(12): p. 1007-1019.
13. Sisson, K., et al., *Evaluation of Cross-Linking Methods for Electrospun Gelatin on Cell Growth and Viability.* Biomacromolecules, 2009. **10**(7): p. 1675-1680.

14. Panzavolta, S., et al., *Electrospun gelatin nanofibers: optimization of genipin cross-linking to preserve fiber morphology after exposure to water.* Acta biomaterialia, 2011. **7**(4): p. 1702-9.
15. Landis, W.J., *The strength of a calcified tissue depends in part on the molecular structure and organization of its constituent mineral crystals in their organic matrix.* Bone, 1995. **16**(5): p. 533-544.
16. Andric T, W.L., Freeman JW, *Rapid Mineralization of Electrospun Scaffolds for Bone Tissue Engineering.* Journal of Biomaterials Science, Polymer Edition, 2011. **22**(11): p. 1535-50.
17. Middleton, J.C. and A.J. Tipton, *Synthetic biodegradable polymers as orthopedic devices.* Biomaterials, 2000. **21**(23): p. 2335-2346.
18. Balasundaram, G. and T.J. Webster, *An overview of nano-polymers for orthopedic applications.* Macromolecular bioscience, 2007. **7**(5): p. 635-642.
19. Huang-Lee, L.L.H., D.T. Cheung, and M.E. Nimni, *Biochemical changes and cytotoxicity associated with the degradation of polymeric glutaraldehyde derived crosslinks.* Journal of Biomedical Materials Research, 1990. **24**(9): p. 1185-1201.
20. Barnes, C.P., et al., *Cross-Linking Electrospun Type II Collagen Tissue Engineering Scaffolds with Carbodiimide in Ethanol.* Tissue Engineering, 2007. **13**(7): p. 1593-1605.
21. Kuwahara K, Y.X., Slack GC, Nimni ME, Han B, *Cell delivery using injectable and adhesive transglutaminase-gelatin gel.* Tissue Eng Part C Meth, 2010. **16**(4): p. 609-618.
22. Fuchs S, K.M., Hertel T, Winter G, Pietzsch, Coester C, *Transglutaminase: new insights into gelatin nanoparticles crosslinking.* J Microencapsul, 2010. **27**(8): p. 747-754.
23. Zhang, Y.Z., et al., *Crosslinking of the electrospun gelatin nanofibers.* Polymer, 2006. **47**(8): p. 2911-2917.
24. Yung, C.W., et al., *Transglutaminase crosslinked gelatin as a tissue engineering scaffold.* Journal of Biomedical Materials Research Part A, 2007. **83A**(4): p. 1039-1046.
25. Bhardwaj, N. and S.C. Kundu, *Electrospinning: A fascinating fiber fabrication technique.* Biotechnology Advances, 2010. **28**(3): p. 325-347.
26. Wright, L.D., T. Andric, and J.W. Freeman, *Utilizing NaCl to increase the porosity of electrospun materials.* Materials Science and Engineering: C, 2011. **31**(1): p. 30-36.
27. Wright, L.D., et al., *Fabrication and mechanical characterization of 3D electrospun scaffolds for tissue engineering.* Biomed. Mater., 2010. **5**(5): p. 055006.
28. Ohgushi, H., et al., *Osteogenic differentiation of marrow stromal stem cells in porous hydroxyapatite ceramics.* Journal of Biomedical Materials Research, 1993. **27**(11): p. 1401-1407.
29. McDermott, M.K., et al., *Mechanical Properties of Biomimetic Tissue Adhesive Based on the Microbial Transglutaminase-Catalyzed Crosslinking of Gelatin.* Biomacromolecules, 2004. **5**(4): p. 1270-1279.
30. Chen, T., et al., *Enzyme-catalyzed gel formation of gelatin and chitosan: potential for in situ applications.* Biomaterials, 2003. **24**(17): p. 2831-2841.

31. Andric, T., et al., *Fabrication and characterization of three-dimensional electrospun scaffolds for bone tissue engineering.* Journal of biomedical materials research. Part A, 2012. **100**(8): p. 2097-105.
32. He, C., et al., *Electrodeposition on Nanofibrous Polymer Scaffolds: Rapid Mineralization, Tunable Calcium Phosphate Composition and Topography.* Adv. Funct. Mater., 2010. **20**(20): p. 3568-3576.
33. He C, J.X., Ma PX, *Calcium phosphate deposition rate, structure and osteoconductivity on electrospun poly(l-lactic acid) matrix using electrodeposition or simulated body fluid incubation.* Acta biomaterialia, 2014. **10**(1): p. 419-27.
34. Bancroft, G.N., et al., *Fluid flow increases mineralized matrix deposition in 3D perfusion culture of marrow stromal osteoblasts in a dose-dependent manner.* Proceedings of the National Academy of Sciences, 2002. **99**(20): p. 12600-12605.
35. He, C., et al., *Electrodeposition on Nanofibrous Polymer Scaffolds: Rapid Mineralization, Tunable Calcium Phosphate Composition and Topography.* Advanced Functional Materials, 2010. **20**(20): p. 3568-3576.
36. Xion Lu, Y.L., Qiyi Zhang, *Electrochemical deposition of octacalcium phosphate micro-fiber/chitosan composite coatings on titanium substrates.* Surface and Coatings Technology, 2008. **202**(13): p. 3142-3147.
37. Shaolin Chen, W.L., Zhijuan Huang, Xiaoguang Liu, Qiyi Zhang, Xiong Lu, *The stimulation of the electrochemical cathodic Ca-P depostion process.* Materials Science and Engineering, C: Materials for Bioligcal Applications, 2009. **29**(1): p. 108-114.
38. Jalota, S., S.B. Bhaduri, and A.C. Tas, *Effect of carbonate content and buffer type on calcium -phosphate formation in SBF solutions.* Journal of materials science. Materials in medicine, 2005. **17**: p. 696-707.
39. Jalota, S., S.B. Bhaduri, and A.C. Tas, *Using a synthetic body fluid (SBF) solution of 27 mM HCO3− to make bone substitutes more osteointegrative.* Materials Science and Engineering: C, 2008. **28**(1): p. 129-140.
40. Samineni, S., C. Glackin, and J.E. Shively, *Role of CEACAM1, ECM, and Mesenchymal Stem Cells in an Orthotopic Model of Human Breast Cancer.* International Journal of Breast Cancer, 2010. **2011**: p. 1-11.
41. Wada S, F.T., Kamiya S, *Osteocalcin and Bone.* Clinical Calcium, 2007. **17**(11): p. 5.
42. Motoki, M., et al., *Glutamine-specific deamidation of .ALPHA.S1-casein by transglutaminase.* Agricultural and Biological Chemistry, 1986. **50**(12): p. 3025-3030.
43. Sarkar, N.K., D.D. Clarke, and H. Waelsch, *An enzymically catalyzed incorporation of amines into proteins.* Biochimica et Biophysica Acta, 1957. **25**: p. 451-452.
44. Clarke DD, M.M., Neidle A, Waelsch H, *The incorporation of amines into protein.* Arch Biochem Biophys, 1959. **79**: p. 338-354.
45. Yung, C.W., et al., *Transglutaminase crosslinked gelatin as a tissue engineering scaffold.* Journal of biomedical materials research. Part A, 2007. **83**(4): p. 1039-46.

46. Allen, E. and W. Zalewski, *Form and Forces: Designing Efficient, Expressive Structures*. 2009: John WIley & Sons.
47. Müller, P., et al., *Calcium phosphate surfaces promote osteogenic differentiation of mesenchymal stem cells.* Journal of Cellular and Molecular Medicine, 2008. **12**(1): p. 281-291.
48. Chen, P.-Y., et al., *Fabrication of large perfusable macroporous cell-laden hydrogel scaffolds using microbial transglutaminase.* Acta Biomaterialia, 2014. **10**(2): p. 912-920.

CHAPTER 3: THE DEVELOPMENT AND *IN VITRO* CHARACTERIZATION OF A PRE-VASCULARIZED CORTICAL SCAFFOLD

3.1. Introduction

Cortical bone is the dense bone type that provides whole bone with its structural integrity. The high compressive properties of cortical bone are due to the highly packed arrangement of cylindrical subunits called osteons. Osteons are hollow structures composed of concentric collagen layers with a hollow canal, known as the Haversian canal. Blood vessels and nerves are housed within this canal. Neovascularization sprouts out from the Haversian canal to the surrounding bone through the Volkmann's canals [1]. This intricate network is vital for bone remodeling and necessary for blood and nutrient transport. Research has shown the development and maturation of bone is coupled with the process of new blood vessel formation, or angiogenesis [2, 3]. For example, non-healing or damaged bone consists of large three-dimensional regions with locally hypoxic environments that lack initial vascularization [4].

Many tissue-engineered (TE) grafts that aim to regenerate bone lack the necessary vascularization for long-term graft integration and viability. Recent vascularization approaches in bone regeneration are largely aimed at promoting early vascularization using the delivery of pro-angiogenic growth factors, stem cells, or pre-vascularization of tissue engineered constructs. While the use of growth factors to promote angiogenesis has shown success *in vitro* and in *vivo*, there is a lack information about the dose to effect ratio and the timing of delivery [4] . Stem cell based therapies are a promising alternative for bone regeneration by increasing vascularized bone formation *in vivo* when co-cultured with endothelial cells [4-6]. Nonetheless, the timing at which specific cell types

are added to the system is a sensitive parameter and play a vital role in vessel development. Furthermore, without a stable structure, vascular networks developed *in vivo* can collapse or display reduced vascular permeability [4] . To address the issues seen with bone vascularization induced by growth factor delivery and co-culture cell therapies, I introduce a neovascularization-inducing three-dimensional scaffold that has the ability to promote differentiation of human bone marrow-derived stem cells (hMSCs) into vascular endothelial cells without added growth factors.

The work presented in this chapter focuses on the development and evaluation of a biomimetic cortical scaffold with concentrically electrospun polymeric-gelatin based fibers to mimic the native osteon structure. I hypothesized the fabricated cylindrical osteon structure will promote circumferential development of endothelial cells into a vascular pro-angiogenic lumen that would provide pro-angiogenic proteins after decellularization. The rationale for this study is to promote the angiogenic differentiation of the stem cells within a stable biomimetic construct. To test our hypothesis, we evaluated the effect of the three-dimensional scaffold structure and composition on endothelial cell proliferation and morphology, validated our decellularization method, and investigated the ability of the decellularized cortical scaffold to induce stem cell differentiation along the vascular endothelial lineage *in vitro*.

3.2. Materials and Methods

PLLA (MW = 152,000) and polyethylene oxide (PEO) (MW=200,000) were purchased from Sigma Aldrich (St. Louis, MO, USA). PDLA (MW=124,000) was purchased from Evonik Birmingham Laboratories (Birmingham, AL, USA). Solvents

dichloromethane (DCM), dimethylformaldehyde (DMF), tetrahydrofuran (THF), and 100% ethanol (EtOH) were purchased from Fisher Scientific (Pittsburgh, PA, USA). PLLA and PDLA were chosen based on their material properties, which are suitable for TE applications. Gelatin, from porcine skin, was purchased from Sigma Aldrich (St. Louis, MO, USA) and included in the scaffold to increase the collagen content and cellular attachment.

3.2.1. Electrospinning the Cortical Scaffold

The base electrospinning solutions were prepared by dissolving PLLA (7% w/v) in DCM and DMF with 10% gelatin and PDLA (22w/v%) in DMF and THF. PEO (10% w/v) solution was prepared by dissolving PEO (10%w/v) in deionized water (dI H_20) and 100% EtOH l. A 5ml syringe with an 18-gauge blunt needle attachment was used to electrospin all the solutions. To create the PEO scaffold, 5ml of the PEO solution was electrospun onto an 8cm diameter rotating aluminum mandrel (~ 2000 RPM) at working distance of 10cm, pump rate 5ml/hr, with +15kV/-11kV voltages. The PEO scaffold was then cut into 7 mm strips. A PLLA scaffold (no gelatin or PDLA) was also electrospun onto the rotating mandrel (working distance = 10cm, voltages =15kV/-10kV, pump rate = 5ml/hr). The PLLA mat was cut into 5 mm strips. The PEO and PLLA strips were then manually twisted together to create a PEO/PLLA twist. The PEO/PLLA twist was then loaded into a rotating device and rotated clockwise while 3mL of PEO was electrospun onto the twist (Fig. 3.1). Then 1.5ml of PLLA followed by .5ml of PDLA was electrospun onto the PEO coated PEO/PLLA twist. All the solutions were electrospun at a working distance of 10cm and extrusion rate of 5ml/hr. The working distance was varied between 7 to 15 cm depending on the polymer and environment conditions.

PDLA was used as the sintering polymer to bind the individual cortical scaffolds together. After electrospinning, the scaffolds were placed into a desiccator to remove any residuals solvents. The next day, the cortical scaffolds were exposed to vapor 25mM glutaraldehyde crosslinking and placed in a desiccator under vacuum to draw out any residual glutaraldehyde. Scaffolds (n=3) were dried overnight and sputter coated with gold and palladium for SEM imaging and qualitative analysis.

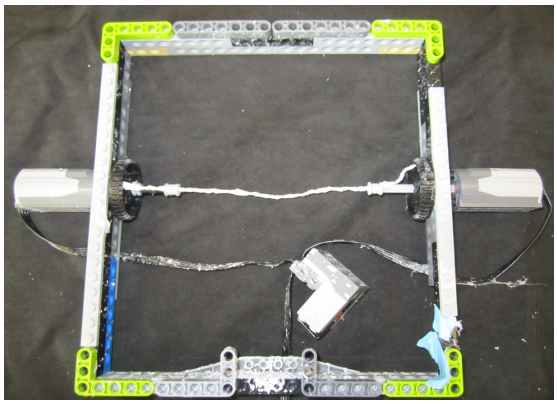

Figure 3.1. Rotating device used to rotate the PEO/PLLA twist.

3.2.2. *In Vitro* Study I: Biocompatibility testing using Human Microvascular Endothelial Cells

The purpose of this study was to test the biocompatibility and interaction of the cortical scaffold with endothelial cells. We used immortalized Human Microvascular Endothelial Cells (HMECs) derived from human foreskin, pulmonary and hepatic endothelium (gifted from Dr. Nicole Rylander's Laboratory at Virginia Tech, VA). HMECs are the primary cell type involved in the development of small vessels and undergo rapid morphological differentiation *in vitro* into capillary-like structures [7-9]. The cells (passage 5) were maintained in MCDB 131 Medium (no glutamine) purchased from Life Technologies (Grand Island, NY, USA), supplemented with 10% FBS and 1%

penicillin streptomycin. HMECs were seeded onto 2D PDLA_PLLA/10%Gel scaffolds at 7,000 cells per substrate. The experimental groups (n=3) were non-mineralized scaffolds (PDLA_PLLA/10%Gel) and scaffolds that were mineralized for 7 days via static mineralization (PDLA_PLLA/10%Gel_Min). We chose these two groups to determine the interaction between endothelial cell activity and mineral content. Many researchers have reported the positive and negative effects of endothelial cell protein secretion on stem cell mineral deposition, but there is limited data on the effects of mineral content on endothelial cell activity [2, 10-14]. The information from this study was crucial in determining the effect of the mineral content and hydroxyapatite in the trabecular scaffold (see Chapter 2) on the development of an endothelial lumen in the cortical scaffold. The control scaffold was a PDLA_PLLA/10%Gel scaffold without cells as a comparison. All substrates were adhered to the well plate with sterile silicone glue and sterilized using 70% ethanol and UV radiation. Substrates were also pre-conditioned with media for 24 hours prior to cell seeding to enhance the hydrophobicity of the scaffold and create a favorable environment for the cells. Cellular viability was indirectly measured over 28 days using Pierce™ BCA Protein Assay Kit. Bicinchoninic acid *(*BCA) protein assays measures total secreted protein in serum. The scaffolds were also stained for collagen using Masson's trichrome stain and quantitatively measured for biocompatibility comparison. The amount of collagen deposited by the HMECs on the scaffold was compared to determine the effect of mineral content on cellular behavior.

3.2.3. *In Vitro* Study II: Developing a Circumferential Endothelial Lumen

The purpose of the study was to evaluate the effect of the scaffold architecture on the cellular growth. We hypothesized the cylindrical 3D cortical scaffold architecture

would promote circumferential cellular growth and lead to the development of an endothelial lumen. To test this hypothesis, we used human umbilical vein endothelial cells (HUVECs). The HUVECs were gifted from Sofou Lab (Rutgers University, NJ). HUVECs are a robust cell line commonly used *in vitro* studies as a model for vasculature physiology and development and has been shown to have a positive influence on bone regeneration [10, 14-16]. The experimental groups were 2D (PDLA_PLLA/10%Gel_2D) and 3D cortical scaffolds(PDLA_PLLA/10%Gel_3D) developed according to section 3.2.1. The control group was HUVECs seeded on TCP. All substrates were sterilized via 70% EtOH soak and UV radiation and pre-conditioned with media for 24 hours prior to cell seeding. The HUVECs (passage 5) were maintained in endothelial growth basal medium (EGM) supplemented with 10% FBS, 2% human fibroblast growth factor (hFGF), 0.02% hydrocortisone, 0.05%vascular endothelial growth factor (VEGF), 0.05% recombinant-3 insulin growth factor (R3-IGF), 0.05% ascorbic acid, 0.05% human endothelial growth factor (hEGF), 0.05% GA-100, and 0.05% heparin (media kit purchased from Lonza, Inc, Allendale, NJ, USA). HUVECs were seeded inside the hollow canal of the 3D cortical scaffolds (10,000 cells per substrate) using a sterile 1ml syringe with a 25-gauge needle tip.

Qualitative analysis was performed to track and evaluate the endothelial cellular growth over 28 days. We performed fluorescent confocal imaging of the phalloidin and DAPI at 7, 14, 21, and 28 days (n=3). The scaffolds were also sliced into 100 μm cross-sectional slices using a cryotome and SEM imaged for morphological analysis. The cross-sectional slices (n=3) were also stained for collagen using Picosirious Red Stain Kit (Polysciences, Inc). The kit also stains yellow and green for collagen type I

type III.

3.2.4. *In Vitro* Study III: Developing and Characterizing a Decellularized Pro-Angiogenic Cortical Scaffold

The objective of this study was to create a decellularized cortical scaffold to promote the differentiation of human bone marrow derived stem cells (hMSCs) along the vascular endothelial lineage. The rationale for this study was to form an endothelial matrix within the osteonic structure by allowing endothelial cells to secret pro-angiogenic factors, and then decellularize the matrix to remove the cells and intercellular content. We hypothesized the remaining pre-vascularized matrix would promote the angiogenic differentiation of hMSCs.

Two-dimensional PDLA_PLLA/10%Gel scaffolds were used for this study. The cells (passage 5) were maintained in Ham's F-12K (Kaighn's) Medium (purchased from Fisher Scientific Co., Suwanee, GA, USA), supplemented with 10% FBS, 2% penicillin streptomycin (P/S), 100μg/ml heparin, 30μg/ml Endothelial cell growth supplement (all purchased from Sigma Aldrich, Atlanta, GA, USA. The scaffolds were attached to well plates with sterile silicone glue, sterilized via UV radiation and pre-conditioned with media for 24 hours prior to cell seeding. The HUVECs were seeding on the scaffolds at 25,000 cells per scaffold.

At Day 14 of post-seeding, PrestoBlue® and Chondrex assays were performed for an indirect measure of cellular viability and to measure the presence of collagen/non-collagenous proteins, respectively (n=3). The positive controls were HUVECs seeded on TCP and the negative controls were the PDLA_PLLA/10%Gel scaffold without cells. The substrates were then decellularized using an FDA approved

freeze-thaw method that has shown success in similar studies [17, 18]. The well plates with the substrates and cells were submerged in a Styrofoam container of liquid nitrogen for 10 minutes and then submerged into a water bath maintained at 37°C for 10 minutes. The substrates were then washed with sterile phosphate buffer saline (PBS) to remove any cell debris. This process was repeated for three cycles. Decellularized substrates (n=3) were analyzed quantitatively for cellular viability and collagen deposition and fluorescently stained for qualitative analysis. This data was compared to the non-decellularized scaffolds (n=3) to determine the efficacy of the decellularization method. The remaining decellularized scaffolds were conditioned with media overnight for hMSCs seeding. The hMSCs (passage 8) were maintained and expanded in Alpha-Modified Minimum Essential Media (α-MEM) supplemented with 10% fetal bovine serum (FBS) and 1% penicillin streptomycin for 1 week prior to seeding. Cells were seeded at 25,00 cells per substrate. The positive control group were PDLA_PLLA/10%Gel scaffolds that were not previously seeded with cells, the negative controls were hMSCs seeded on a TCP, and the experimental group was the decellularized PDLA_PLLA/10%Gel scaffolds. Cellular viability and collagen deposition was assessed at Day 7. The presence of secreted vascular endothelial growth factor (VEGF) expressed by the hMSCs was evaluated qualitatively via immunohistochemistry (IHC) and quantitatively with ELISA (n=3) (novex by Life Technologies VEGF ELISA kit, USA). VEGF is the primary protein active in early angiogenesis and has been shown to play a significant role in bone regeneration [16, 19, 20]. Cellular morphology was also evaluated using fluorescence microscopy for actin (cytoskeleton) and DAP (nucleus. The vascularization formation was quantified using

ImageJ software by measuring the lumen areas.

3.2.5. Statistical Analysis

Statistical analysis was performed using KaleidaGraph Synergy Software. All data was subjected to an one-way analysis of variance (ANOVA) with post-hoc analysis (Tukey test) to determine the statistical significance of differences between groups, $p < 0.05$.

3.3. Results & Discussion

3.3.1. SEM Analysis of Scaffold Fabrication

SEM images of the cortical scaffold confirmed the ability to replicate the cylindrical structure of native osteon using electrospinning (Fig. 3.2). Figure 3.2A is the fabricated osteon with the inner PEO/PLLA fiber twist and Figure 3.3B after the PEO/PLLA twist is removed. As seen in this image, the cylindrical structure with the hollow center was maintained. The fibers are also oriented concentrically similar to the native osteon collagen fiber formation, Figure 3.2C.

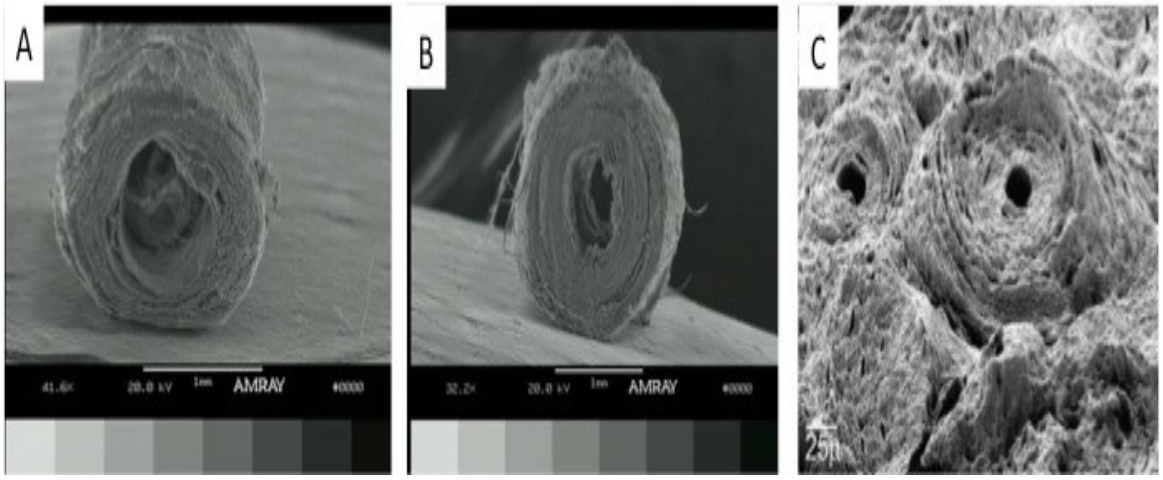

Figure 3.2. SEM image (scale bar = 1 mm) of the fabricated osteon scaffold (A) with the PEO/PLLA fiber twist, (B) after the PEO/PLLA twist was removed to yield a structure that mimics (C) native osteons structure (scale bar = 25µm).

3.3.2. *In Vitro* Study I Results: Biocompatibility Testing using Human Microvascular Endothelial Cells

BCA protein assay was performed on the HMECs seeded on the 2D PDLA_PLLA/10%Gel mineralized and non-mineralized scaffolds, Figure 3.3. HMECS seeded on the non-mineralized and mineralized scaffold had higher levels of protein activity than the HMECs seeded on TCP up to Day 21. This suggests the fibrous network provides a favorable environment for the endothelial cells. At Day 21, cellular viability was significantly greater for the cells seeded on the scaffolds than on the TCP. At Day 28, there was a decrease in cellular viability witnessed with all the groups. This could be due to over confluency of the cells leading to cellular contact and protein activity inhibition.

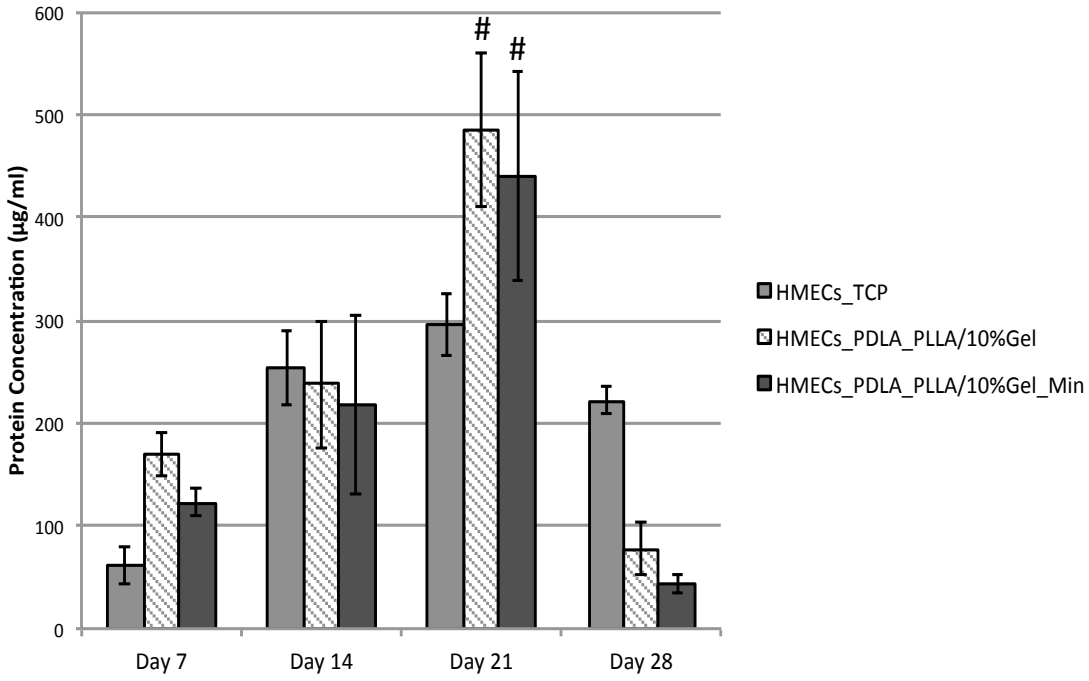

Figure 3.3. Protein activity of HMECs on the control (HMECs_TCP), non-mineralized (PDLA_PLLA/10%Gel) and mineralized (PDLA_PLLA/10%Gel_Min) scaffolds. Statistical analysis: # denotes ANOVA Tukey Test (post-hoc) $p < 0.05$ in comparison to the control scaffold at Day 21.

As seen from BCA assay results in Figure 3.3, there is greater protein activity from the HMECs seeded on the non-mineralized scaffolds (PDLA_PLLA/10%Gel) than the cells seeded on the mineralized scaffolds (PDLA_PLLA/10%Gel_Min). This trend was also seen with collagen deposition measured using Masson's trichrome stain at Day 28 (Fig. 3.4). The red hue is directly related to the amount of collagen content. The non-mineralized scaffolds were darker red than the mineralized scaffold, suggesting a higher cellular proliferation on the non-mineralized scaffolds. The mineralized scaffolds have a rougher surface due to the deposited crystals. Research shows endothelial cells prefer

smooth surfaces and therefore the HMECs did not proliferate as well on the rough mineralized scaffolds. The data in this study evaluated endothelial cell activity on non-mineralized and mineralized scaffolds.

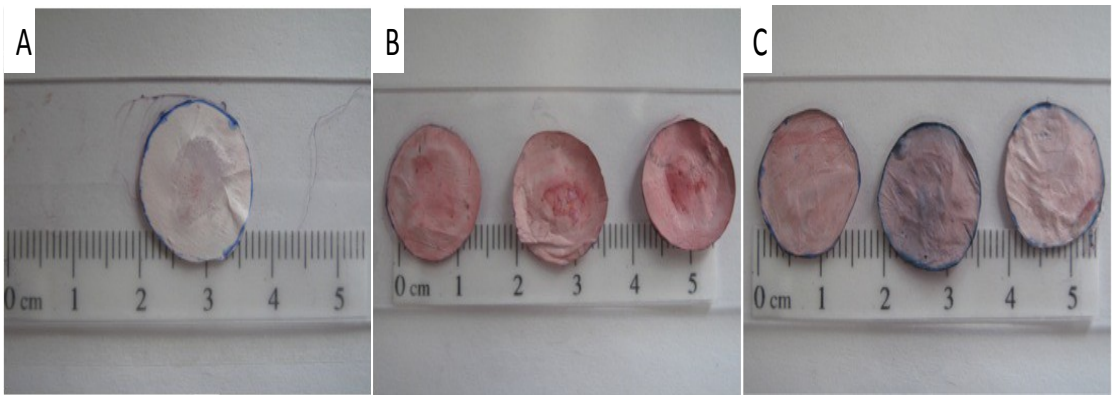

Figure 3.4. Masson's Trichrome (cytoplasmic) stain of the control scaffold (A), non-mineralized (PDLA_PLLA/10%Gel) scaffolds (B), and mineralized (PDLA_PLLA/10%Gel_Min) scaffolds (C) at Day 28.

3.3.3. *In Vitro* Study II Results: Developing a Circumferential Endothelial Lumen

Endothelial growth in response to the scaffolds' architecture and fiber orientation was evaluated using HUVECs. Figure 3.5 is a collection of the fluorescent confocal images of the HUVECs on TCP, on a 2D scaffold (PDLA_PLLA/10%Gel_2D), and within the cortical scaffold (PDLA_PLLA/10%Gel_3D). Figures 3.5A and 3.5D are the HUVECs at Day 14 on TCP. The HUVECs are attached to the TCP with a spread out morphology. The cells on TCP appear to be growing and elongating in random directions. Figures 3.5B and 3.5E are the HUVECs seeded on the 2D scaffold. The HUVECs cytoskeleton morphology is similar to the cells seeded on TCP. Figures 3.5C

and 3.5F are the HUVECs seeded within the 3D cortical scaffold. Figure 3.5C is the same image taken at 10X. The HUVECs in this image are oriented diagonally from the lower left corner to the upper right corner. The scaffold was orientated in the same direction. Figure 3.5F shows the cells beginning to elongate in the direction of the osteon canal. Cross- sectional slices of the three-dimensional scaffold stained with phalloidin and DAPI also demonstrated the ability of the cells to attach to the inner lumen, Figure 3.6. Z-stack images of the 3D scaffold were also taken and compiled into a movie. The movie shows slices taken in the x-plane going from bottom to top in the y-direction and the location of the endothelial cells. The movie further suggests circumferential endothelial growth due to the scaffold architecture and cellular infiltration in the nanofibrous structure.

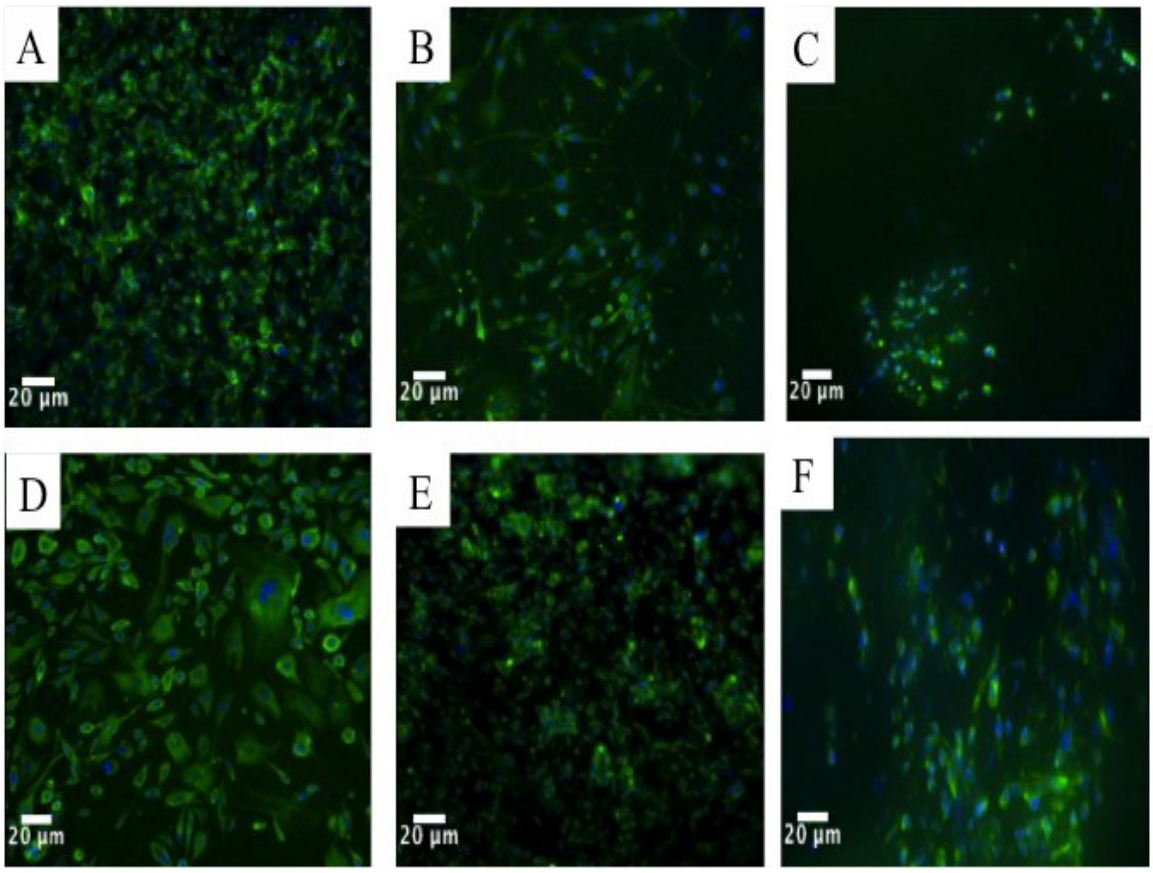

Figure 3.5. Fluorescent confocal images of HUVECs on TCP, 2D and 3D cortical scaffold (blue = nucleus, green = cytoskeleton). A.) Widefield image (10x) of HUVECs on TCP at Day 7, B.) Confocal image (10x) of HUVECS on PDLA_PLLA/10%Gel_2D scaffold at Day 7, C.) Confocal image (10x) of HUVECS on PDLA_PLLA/10%Gel_3D scaffold at Day 7 (top view), D.) Widefield Image (10x) of HUVECS on TCP at Day 14, E.) Confocal image (10x) of HUVECs on PDLA_PLLA/10%Gel_2D scaffold at Day 14, F.) Confocal image (top view) of HUVECs on PDLA_PLLA/10%Gel_3D at Day 14 (40x)

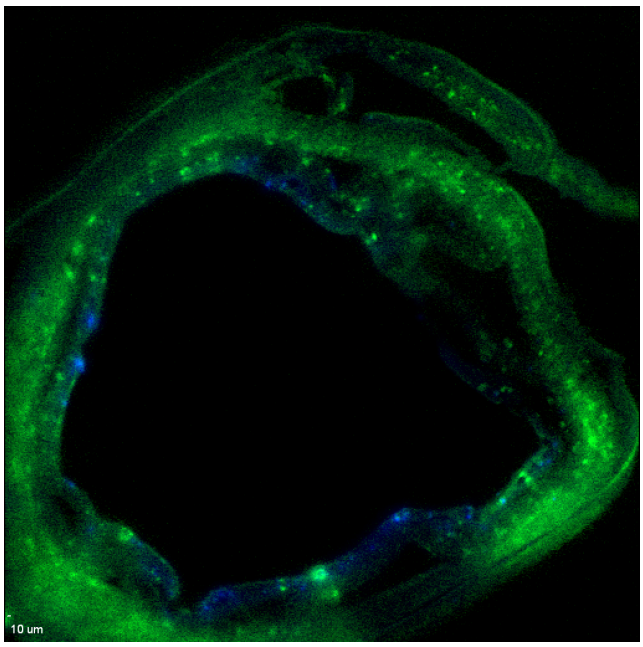

Figure 3.6. Cross-sectional image of HUVECS seeded on the PDLA_PLLA/10%Gel_3D scaffold stained with phalloidin (green) for actin and DAPI (blue) for nucleus (Scale bar = 10μm).

The PDLA_PLLA/10%Gel cortical scaffold (osteon) was also SEM imaged at Day 14, Figure 3.7A. The images suggest development of an endothelial lumen within the cortical structure. This endothelial lumen is developed by the HUVECS. The lumen was further characterized using Picosirous stain for collagen types I and III. Collagenous structures results in a bright red stain bright whereas collagen type I and type III will stain yellow and green, respectively. An orange color indicates a mix of collagen (types outside of I and III) and collagen type I. An overlap in the collagen (red) and collagen type III (green) stains would result in grey. The orange color of the scaffold, Figure 3.7B, is a mix of the denatured collagen in the scaffold due to the addition of the 10% bovine gelatin (red) and

collagen type I (yellow). Collagen type I is an extracellular matrix protein that is essential for many extracellular matrix-dependent cell functions, such as cell migration and proliferation. Moreover, collagen I is a major protein present in the endothelial wall of the blood vessels [21-23].

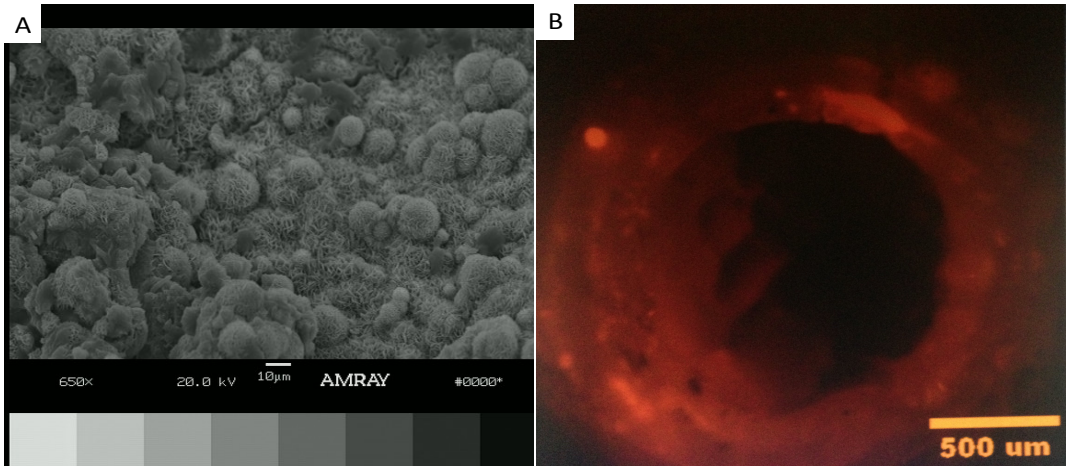

Figure 3.7. A.) SEM image of the inner canal of the fabricated osteon at Day 14 of HUVECs *in vitro* (scale bar = 10µm), B.) Collagen matrix stain indicates collagen network (red) and presence of collage type I (yellow) (scale bar = 500µm).

3.3.4. *In Vitro* Study III: Developing and Characterizing a Decellularized Cortical Scaffold

In this study, PDLA_PLLA/10%Gel scaffolds were seeded with HUVECs and then decellularized using a freeze-thaw method at Day 14. Figure 3.8 shows the presence of HUVECs nuclei stained with DAPI before (left) and after (right) decellularization. Qualitatively, there is a significant decreased in cellular viability after decellularization.

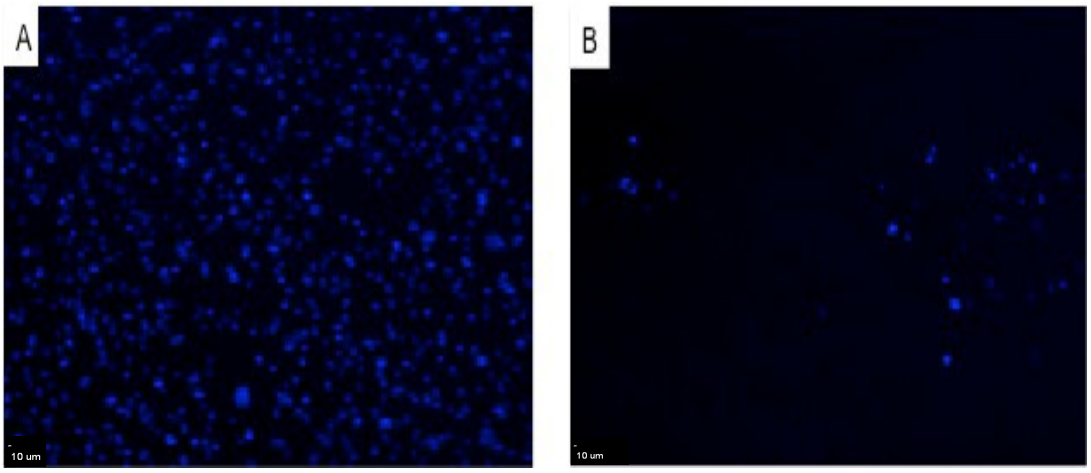

Figure 3.8. Fluorescent DAPI images of HUVECs nuclei on PDLA_PLLA/10%Gel scaffolds (A) before and (B) after decellularization indicate a significant decrease in cellular viability after decellularization (scale bar = 10μm).

To further validate the freeze-thaw decellularization method, metabolic activity and collagen deposition of the HUVECs was evaluated before and after decellularization using a PrestoBlue® and Chondrex assay. As seen in Figure 3.9, there is an 86% decrease in cellular viability due to the decellularization method. Even through the cellular viability decreased, 96% of the collagenous/non-collagenous matrix was maintained post decellularization. The preservation of this protein matrix is essential for promoting the differentiation of the hMSCs into vascular endothelial cells. This data supports the efficacy of our decellularization technique.

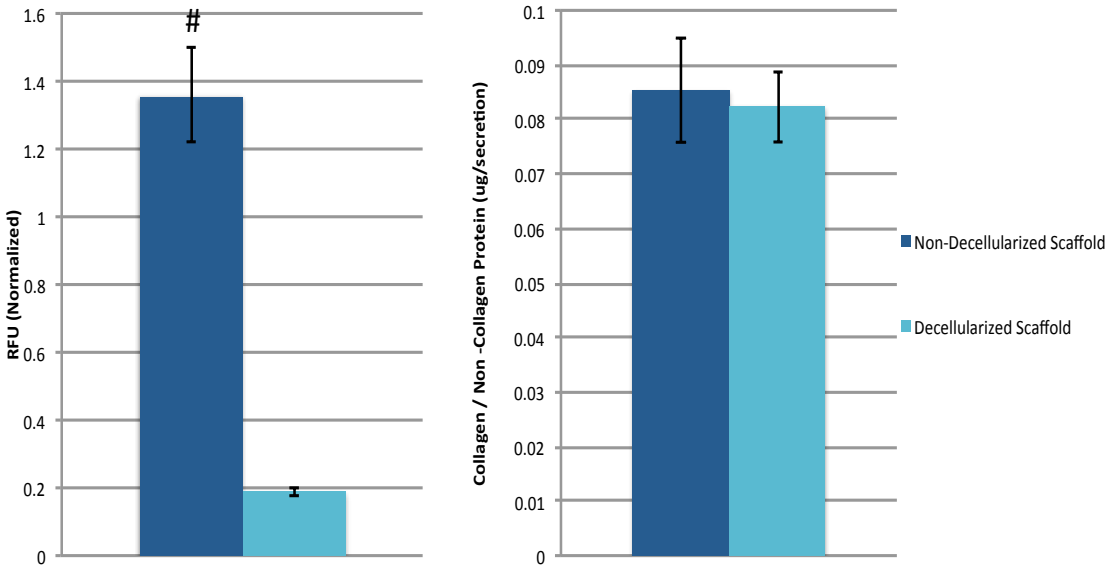

Figure 3.9. (Left) Metabolic activity (indirect measurement of cellular viability) of HUVECs on PDLA_PLLA/10%Gel scaffolds decreased by 86% after decellularization. (Right) Collagenous/non-collagenous protein matrix secreted by HUVECs was maintained by 96% after decellularization. Statistical analysis: # denotes ANOVA Tukey Test (post-hoc) $p<0.05$.

Next, we evaluated the cellular response of hMSCs to the preserved decellularized PDLA_PLLA/10%Gel scaffold at Day 7. The hMSCs seeded on the decellularized scaffold had a statistically significant higher level of metabolic activity at Day 7 in comparison to the hMSCs seeded on the control scaffold. The control scaffold was a scaffold that was not previously seeded with cells. This data suggest the hMSCs preferred the maintained endothelial matrix deposited by the HUVECs. Figure 3.10 also shows the hMSCs secreted similar levels of collagenous/non-collagenous proteins in response to the material as the hMSCs on the control scaffold; suggesting the matrix did

not inhibit the hMSCs innate functions.

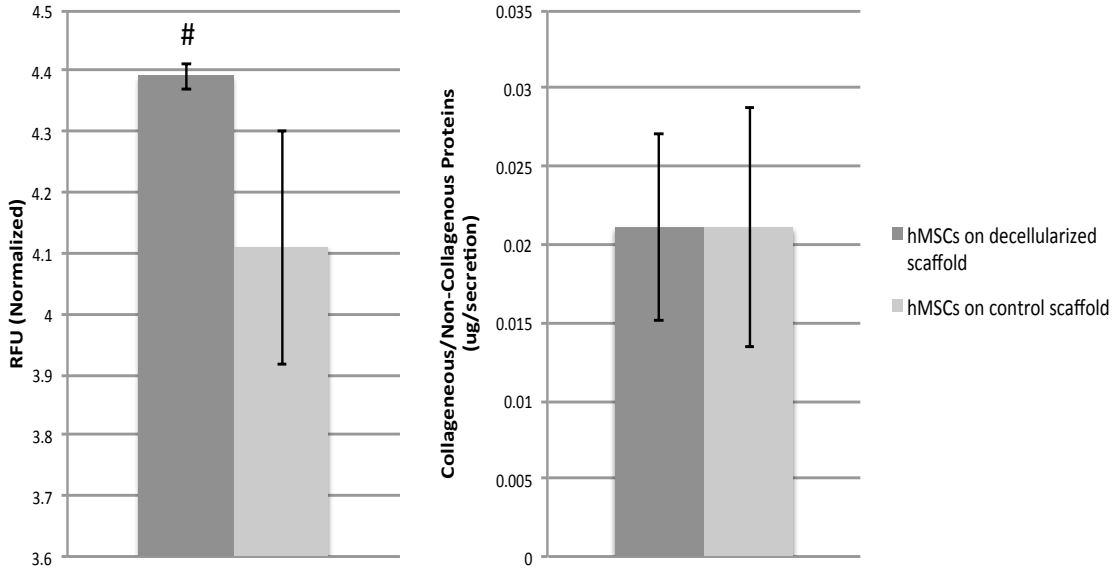

Figure 3.10. (Left) Metabolic activity of hMSCs on the decellularized PDLA_PLLA/10%Gel scaffolds was significantly higher than on the control non-decellularized scaffold at Day 7. (Right) Collagenous/non-collagenous protein matrix secreted by the hMSCs on the decellularized PDLA_PLLA/10%Gel scaffold was similar to the hMSCs on the control non-decellularized scaffold at Day 7. Statistical analysis: # denotes ANOVA Tukey Test (post-hoc) $p<0.05$.

The protein expression of VEGF was evaluated using IHC, Figure 3.11. The green indicates the presence of intercellular VEGF stained with phalloidin. The negative control, decellularized scaffold without cells, was also imaged and compared to confirm the VEGF expression was from the hMSCs and not residual VEGF on the scaffold, Fig.

3.11B. This image qualitatively confirms the ability of the decellularized cortical scaffold to promote stem cell differentiation into vascular endothelial cells without the addition of any growth factors. The protein secretion was also measured quantitatively using an ELISA kit for human VEGF, Figure 3.12. In this study, HUVECs on TCP was added as a comparison group. There was a significantly higher concentration of VEGF secreted from the hMSCs seeded on the decellularized scaffold (hMSCs_PDLA_PLLA/10%Gel_Decell) than the hMSCs seeded on the control scaffold, (hMSCs_PDLA_PLLA/10%Gel). As expected the secretion of VEGF from the HUVECs was significantly greater than the hMSCS seeded on the decellularized scaffold. It is important to note this was the amount of VEGF measured in the cell supernatant at Day 7. We would expect an increase in secreted VEGF at later time points as the hMSCS continued to differentiate in response to the pro-angiogenic matrix.

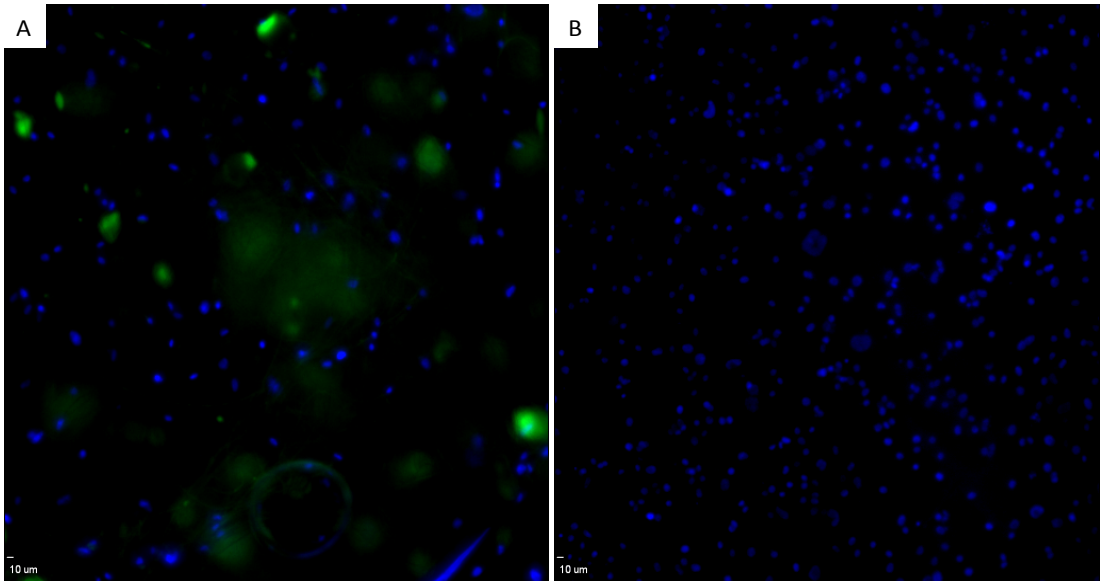

Figure 3.11. VEGF immunostain of hMSCs seeded on the previously seeded decellularized PDLA_PLLA/10%Gel scaffolds (left) and the control non-decellularized

scaffold. GFP (green) is the presence of VEGF and DAPI (blue) is the hMSCs nuclei (scale bar = 10μm).

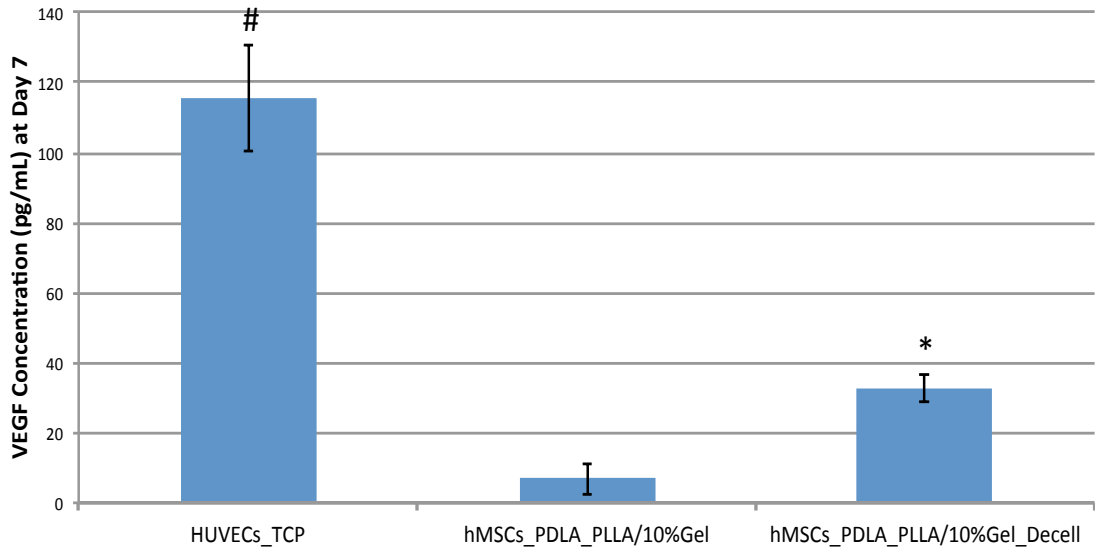

Figure 3.12. Quantitatively measured VEGF secretion from HUVECs on TCP (HUVECs_TCP), hMSCs on the control scaffold (hMSCS_PDLA_PLLA/10%Gel) and hMSCs on the decellularized scaffold (hMSCs_PDLA_PLLA/10%Gel_Decell). hMSCs seeded on the pre-vascularized decellularized scaffold secreted statistically significant higher levels of VEGF (N=6 for all the groups). Statistical analysis: # denotes ANOVA Tukey Test (post-hoc) $p<0.05$ from the other groups, * denotes $p<0.05$ significance from hMSCS_PDLA_PLLA/10%Gel scaffold.

The scaffolds were also stained with actin/DAPI to evaluate the effect of the decellularized matrix on the cellular morphology. Blood vessels develop in 2D by the

connection of collagen fibers. The images were taken at 10x to visualize a larger area. The percent area of enclosed lumens was quantified using ImageJ. The images and percent area values are shown in Figure 3.13. The hMSCS seeded on the decellularized scaffold, Figure 3.13A, have elongated along the fibers and start to created lumens in 2D. The percent of enclosed area, approximately 13%, was comparable to the HUVECs seeded on TCP, Figure 3.13C. Figure 3.13B shows the hMSCs randomly seeded on TCP due to the lack of guidance cues provided by the aligned electrospun fibers. The influence of the aligned fibers are seen in Figure 3.13D, hMSCs seeded on the control scaffold.

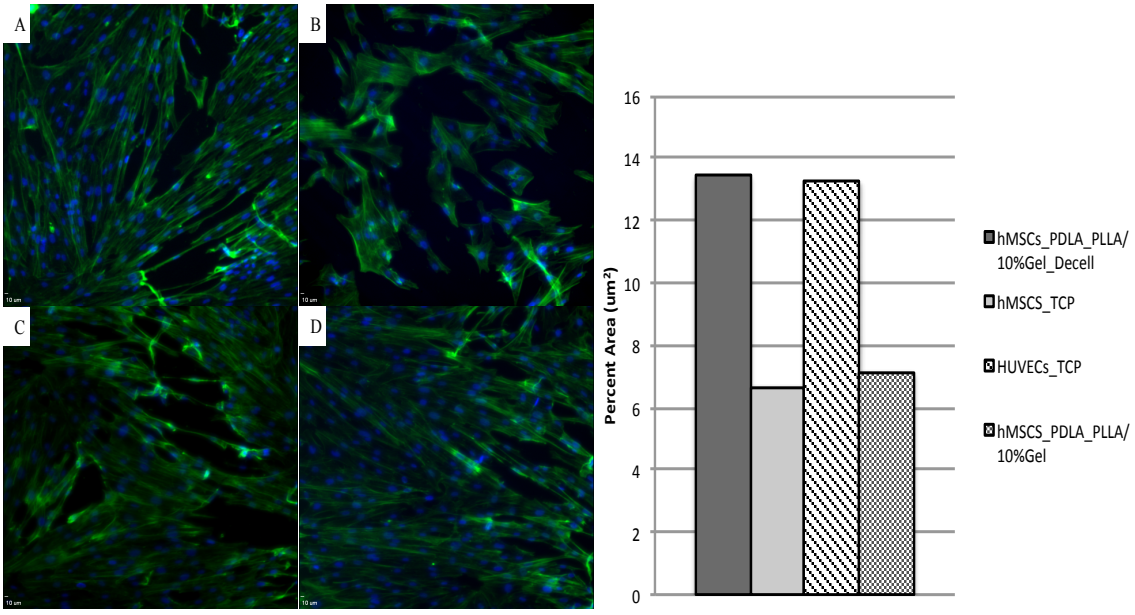

Figure 3.13. Representative fluorescent images (10X) of A) hMSCs seeded on the decellularized scaffold, B) hMSCs on TCP, C) HUVECs on TCP, D.) hMSCs on the control scaffold (scaffold not previously vascularized). hMSCs seeded on the decellularized scaffolds exhibited morphology indicative of lumens in 2D with areas comparable to endothelial cells. (Scale bar = 10μm).

3.4. Conclusion

The results presented in this chapter validate the development of a decellularized cortical scaffold that promotes endothelial growth. SEM images of the fabricated osteon confirmed the scaffold mimics the hollow cylindrical architecture of native osteons. Although the fabricated osteons were about 10x greater in size than native osteons, the size can be reduced using less electrospun polymer. The data demonstrates the ability of the PDLA_PLLA/10%Gel, non-mineralized and mineralized, cortical scaffolds to promote endothelial cellular attachment and proliferation. This was confirmed with two human endothelial cell lines, human microvascular endothelial cells (HMECs) and human umbilical vein endothelial cells (HUVECs). The concentric electrospun fibers also guided cellular growth circumferentially and organized collagen network within the canal of the cortical scaffold. Qualitative and quantitative analysis was performed to validate the freeze-thaw decellularization method. Cellular viability significantly decreased by 86% in response to the freeze-thaw process. The HUVECs deposited a collagenous/non-collagenous protein matrix that was maintained post-decellularization. hMSCs seeded on the collagenous matrix exhibited cellular morphology indicative of lumens in 2D with areas comparable to endothelial cells. Furthermore, the maintained protein matrix promoted angiogenic differentiation of hMSCs confirmed qualitatively and quantitatively by the secretion of VEGF. VEGF has been shown to enhance angiogenesis and bone regeneration and have a direct effect on osteogenesis by recruiting and promoting osteoblast and osteoclast activity [4, 24, 25]. The pre-vascularized cortical scaffold combines the advantages of cell-based therapies, pro-

angiogenic factors, and a stable biomimetic construct to promote early vascularization *in vitro*.

3.5. References

1. Clarke, B., *Normal Bone Anatomy and Physiology.* Clinical Journal of the American Society of Nephrology, 2008. **3**: p. S131-S139.
2. Kaigler, D., Krebsbach PH, West ER, Horger K, Huang YC, Mooney DJ, *Endothelial cell modulation of bone marrow stromal cell osteogenic potential.* The FASEB Journal, 2005. **19**: p. 665-667.
3. Gerber, H., Vu, TH, Ryan, A.M., Kowalkski J., Werb, Z., Ferrara, N, *VEGF couples hypertrophic cartilage remodeling, ossification, and angiogenesis during endochodral bone formation.* Nat. Med, 1999. **5**: p. 623-628.
4. Krishnan, L., N.J. Willett, and R.E. Guldberg, *Vascularization strategies for bone regeneration.* Annals of biomedical engineering, 2014. **42**(2): p. 432-44.
5. Fedorovich, N.E., Haverslag, RT, Dhert WJA, Alblas J, *The Role of Endothelial Progenitor Cels in Prevascularized Bone Tissue Engineering: Deveopment of Heterogeneous Constructs.* Tissue Engineering Part A, 2010. **16**(7): p. 2355-2367.
6. Liu, X., et al., *Vascularized bone tissue formation induced by fiber-reinforced scaffolds cultured with osteoblasts and endothelial cells.* BioMed research international, 2013. **2013**: p. 854917.
7. Kubota Y., K.H., Martin GR, Lawley TJ, *Role of laminin and basement membrane in the morphological differentiation of human endothelial cells into capillary-like structures.* J Cell Biol, 1988. **107**: p. 1589-1598.
8. Ades, E.W., et al., *HMEC-1: Establishment of an Immortalized Human Microvascular Endothelial Cell Line.* Journal of Investigative Dermatology, 1992. **99**(6): p. 683-690.
9. Madri JA, P.B., *The Molecular and Cellular Biology of Wound Repair*, ed. H.P. Clark RF. 1988, New York: Flenum Press.
10. Meury, T., S. Verrier, and M. Alini, *Human endothelial cells inhibit BMSC differentiation into mature osteoblasts in vitro by interfering with osterix expression.* Journal of Cellular Biochemistry, 2006. **98**(4): p. 992-1006.
11. Correia, C., et al., *In Vitro Model of Vascularized Bone: Synergizing Vascular Development and Osteogenesis.* PLoS ONE, 2011. **6**(12): p. e28352.
12. Clarkin, C.E., et al., *Heterotypic contact reveals a COX-2-mediated suppression of osteoblast differentiation by endothelial cells: A negative modulatory role for prostanoids in VEGF-mediated cell: cell communication?* Experimental Cell Research, 2008. **314**(17): p. 3152-3161.
13. Tsigkou, O., Pomerantseva, I., Spencer, JA, Redondo PA, Hart AR, O'Doherty E., Lin Y., Friedrich CC., Daheron L., Lin CP, Sundback CA, Vacanti JP, Nevile C, *Engineered vascularized bone grafts.* Proceedings of the Natioanl Academy of Sciences of the United States of America, 2010. **107**: p. 3311-3316.
14. Grellier, M., et al., *The effect of the co-immobilization of human osteoprogenitors and endothelial cells within alginate microspheres on mineralization in a bone defect.* Biomaterials, 2009. **30**(19): p. 3271-3278.

15. Guillotin, B., et al., *Human Primary Endothelial Cells Stimulate Human Osteoprogenitor Cell Differentiation.* Cellular Physiology and Biochemistry, 2004. **14**(4-6): p. 325-332.
16. Villars, F., et al., *Effect of human endothelial cells on Human Bone Marrow Stromal Cell phenotype: Role of VEGF?* Journal of Cellular Biochemistry, 2000. **79**(4): p. 672-685.
17. Liao, J., et al., *Modulation of osteogenic properties of biodegradable polymer/extracellular matrix composite scaffolds generated with a flow perfusion bioreactor.* Aca Biomaterialia, 2010. **6**(7): p. 2386-2393.
18. N, D., et al., *Effect of bone extracellular matrix synthesized in vitro on the osteoblastic differentiation of marrow stromal cells.* Biomaterials, 2005. **26**(9): p. 971-977.
19. Kaigler, D., Krebsbach PH, Polverini PJ, Mooney DJ, *Role of Vascular Endothelial Growth Factor in Bone Marrow Stromal Cell Modulation of Endothelial Cells.* Tissue Engineering, 2004. **9**(1): p. 95-103.
20. N, F., *Vascular endothelial growth factor.* Eur. J. Cancer, 1996. **32A**.
21. Sgarioto, M., et al., *Collagen type I together with fibronectin provide a better support for endothelialization.* Comptes Rendus Biologies, 2012. **335**(8): p. 520-528.
22. Shekhonin, B.V., et al., *Distribution of Type I, III, IV and V Collagen in Normal and Atherosclerotic Human Arterial Wall: Immunomorphological Characteristics.* Collagen and Related Research, 1985. **5**(4): p. 355-368.
23. RIcard-Blum, S., *The Collagen Family.* Cold Spring Harb Perspect Biol, 2011. **3**(1): p. 1-58.
24. Dai, J., Rabie, A.B. , *Vegf: an essential mediator of both angiogenesis and endochondral ossification.* J. Dent. Res, 2007. **86**: p. 937-950.
25. Tang, Y.L., et al., *Autologous mesenchymal stem cell transplantation induce VEGF and neovascularization in ischemic myocardium.* Regulatory Peptides, 2004. **117**(1): p. 3-10.

CHAPTER 4: FINITE ELEMENT ANALYSIS AND OPTIMIZATION OF HYDROXYAPATITE POSTS

4.1. Introduction

A major disadvantage of tissue-engineered (TE) grafts is that they lack mechanical strength comparable to native bone. Load-bearing metallic bone grafts provide the adequate mechanical strength, but they tend cause stress shielding *in vivo* or lack the ability to osseointegrate with surrounding bone leading to potential long-term failures. Our proposed TE bone graft aims to provide mechanical strength for load-bearing applications through the use of stable hydroxyapatite (HAp) columns as mechanical reinforcement structures. HAp is a natural inorganic component of bone that is responsible for bone's rigidity, and it has also been found to promote osteoinduction *in vitro* [1-4]. Researchers have concluded the mechanical properties of packed HAp matches the mechanical properties or native bone [5, 6]. The studies discussed in this chapter specifically focus on the incorporation of sintered hydroxyapatite (HAp) columns into the complete scaffold as a load-bearing structure. Cylindrical HAp columns will be integrated throughout the scaffold, specifically within the cortical scaffold section in order to obtain the appropriate inorganic (mineral) to organic (polymer) ratio. We hypothesized that incorporating sintered HAp columns into the complete scaffold would increase the overall mechanical strength. In this chapter, we investigated the effect of packing methods, sintering duration, and HAp powder type on the mechanical strength of the stable HAp columns.

4.2. Materials and Methods

4.2.1. Optimizing HAp Column Development

In this study, the effects of sintering and packing methods were explored to yield a mechanically enhanced biocompatible ceramic product. Sintering is a process whereby consolidation and densification of a material is achieved via the application of heat [7] . The three experiments were tested in sequence, so the packing method that yielded the highest mechanical properties was used in the sintering time experiment and the optimal sintering time was used in the type of HAp powder experiment. Table 1 outlines the parameters investigated in each experiment. Approximately 1 gram of the HAp nanopowder (purchased from Sigma Aldrich , Atlanta, GA, USA) was mixed with distilled water (dI H_2O) and compacted into a cylindrical wooden framework either manually or with the Instron 5869 at constant load of 44MPa. The columns were then pushed out using the Instron and sintered in a conventional furnace at 1200°C. This temperature was selected based on research showing HAp undergoes structural transformations into α-tri calcium phosphate (TCP) when sintered above 1250°C [7, 8]. The sintering times tested were 3 and 5 hours. In a following, experiment, we used the packing pressure and sintering time that yielded the best results and created columns from two different forms of HAp powder, synthetic powder and nanopowder. The sintered HAp columns were mechanically tested using an Instron 5869 at a rate of 1mm/min and the compressive moduli and ultimate compressive strengths were computed and compared. The samples were dried completely prior to mechanical testing (n=6).

	Parameters Tested	Condition 1	Condition 2
Experiment 1	Packing Method	Manually Packed (N=6)	Instron Packed (44 MPa) (N=6)
Experiment 2	Sintering Time	3 Hours (N=6)	5 Hours (N=6)
Experiment 3	Type of HAp	Synthetic Powder (N=6)	Nanopowder (N=6)

Table 4.1: Experimental design of HAp column study

4.2.2. Finite Element Analysis of HAp Column

Finite Element Analysis (FEA) is a mathematical computerized method used to predict how a product reacts to various applied forces. FEA was performed using Abaqus software on multiple three-dimensional scaffold models featuring various shapes and arrangements of HAp columns to determine the modeled scaffold's compressive yield strength. Mechanical properties of the trabecular and cortical scaffold determined from previous work were inputted and assigned to the appropriate sections. A pressure load of 44MPa at 1mm/min was applied to the top face of each sample while translational and rotational constraints were applied to the bottom face of each sample. This force was chosen based on loading studies performed on subjects of varying ages [9]. Results from the finite element analysis were outputted as principal stresses and were used to calculate von Misses stresses. The FEA models and corresponding stresses were compared to determine the optimal HAp column shape and arrangement.

4.2.3. HAp Columns in Complete Scaffold Mechanical Testing

The purpose of this study was to determine the mechanical properties of the complete scaffold containing the trabecular and cortical scaffolds with and without HAp columns. The columns were created by hand packing HAp nanopowder and dI H_2O into a wooden mold with 1 x 10 mm drilled holes. The columns were then Instron packed at a constant 140N compressive force for 10 minutes. The HAp columns were pushed out using the Instron and inspected for any cracks. The columns that passed inspection were sintered in a conventional furnace for 5 hours at 1200°C (Figure 4.1A). The trabecular scaffolds was constructed according to the methods discussed in Chapter 2 (PDLA_PLLA/10%Gel/HAp) and the cortical scaffolds was created as mentioned in Chapter 3 (PDLA_PLLA/10%Gel). The control group was complete non-mineralized scaffolds that did not have HAp columns (Figure 4.1B). The experimental groups were mineralized complete scaffolds with (NoColumns_Min) and without (HApColumns_Min) HAp columns, Figures 1C and 1D. The mineralized scaffolds were mineralized via electrodeposition for 2 hours at 5V. The complete scaffolds (n=6) were mechanically tested in compression using the Instron 5869 at 1mm/min strain rate. After mechanical testing, the percent of inorganic content was evaluated through an ash weight study. Remaining HAp column pieces were removed from the scaffolds and the scaffolds were heated up to 700°C for 24hrs in a conventional furnace to burn off all organic matter. We hypothesized the addition of the HAp columns in the scaffold would increase mineral deposition during the electrodeposition mineralization.

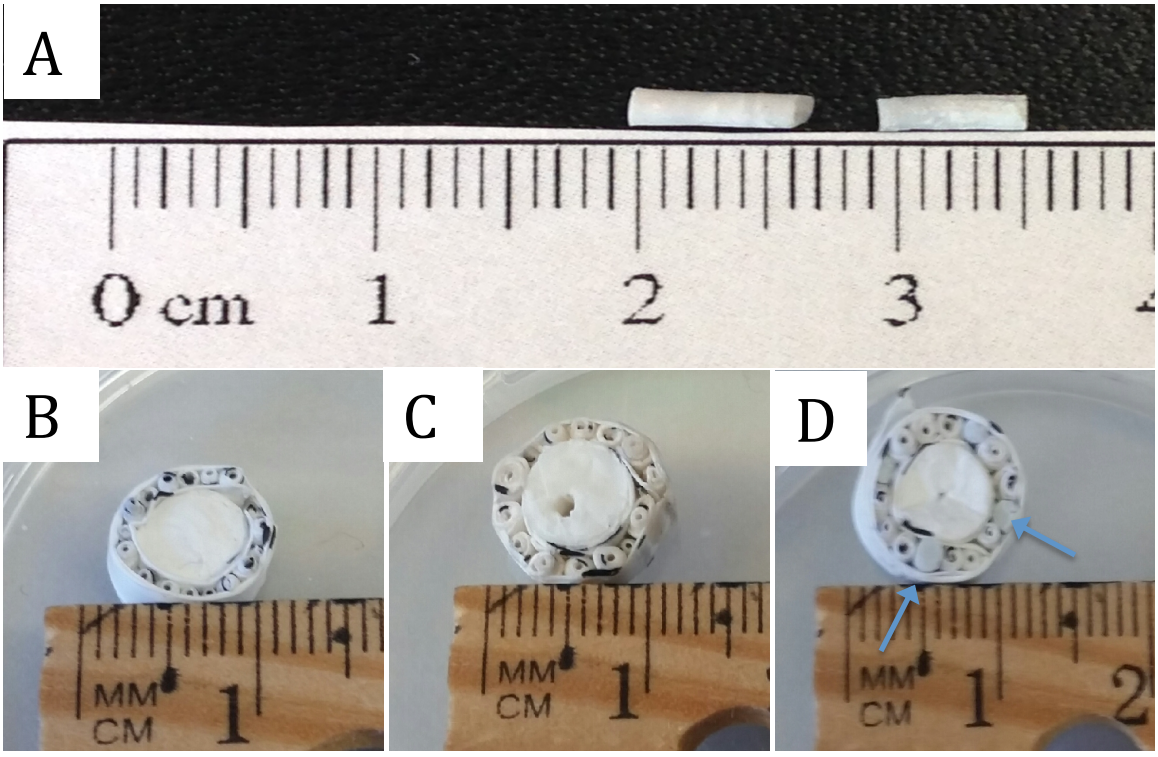

Figure 4.1. A) Sintered HAp columns, B) Control scaffold (no HAp columns and non-mineralized), C) Mineralized complete scaffold without HAp columns (NoColumns_Min), and D) Mineralized complete scaffold with HAp columns (HApColumn_Min)

4.2.4. Statistical Analysis

Statistical analysis was performed using KaleidaGraph Synergy Software. All data was subjected to an one-way analysis of variance (ANOVA) with post-hoc analysis (Tukey test) to determine the statistical significance of differences between groups, $p < 0.05$.

4.3. Results & Discussion

4.3.1. Optimizing HAp Column Development Results

The effects of packing methods, manually or machine, on the mechanical strength of the sintered HAp columns were evaluated. One group of HAp columns (n=6) were hand packed and the other group (n=6) was machined packed with an Instron 5869 at a constant pressure of 44 MPa for 10 minutes Both groups were sintered at 1200°C for 5 hours. The compressive moduli of the two samples are shown in Figure 4.3. The HAp columns packed with the Instron exhibited statistically significant higher compressive moduli (1059.46 ± 405.57 MPa) than the columns packed manually (329.896 ± 206.31 MPa).

The HAp columns were sintered at a temperature of 1200°C for 5 and 3 hours. All samples were Instron packed into cylindrical molds at a constant 44 Mpa load for 10 minutes. It was concluded that longer sintering times maximize the mechanical properties of the HAp columns. A comparison of their compressive modulus can be seen in Figure 4.3. The columns sintered for 5 hours yielded significantly higher compressive moduli (1059.46 ± 215.43 MPa) than the columns sintered for 3 hours (475.035 ± 197.99 MPa).

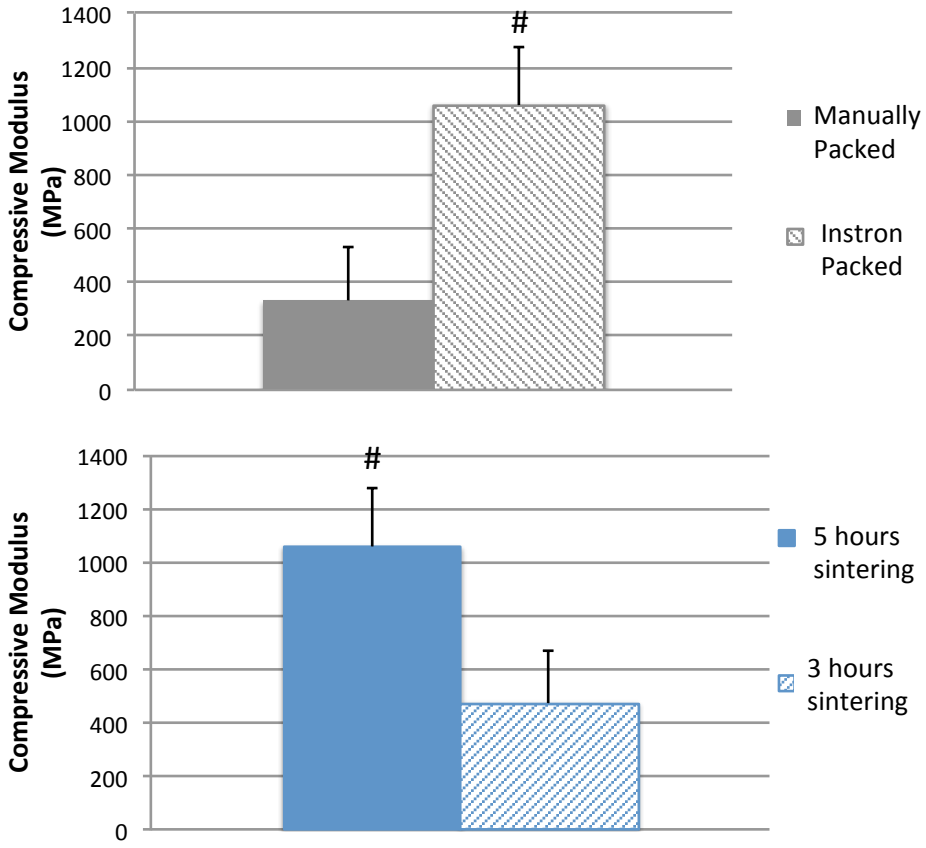

Figure 4.2. (Top) The compressive moduli of HAp columns packed with the Instron (1059.46 ± 405.57 MPa) was significantly greater than the compressive moduli of the columns packed manually (329.896 ± 206.31 MPa). (Bottom) The compressive moduli of HAp columns sintered for 5 hours (1059.46 ± 215.43 MPa) was significantly greater than the compressive moduli of the columns sintered for 3 hours (475.035 ± 197.99 MPa). Statistical analysis: # denotes ANOVA Tukey Test (post-hoc) $p<0.05$.

Synthetic HAp powder and HAp nanopowder were Instron packed for 10 minutes at a constant 44 MPa load and sintered at 1200°C for 5 hours. A comparison of their compressive moduli is shown in Figure 4.3. HAp nanopowder was found to be significantly stronger than the synthetic HAp powder, with average compressive moduli of 1079.0667± 300.82 MPa and 319.243± 58.34 MPa respectively. One explanation for this is that the nanopowder HAp exhibited a greater degree of densification. As a result, the final HAp columns for the scaffold will be composed of Instron packed (44 MPa for 10 minutes) nanopowder HAp sintered at 1200°C for 5 hours.

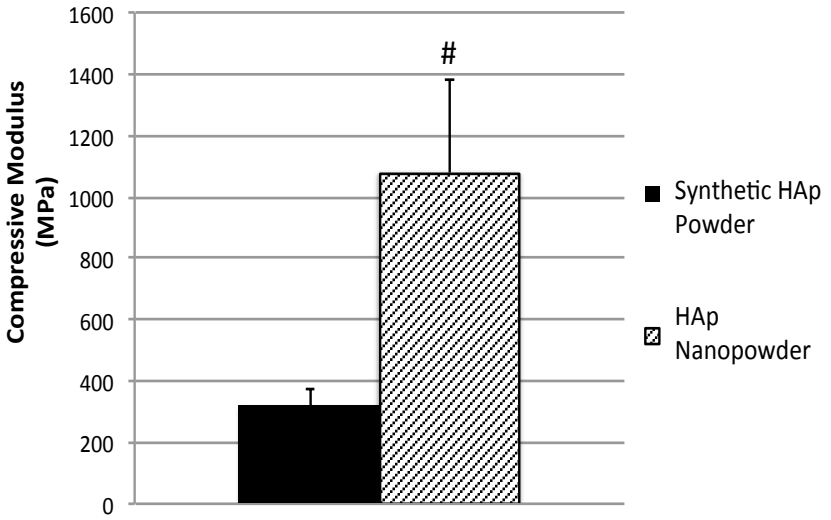

Figure 4.3. The HAp columns composed of synthetic HAp powder (1079.0667 ± 58.34 MPa) exhibited statistically significant greater compressive moduli than the HAp nanopowder columns (319.243 ± 300.82 MPa). Statistical analysis: # denotes ANOVA Tukey Test (post-hoc) $p<0.05$.

4.3.2. Finite Element Analysis Results

FEA was performed on complete scaffold models to determine the appropriate shape, arrangement and amount of HAp columns (% wt/volume) necessary to match the mechanical properties of native bone. The results from the mechanical modeling are depicted in Figure 4.4. The color scale bar corresponds to Von Mises stresses with red representing the higher stresses and blue indicating lower stresses. The scaffold modeled in Figure 4.4A is one large circle cylinder and the model in Figure 4.4B is one large square HAp columns within the complete scaffold. A scaffold with 4 square columns with and without fillets is shown in Figures 4.4C and 4.4D. The models depicted in Figures 4.4A –D show the trabecular and cortical scaffold sections taking on a large amount of the compressive load, as indicated by the green surrounding the HAp column. This is undesirable outcome as it could lead to scaffold shearing and failure *in vivo*. Whereas, in Figure 4.4E the majority of the compressive load is being taken on by the multiple embedded HAp columns.

FEA was also performed using SolidWorks software to validate the Abaqus FEA results and further determine the HAp percent amount to include in the complete scaffold. The calculated Von Mises yield stresses from this analysis are graphed in Figure 4.5. The compressive yield strength of cortical bone, 193 MPa, was the reference value. Assemblies 1, 2, and 3 yielded Von Mises stressed within the range of cortical bone, but it was difficult to create square columns. We decided to select the Assembly 3 design of four 1.5 mm cylindrical columns (8.9% total HAp in scaffold), as our final HAp shape and arrangement due its yield strength of 206 MPa and feasibility.

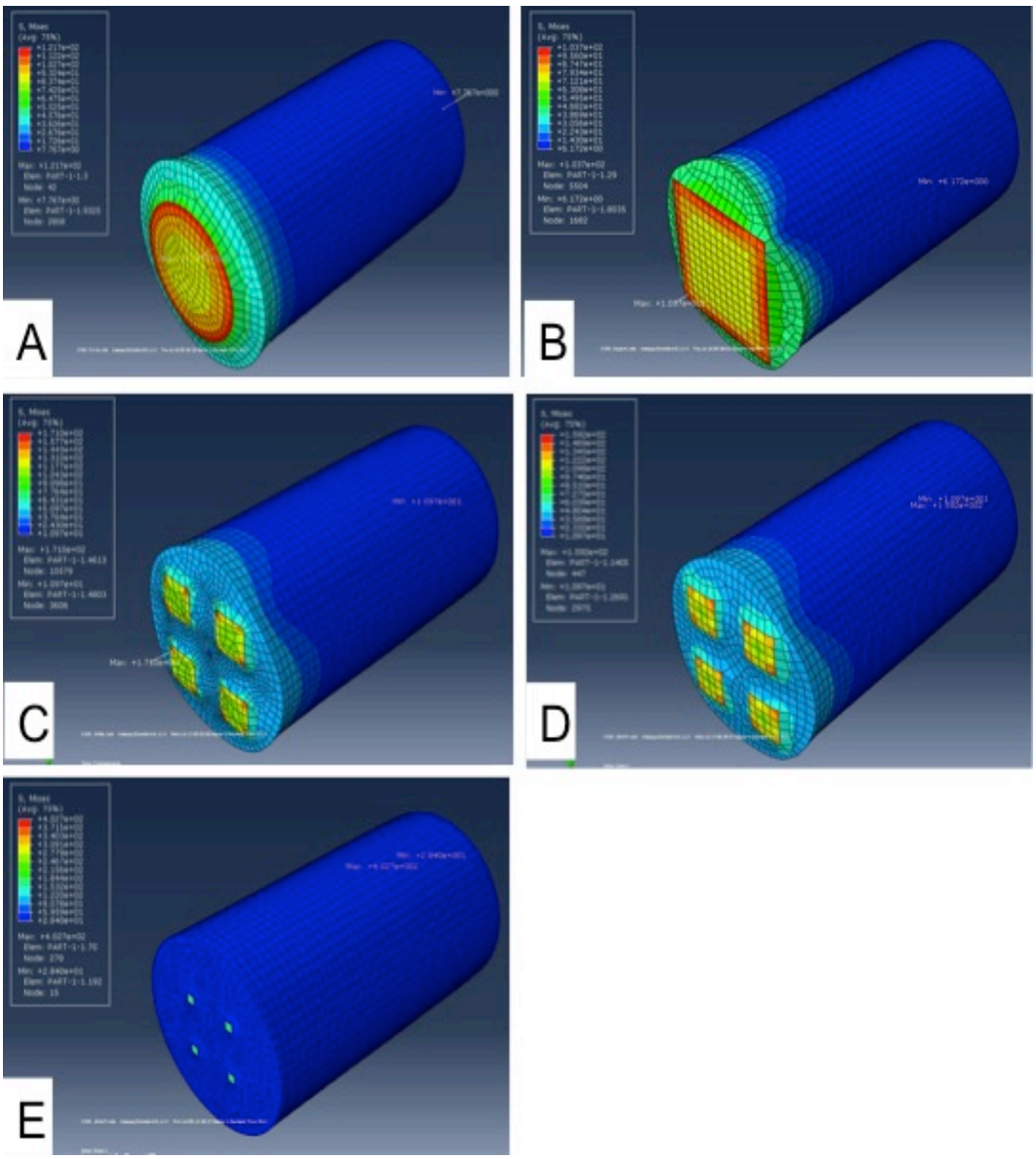

Figure 4.4. Abaqus FEA model results of varying HAp column shapes and arrangements (red and blue indicate the maximum and minimum von Misses stresses respectively) A.) One circular HAp column, B.) One square HAp column, C.) 4 squares, 26% HAp 0.1mm fillets, D.) 4 squares, 26% HAp, E.) 4 squares, 10% HAp

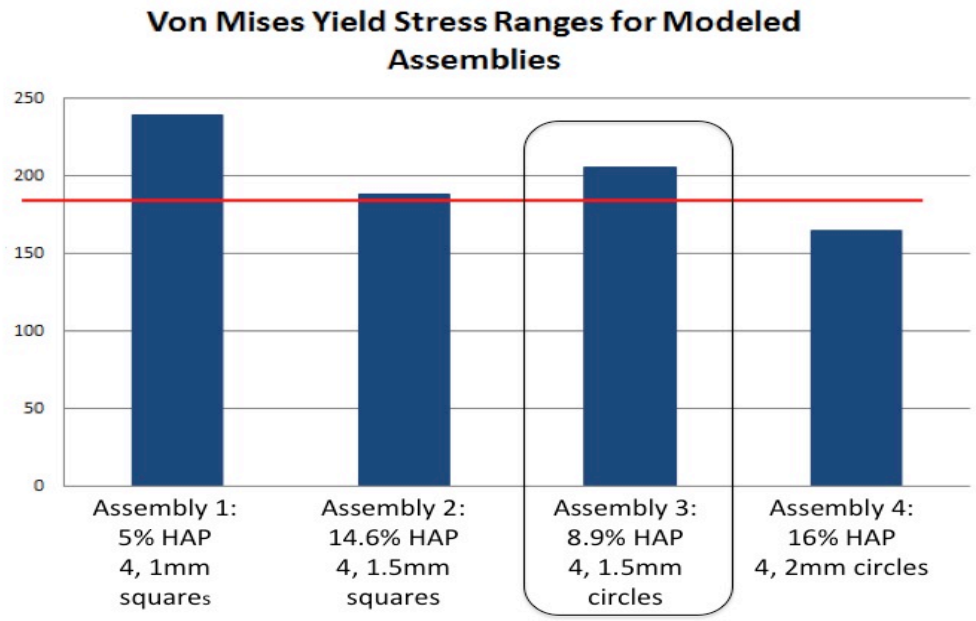

Figure 4.5. Calculated Von Mises yield stresses of varying HAp shape and assembly using SolidWorks. The red line indicates the von misses stress of cortical bone, 194 MPa

4.3.3. HAp Columns in Complete Scaffold Mechanical Analysis & Ash Weights

Complete scaff0lds (n=6) were mechanically tested in compression to determine the effect of the embedded HAp columns and mineralization on the scaffold's overall mechanical strength (Figure 4.6). The stiffness of the complete scaffolds significantly increased by 42% with the addition of the HAp columns when comparing the ultimate compressive strength of the scaffolds with the HAp columns (274.72±4.98 MPa) and without the HAp columns (157.40 ±22.17 MPa). Furthermore, the compressive modulus and ultimate compressive strength increased by 83% and 73% r*espectively* when comparing the mineralized scaffold without HAp columns and the non-mineralized scaffold, Fig. 4.6. The mineralized scaffold with HAp columns yielded a compressive modulus of 574 MPa, which is about three times greater than the compressive modulus f

native bone. Figure 4.7 depicts the percent inorganic content of the scaffolds' total mass. The percent inorganic content in the scaffolds were 35.95 ± 1.66, 53.89 ± 2.44, and 61.40 ± 1.80 for the control, HApColumns_NonMin and HApColumns_Min scaffolds respectively. The electrodeposition mineralization deposited a significant amount of mineral throughout the scaffold as evident by the statistically significant increase in inorganic content between the non-mineralized and mineralized scaffolds.

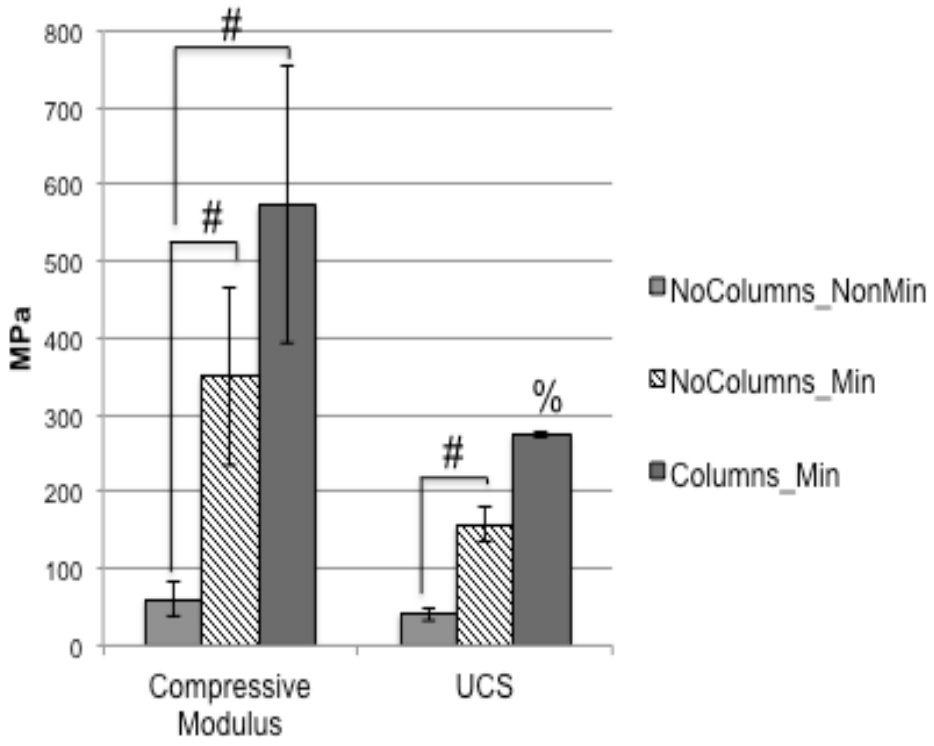

Figure 4.6. Compressive testing performed at 1mm/min using the Instron 5869 exhibited significant differences in compressive modulus and ultimate compressive strength with the addition of mineralization and/or HAp columns. The HAp columns added a 42% increase in compressive strength, while mineralization increased the compressive

modulus by 73%. Statistical analysis: # denotes ANOVA Tukey Test (post-hoc) $p<0.05$ from control, % denotes ANOVA Tukey Test (post-hoc) $p<0.05$ from all other groups.

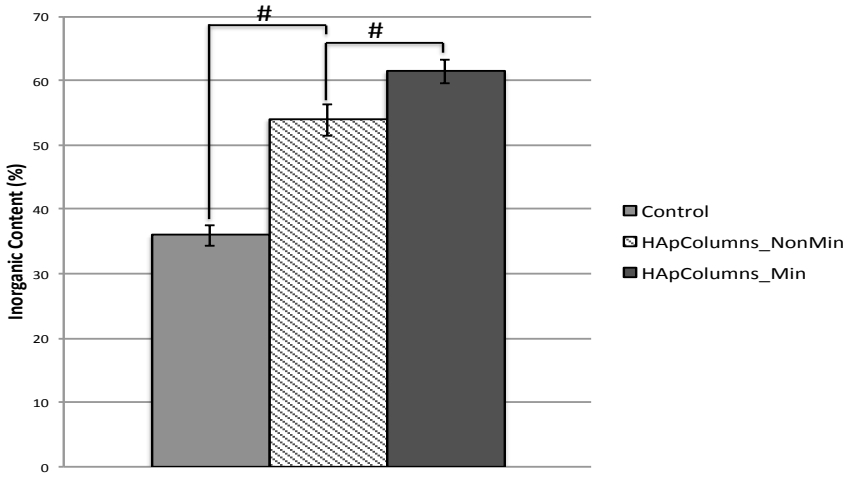

Figure 4.7. The percent inorganic content increased with the electrodeposition mineralization. The HAp columns also lead to an increase in mineral deposition during mineralization. Statistical analysis: # denotes ANOVA Tukey Test (post-hoc) $p<0.05$.

4.4. Conclusion

HAp is a naturally occurring mineral found in native bone, making it an ideal osteoinductive material for bone regeneration. The integration of mechanically enhanced HAp columns serves as a promising step towards developing one of the first biomimetic bone scaffolds that exhibits the mechanical properties of native bone, while simultaneously promoting osteoblastic and vascular differentiation. In order to optimize the mechanical properties of HAp columns, we investigated packing method, sintering time, and HAp powder type. Instron packed nanopowder HAp sintered for 5hrs at

1200°C yielded the most mechanically enhanced HAp columns with a compressive modulus of 1079.07 ± 58.34 MPa. Two FEA modeling systems confirmed four 1mm in diameter cylindrical HAp columns, making up 8.9% of the total scaffold mass, would be the optimal HAp column shape and arrangement in terms of Von Misses stress. Complete scaffolds, including the trabecular and cortical scaffolds, were created according to the FEA model results and tested in compression. The compressive modulus of the mineralized scaffold with HAp columns was 2-3 times greater than native bone. Furthermore, the electrodeposition was successful at mineralizing the full-thickness of the scaffolds and increased the mineral content by 25% with 62% inorganic content. The results presented in this chapter validate the ability to development a synthetic bone scaffold with mechanical properties comparable to native bone by incorporating a sintered hydroxyapatite structure.

4.5. References

1. Lin, L., K.L. Chow, and Y. Leng, *Study of hydroxyapatite osteoinductivity with an osteogenic differentiation of mesenchymal stem cells.* Journal of biomedical materials research. Part A, 2009. **89**(2): p. 326-35.
2. RZ, L., *Properties of osteoinductive biomaterials: calcium phosphates.* Clin Orthop Rel Res, 2002. **395**: p. 81-95.
3. M, J., *Biological ascpects of calcium phosphates: properties and applications.* Dental clinics of North America, 1986. **30**: p. 25-47.
4. Bucholz RW, C.A., Holmes FE, *Hydroxyapatite and tricalcium phosphate bone graft substitutes.* Orthop Clin North Am, 1987. **18**: p. 323-334.
5. Rootare HM, P.J., Craig RG, *Sintered Hydroxyapatite Ceramic for Wear Studies* Journal of dental research, 1978. **57**(7): p. 77-83.
6. Ramay HR, Z.M., *Biphasic calcium phosphate nanocompositite porous scaffolds for load-bearing bone tissue engineering.* Biomaterials, 2003. **25**: p. 5171-5180.
7. Gu, Y.W., et al., *Spark plasma sintering of hydroxyapatite powders.* Biomaterials, 2002. **23**(1): p. 37-43.
8. Pramanik, S., et al., *Development of high strength hydroxyapatite by solid-state-sintering process.* Ceramics International, 2007. **33**(3): p. 419-426.

9. Crandall JR, M.B., Meaney DF, Schmidtke SZ, *Pediatric Injury Biomechanics*, ed. P.I.B.A. Textbook. 2012: Springer.
10. Erickson, G.M., J. Catanesem, and T. Keaveny, *Evolution of the biomechanical material properties of the femur.* The Anatomical Record, 2002. **268**(2): p. 115-1124.

CHAPTER 5: *IN VIVO* ANALYSIS OF AN OSTEOINDUCTIVE PRE-VASCULARIZED BONE REGENERATIVE SCAFFOLD

5.1. Introduction

Subcutaneous scaffold implantation is the gold standard for *in vivo* evaluation of biocompatibility and biological response at the cellular and tissue level [1] . Recent subcutaneous nanofibrous bone scaffold implantation studies have shown success in terms of cellular infiltration [2-5]. The purpose of the following *in vivo* study is to characterize the osteoblastic and vascular phenotype expression in response to the 3D pre-vascularized osteoinductive scaffold implanted into the dorsum of BALB/c mice. We hypothesized the added HAp and mineral content and vascularized lumen will promote scaffold integration, vascularization and differentiation of stem cells along the osteoblastic and angiogenic lineages.

5.2. Materials and Methods

The scaffold groups for the subcutaneous *in vivo* study are outlined in Table 5.1. The rationale for these groups were to assess the biocompatibility, osteogenic and angiogenic potential of the complete scaffold *in vivo* (Groups I vs. II & Group III), evaluate the effect of mineralization and HAp on vasculature development *in vivo* (Group II vs. Group III) and investigate the effect of the pre-vascularized lumen on vasculature integration (Group I vs. Group II). Modified versions of the complete scaffold were created for this study. Porous electrospun PDLA_PLLA/10%Gel scaffolds were wrapped around a single fabricated osteon. The trabecular scaffold and osteon were developed as previously mentioned. The entire assembly was wrapped with a nanofibrous PDLA_PLLA/10%Gel

scaffold, secured with tape and sintered at 54°C for 45 minutes to yield a stable scaffold 5 mm diameter by 10 mm in length. The scaffolds in the Min_HAp groups had 10%HAp in the trabecular scaffold and were mineralized via static mineralization for 3 hours at 5V in simulated body fluid (SBF), yielding approximately 20% mineralization. All the scaffolds, n=6 per group for two time points, were attached to well plates with sterile silicone glue, sterilized with 70% EtOH and UV radiation and conditioned with endothelial media for 24 hours.

Group	Mineralized	HAp	Pre-Vascularized Lumen	hMSCs
I (NonMin-Lumen)	-	-	-	+
II (NonMin+Lumen)	-	+	+	+
III (Min+Lumen)	+	+	+	+

Table 5.1. Outline of scaffold groups for subcutaneous scaffold implantation study.

To create the pre-vascularized lumen, human umbilical vein cells (HUVECs) were seeded inside the cortical scaffold at 25,000 cells per scaffold. The cells (passage 5) were maintained in Ham's F-12K (Kaighn's) Medium (purchased from Fisher Scientific Co., Suwanee, GA, USA), supplemented with 10% FBS, 2% penicillin streptomycin (P/S), 100μg/ml heparin, 30μg/ml Endothelial cell growth supplement (all purchased from Sigma Aldrich, Atlanta, GA, USA). At Day 14, the scaffolds were decellularized via the freeze-thaw procedure as discussed in Chapter 3. The scaffolds were then conditioned for 24 hours in the endothelial media with increased antibiotics to eliminate the risk of contamination. Prior to scaffold implantation, human bone marrow derived cells (hMSCs) at passage 1, obtained from Texas A&M Health Science Center, were seeded throughout the scaffolds at 100,000 cells per scaffold. The scaffolds with hMSCs were maintained for seven days in Media (α-MEM) supplemented with 10% fetal bovine

serum (FBS) and 5% penicillin.

5.2.2. Subcutaneous Scaffold Implantation

All surgeries were performed in compliance with Rutgers Institutional Animal Care and Use of Committee (IACUC) under protocol #14-062. Female BALB/c mice (6 weeks and approximately 18-21g) were used for this study. BALB/c mice are a common mouse type selected for scaffold implantation compatibility studies [2-4, 6]. On the day of surgery, the mice were anesthetized via mask induction of isoflurane and oxygen 1-5% or to effect on a heating pad at 37°C and the area of interest was shaved. Local anesthetic of Marcaine 0.25% (not to exceed 2mg/kg) was administered subcutaneously at the incision site. The desired surgical area was then aseptically prepared with a three-fold alternating application of Betadine scrub followed by wiping with 70% ethanol. A skin incision was created on the dorsum of the mice using a poke incision method. The skin was pulled up with forceps and a small incision was made at the base of the raised skin with a razor. Closed scissors were inserted into the incision and opened up to create a subcutaneous pocket. The skin margin was then elevated using forceps, and the scaffold was implanted into the subcutaneous pocket. This incision and implantation method reduced scarring. To minimize the number of mice used for study, two scaffolds one from Group II and one from Group III, were implanted in two separate subcutaneous pockets of the same mouse. The control scaffolds were implanted one per mouse. The skin around the incision was then pulled together and closed with sterile adhesive tissue glue. Animals were removed from anesthesia and placed into their recovery cage. Mice (6 per group) were sacrificed at 4 and 8 weeks postoperatively via CO_2

inhalation. The scaffolds were extracted and placed in 70% EtOH for up to 24 hours following by formalin. Scaffolds were sliced horizontally to yield circle cross-sections and prepared for histology at the Digital Imaging and Histology Core laboratory at the Rutgers-NJMS Cancer Center in Newark, New Jersey. The sections were stained with H&E to qualitatively assess cellular infiltration and tissue development. Masson's trichrome and Alizarin red stain was also performed to visualize collagen and mineral content, respectively.

The scaffolds were mechanically tested under compression with an Instron 5869 at a crosshead speed of 10%/min. All samples were vacuum soaked in PBS for 30 minutes prior to testing and the fibrous capsule was removed. Compressive moduli, yield stresses, and ultimate compressive stresses were computed and compared between groups to determine change in scaffold properties due to degradation and/or tissue integration. Toughness was measured using the trapezoidal method to measure the area under the stress-strain curve. The thickness of the fibrous capsules at varying location was measured using light microscopy and ImageJ analysis and validated using calipers.

5.2.3 Statistical Analysis

Statistically significance was determined at a p-value of 0.05, a standard deviation of 10%, and a sample size (n=6) yields a power of 0.98. Statistical analysis was evaluated using KaleidaGraph Synergy Software.

5.3. Results and Discussion

5.3.1. Qualitative Analysis and Histology

The scaffolds were extracted at timepoints 4 and 8 weeks and qualitatively assessed. This

dissertation only features the histology of the 4 week samples. Figure 5.1A is the Min+Lumen scaffold with the pre-vascularized lumen and hMSCs before implantation. Figure 5.1B is the same scaffold extracted at 4 weeks encapsulated in a fibrous network. Fibrous capsule thickness (FCT) was measured at the bottom (inferior side) and at the middle. The representative locations are marked in red (bottom) and in blue (middle) in Figure 5.1D. Figure 5.1C is the same scaffold from Figure 5.1A extracted at 4 weeks. At this time point, the scaffold was encapsulated and the inner pre-vascularized lumen appeared to be integrated with new vasculature tissue.

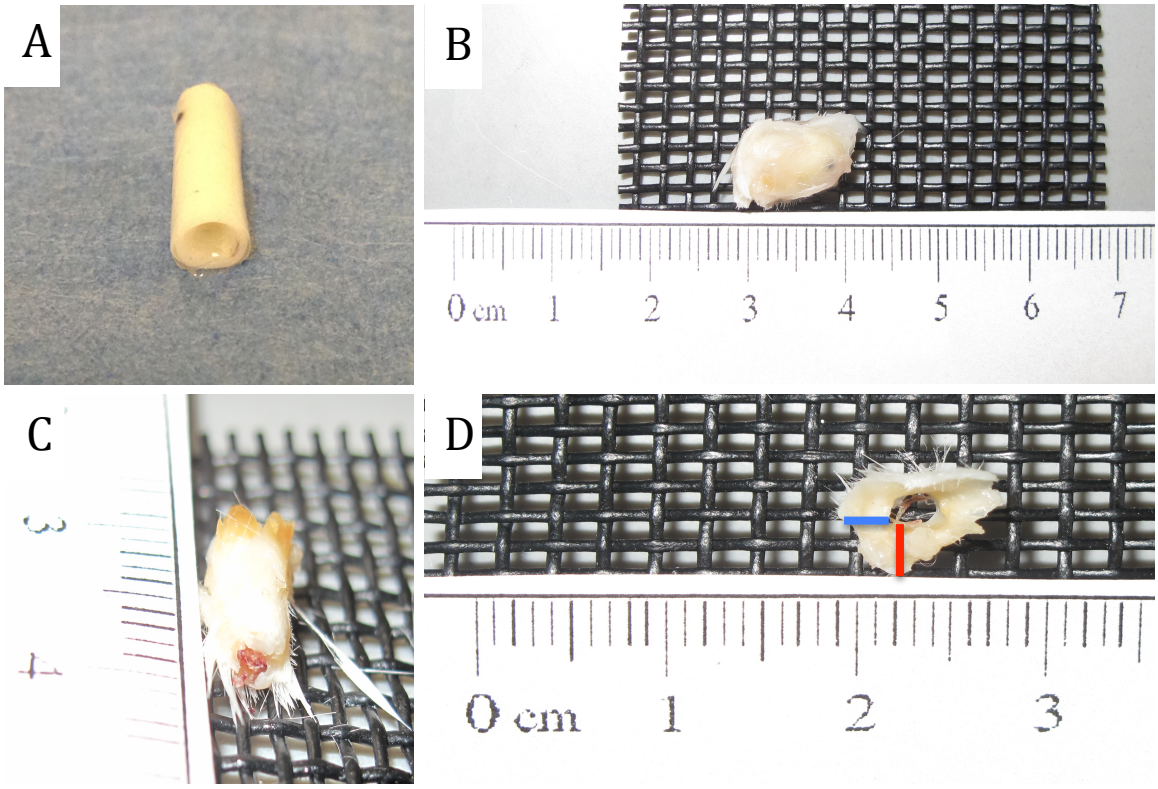

Figure 5.1. A) Scaffold, 5mm in diameter and 10mm in length, before implantation. B) Scaffold excised at 4 weeks in a fibrotic capsule. C) Scaffold with integrated vasculature

in the pre-vascularized lumen without the addition of hMSCs. D) Fibrous capsules were measured at the bottom (red) and middle (blue).

Fibrous encapsulation is indicative of the early wound healing response elicited by the foreign body reaction at the tissue-implant interface [7-9]. During this process, monocytes/macrophages are activated, which leads to collagen matrix deposition. Macrophages play an important role in angiogenesis of implants [10, 11]. The measured thicknesses at the middle and bottom are shown in Table 5.2 and graphically depicted in Figure 5.2. The FCT at the bottom was thicker than at the middle at 4 weeks for all the scaffold groups. The FCT at the bottom decreased at 8 weeks for all the scaffold groups in comparison to the 4 weeks. This could be due to the presence of local vasculature in the mice dorsum area and the supply of nutrients to the implantation site. Additionally, the fibrous capsule at the bottom was significantly thicker for the NonMin-Lumen scaffolds than the scaffold with the lumen. This could be attributed to the pre-existing vascularized matrix allowing for the influx of nutrients.

	Scaffold Group	FCT (Middle)	FCT (Bottom)
4 weeks	NonMin-Lumen	326.67±65.06	1076.67±372.20
	Min+Lumen	310.01±50.29	450.02±182.48
	NonMin+Lumen	570.15±141.77	573.33±109.70
8 weeks	NonMin-Lumen	403.33±95.04	576.67±104.08
	Min+Lumen	663.33±124.23	306.67±25.17
	NonMin+Lumen	430.12±60.83	556.67±242.14

Table 5.2. Fibrous capsule thickness (FCT) measurements (units = μm) taken at the middle and bottom of the scaffold over 8 weeks demonstrated an increased FCT at the

bottom of the scaffold. The values are shown as mean ± standard The FCT also decreased at the bottom over 8 weeks.

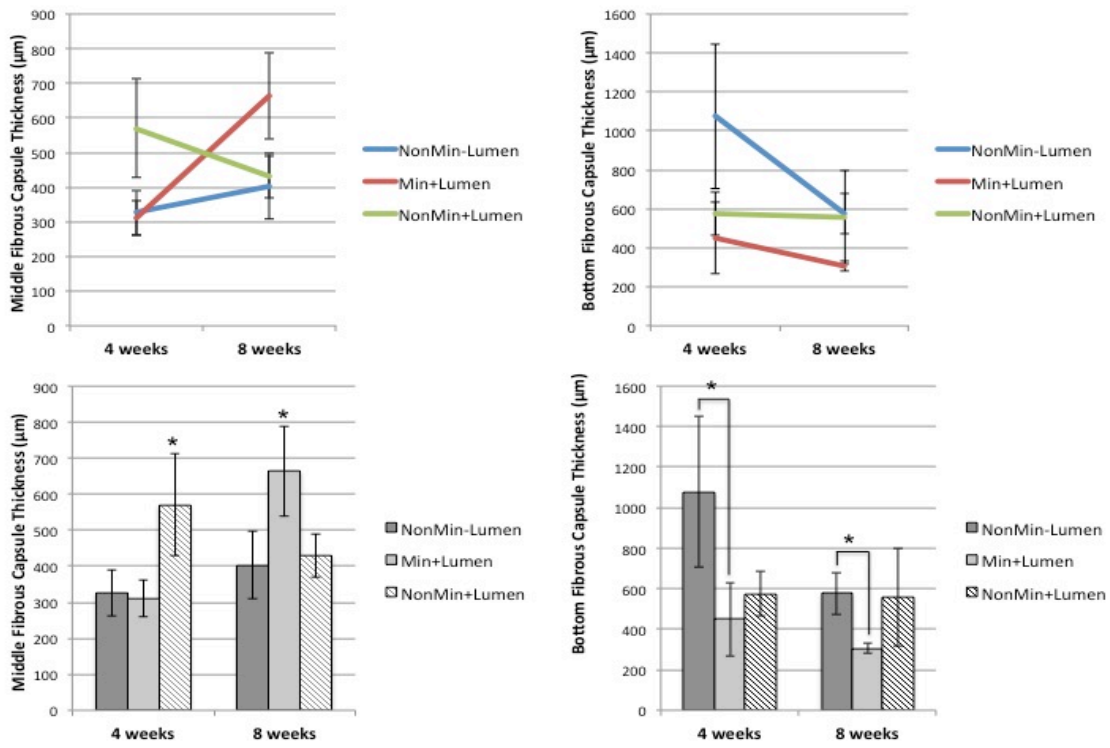

Figure 5.2. Fibrous capsule thicknesses (FCT) at the bottom and middles graphically showed a decrease in the thickness over 8 weeks at the bottom location. The thickness of the fibrous capsules surrounding the NonMin-Lumen scaffold was significantly greater then the scaffold groups with the lumen. Statistical analysis: * denotes ANOVA tukey Test (post-hoc) $p<0.05$

Histology was performed to qualitatively assess cellular infiltration, scaffold integration and vasculature within or surrounding the scaffold. Cell infiltration is a critical process in promoting tissue integration between implanted material and the host tissue [12-14].

Figure 5.3 are the H&E images of the scaffolds extracted at 4 weeks. These scaffolds were previously seeded with hMSCS and were either non-mineralized without a lumen (NonMin-Lumen), mineralized with the endothelial lumen (Min+Lumen), or non-mineralized with an endothelial lumen (NonMin+Lumen). As seen in all the figures, there was infiltration of a mixed population of cells within the scaffolds ('S'). Structured vasculature was also evident in some sections of the scaffolds as seen in Figures 5.3D-F at 10X and also in Figures 5.3G-I at 20X as indicated by 'BV' for blood vessels filled with erythrocytes. The beginning of a collagen network (pink) and cellular infiltration on the inner lumen of the non-mineralized scaffold without a lumen (NonMin-Lumen) is shown in Figure 5.3A. Integration of the scaffold with the surrounding tissue is evident in Figure 5.3G and Figure 5.3H. Masson's trichrome analysis of the excised scaffold at 4 weeks further confirmed the presence of scaffold integration and vasculature, Figure 5.4. The circular layers of the scaffold are apparent in Figure 5.4A with naïve collagen (dark pink) between the layers. The separation of the scaffold layers may have occurred during the sectioning process for histology. Infiltration of collagen and stable blood vessels within a scaffold section are seen in Figure 5.4B. Mineral content was detected in the Min+Lumen excised scaffolds at 4weeks, Figure 5.4E. This indicates the mineralization process was successful at mineralizing the full-thickness and that the mineral remains within the scaffold structure *in vivo*. The presence of mineral content, evaluated using an Alizarin red assay, was detected in the non-mineralized+Lumen samples can be contributed to the HAp in the scaffold, Figure 5.4F.

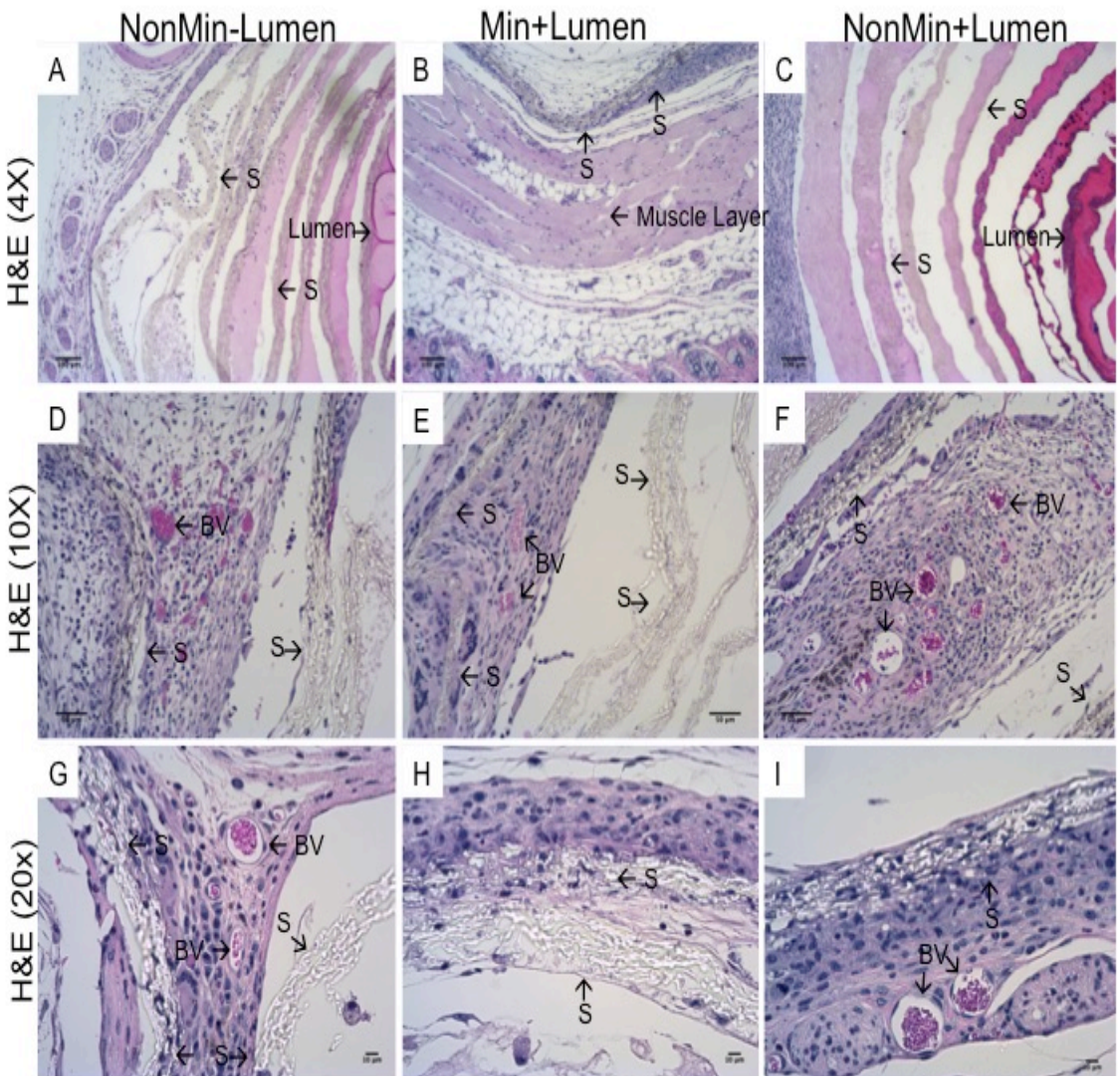

Figure 5.3. Cross-sectional H&E images of the explants at 4 weeks showed the presence of blood vessels ('BV'), cellular infiltration (purple) and scaffold integration in all the scaffold groups. The label 'S' indicates the location of the scaffold. Top row: 4X images (scale bar = 100μm) of the A) non-mineralized scaffold without the endothelial lumen (NonMin-Lumen), B) mineralized scaffolds with the endothelial lumen (Min+Lumen), and C) non- mineralized scaffold with the endothelial lumen (NonMin+Lumen). Middle row: 10X images (scale bar = 50μm) of the D) NonMin-Lumen scaffold, E) Min+Lumen

scaffold, and F) NonMin+Lumen scaffold. Bottom row: 20X images (scale bar = 10 μm) of the G) NonMin-Lumen, H) Min+Lumen scaffold, and I) NonMin+Lumen scaffold.

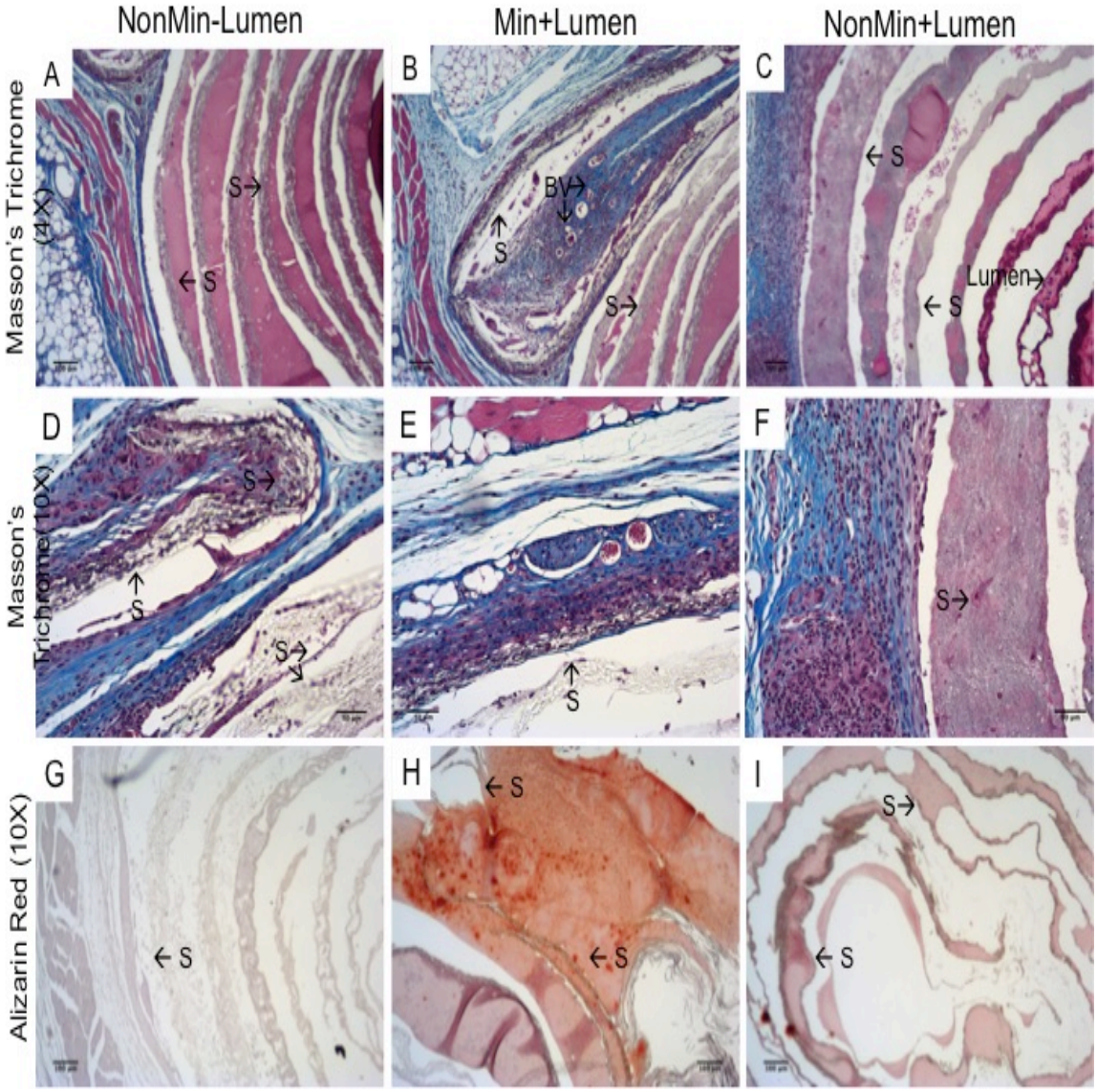

Figure 5.4. Masson's Trichrome and Alizarin Red stained images of the scaffolds at 4 weeks showed scaffold integration and mineral content (red). Collagen (blue) and neomatrix (pink) are seen surrounding and integrating with the scaffold. The labels 'S' indicate the location of the scaffold. Top row: 4X images (scale bar = 100μm) of the A)

non-mineralized scaffold without the endothelial lumen (NonMin-Lumen), B) mineralized scaffolds with the endothelial lumen (Min+Lumen), and C) non- mineralized scaffold with the endothelial lumen (NonMin+Lumen). Middle row: 10X images (scale bar = 50μm) of a D)NonMin-Lumen scaffold, E) Min+Lumen scaffold, and F) NonMin+Lumen scaffold. Bottom row: Alizarin Red 10X images (scale bar = 50μm) of the D)NonMin-Lumen scaffold, E) Min+Lumen scaffold, and F).NonMin+Lumen scaffold.

5.3.2. Mechanical Testing of Excised Scaffolds

The excised scaffolds were subjected to compressive testing at 1mm/min using an Instron 5869. Scaffolds that were not implanted were also tested as negative controls (NegControl_Min and NegControl_NonMin). Including these groups in the mechanical testing study provides us with information about the change in the scaffold's structural properties due to the *in vivo* conditions. The calculated yield strengths, ultimate compressive strengths, young's moduli and toughness values are shown in Figure 5.5 and Table 5.3. There were no significant differences in the ultimate compressive strength, yield strength and toughness of the excised experimental scaffolds, 4wks_NonMin_NoHAp and 4wks_Min_HAp, in comparison to their corresponding negative controls, NegControl_Min and NegControl_NonMin respectively. This indicates the scaffolds did not undergo any significant structural changes due to rapid degradation *in vivo* and were able to maintain their strength up to 4 weeks. Furthermore, the mechanical properties of the experimental scaffolds seeded with hMSCs prior to

implantation had significantly increased strength and toughness in comparison to the unseeded positive control scaffolds, 4wks_PosControl. This increase in mechanics can be contributed to the early tissue development and integration initiated by the hMSCs in the scaffolds. The ability to maintain the mineral content and strength *in vivo* was demonstrated by the statistically significant increase in compressive strength, yield strength, and toughness of the mineralized scaffolds with HAp in comparison to the non-mineralized scaffolds without HAp. All of the implanted scaffolds had similar areas with fibrous capsule, therefore this increase was not due to differences in area, but yet a difference in the forces the scaffolds were able to withstand. All the scaffolds exhibited ductile behavior and therefore there was no single clear point of failure for most of the scaffolds. This slow barreling effect causes a change in area as the load is applied; leading to variations in the computed stresses and strains of samples within the same group [15]. The mechanical properties of the excised scaffolds were also analyzed at 8 weeks and compared to the mechanics of the scaffold excised at 4 weeks. The results shown in Figure 5.6 indicate integration of fibrous tissue leading to significant increase in mechanical properties for all the groups.

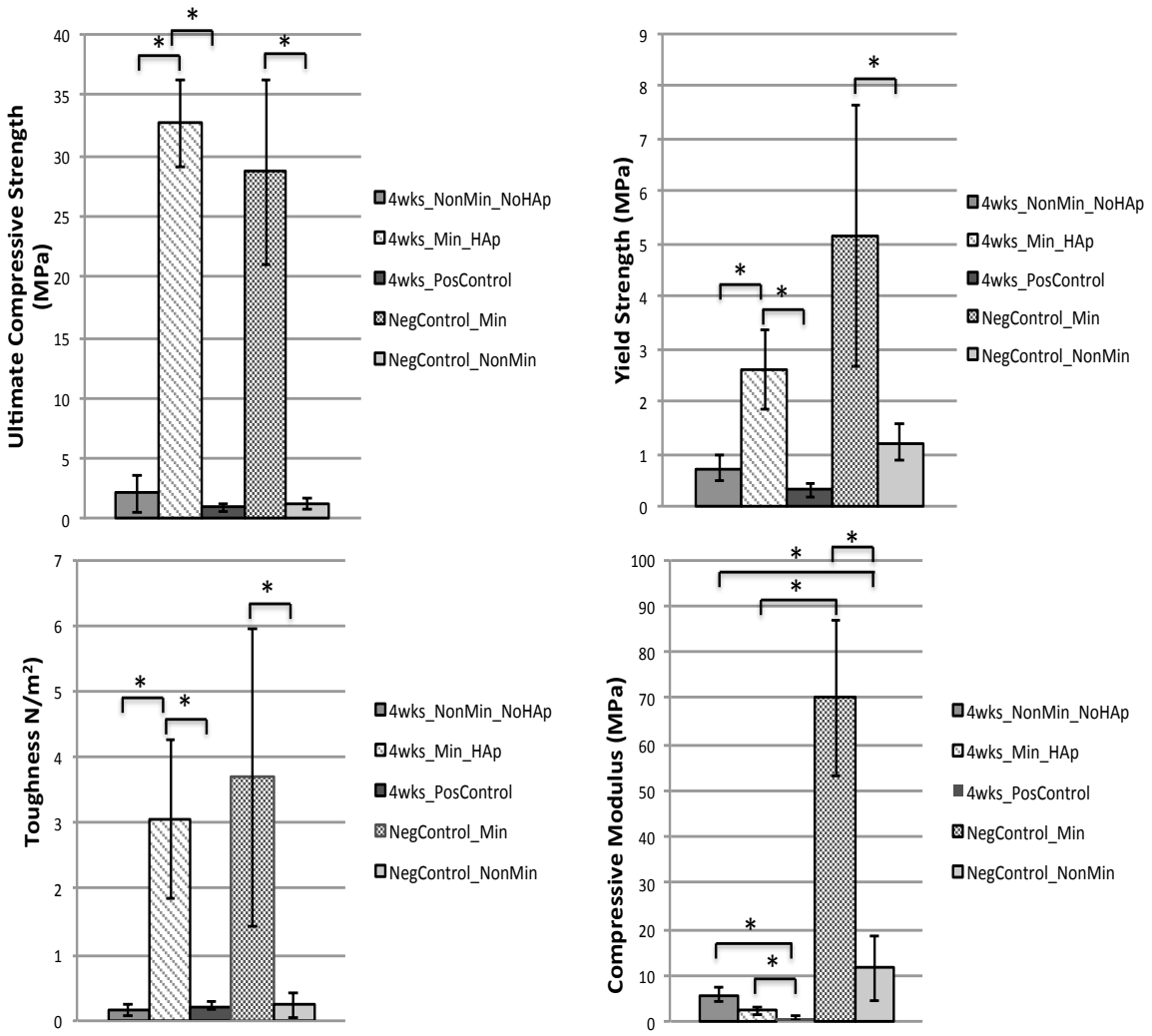

Figure 5.5. Compressive testing of excised scaffolds exhibited no significant difference in ultimate compressive strength, yield strength and toughness in comparison to their negative controls. The scaffolds with hMSCs and pre-vascularized lumens had increased mechanics in comparison to the control scaffolds. Statistical analysis: * denotes ANOVA tukey Test (post-hoc) $p<0.05$

	Ultimate Compressive Strength (MPa)	Yield Strength (MPa)	Toughness (N/m^2)	Young's Modulus (MPa)
4wks_NonMin+Lumen	2.49 ± 0.65	0.74 ± 0.27	0.16 ± 0.10	5.86 ±1.57*#
4wks_Min_Lumen	32.63 ± 3.55* %	2.60 ± 0.74*%	3.06 ± 1.20 *%	2.41 ± .081*
4wks_NonMin-Lumen	1.02 ± 0.58	0.31 ± 0.13	0.23 ± 0.05	0.79 ± 0.37
NegControl_Min	28.66 ± 7.65 **	5.17 ± 2.50 **	3.70 ± 2.27 **	70.07 ± 16.83#**
NegControl_NonMIn	1.26 ± 0.41	1.23 ± 0.34	0.23 ± 0.18	11.57 ± 6.94

Table 5.3. Mechanical properties of excised scaffolds shown as mean ± standard deviation. Negative controls were scaffolds that were not implanted as a comparison. No significant differences in UCS, yield strength, and toughness between experimental scaffolds and their corresponding negative controls. Statistical analysis performed with ANOVA tukey Test (post-hoc) $p<0.05$: * denotes significance compared to positive control group, % denotes significance compared to 4wks_NonMin_+Lumen scaffolds, # denotes significance compared to, ** denotes significance compared to NegControl_NonMin

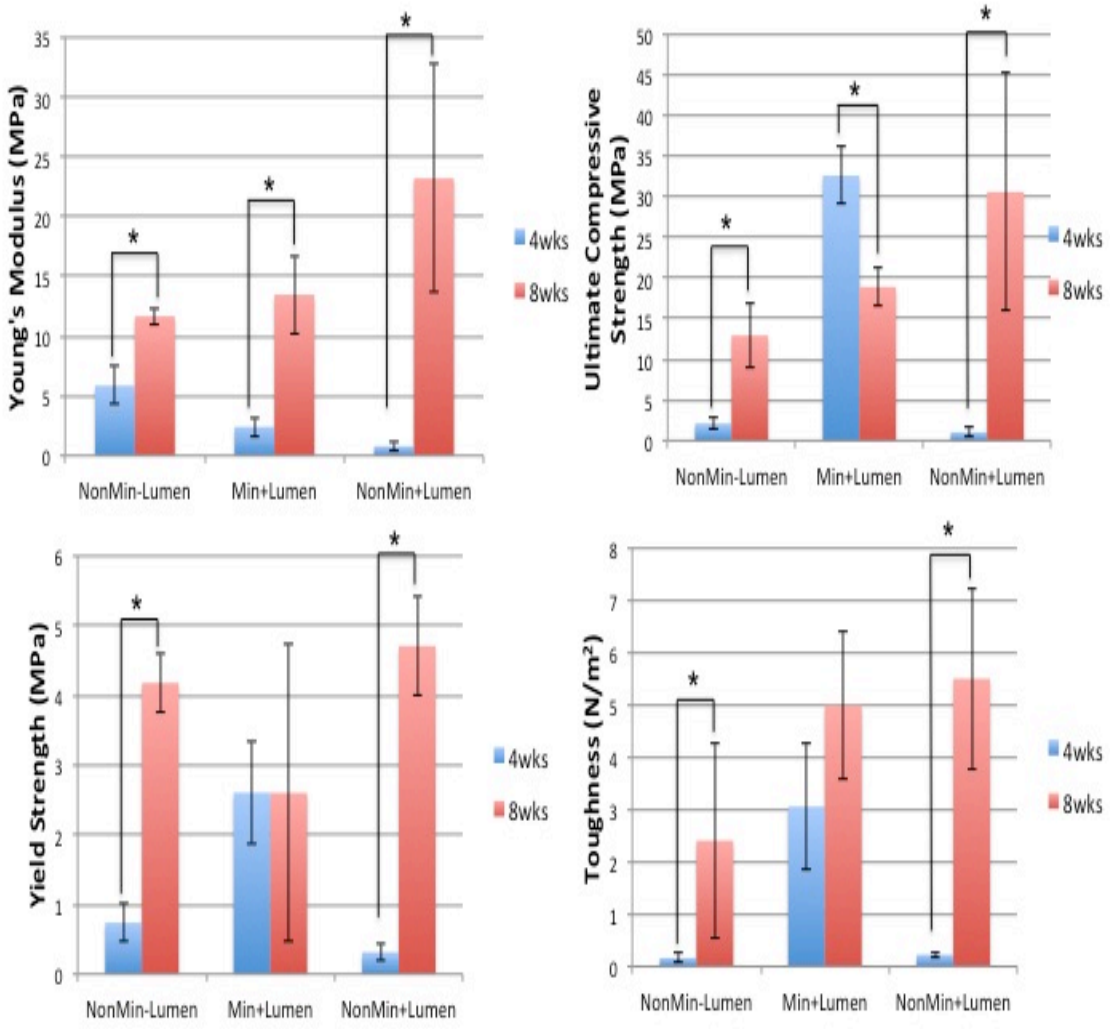

Figure 5.6. Mechanical properties of scaffold excised at 8 weeks post operation compared to the scaffolds excised at 4 weeks. There was a statistically significant increase in Young's modulus for all the groups from 4 to 8 weeks. Statistical analysis: * denotes ANOVA tukey Test (post-hoc) $p<0.05$

5.4. Conclusion

In vivo evaluation of the composite scaffold was discussed in this chapter. The scaffolds, 5mm in diameter and 10mm in length, were implanted into the dorsum of BALB/c mice

and qualitatively and quantitatively assessed for cellular infiltration and tissue development at 4 and 8 weeks. Qualitatively, the scaffolds were encapsulated in fibrous tissue, about 500μm thick, and the hollow lumen was infiltrated with vascularized tissue. The fibrotic capsule was thicker at the bottom for the scaffolds without the lumen, suggesting the lumen allowed for nutrient infiltration leading to a lesser immune response. H&E also confirmed significant cellular infiltration and the presence of blood vessels with erythrocytes at 4 weeks. There was an abundance of collagen present between the scaffold layers and mineral content in the mineralized scaffold at 4 weeks. Mechanical testing (1mm/min) was performed to determine the impact of the in vivo conditions on the structural integrity of the scaffolds. There was no significant decrease in the mechanical properties for the experimental scaffolds. The scaffolds seeded with hMSCs exhibited significantly greater strength and toughness than the control scaffolds. Furthermore, there was a significant increase in mechanical properties exhibited by the 8 week explants in comparison to the scaffolds excised at 4 weeks. The increase in mechanical properties indicates a possible increase in tissue integration. The results from this study confirm the biocompatibility of the scaffold and its ability to maintain its structure *in vivo*.

5.5. References

1. Viateau, V. and G. Guillemin, *Experimental animal modesl for tissue-engineerined bone regeneration*, in *Engineered Bone* H.P.a.R. Quatro, Editor. 2004. p. 1-17.
2. Poldervaart, M.e.a., *Prolonged presence of VEGF promotes vascularization in 3D bioprinted scaffolds with defined architecture.* Journal of controlled release, 2014.

3. Ma, J., et al., *Bone forming capacity of cell- and growth factor-based constructs at different ectopic implantation sites.* Journal of biomedical materials research. Part A, 2014.
4. Kim, K.I., S. Park, and G.I. Im, *Osteogenic differentiation and angiogenesis with cocultured adipose-derived stromal cells and bone marrow stromal cells.* Biomaterials, 2014. **35**(17): p. 4792-804.
5. Qiao, P., et al., *Injectable calcium phosphate-alginate-chitosan microencapsulated MC3T3-E1 cell paste for bone tissue engineering in vivo.* Materials science & engineering. C, Materials for biological applications, 2013. **33**(8): p. 4633-9.
6. Poldervaart, M., Wang, H., van der Stok, j., Weinans, H., Leeuwenburgh, S.C.G., Cumhur, F., Oner, C., Dhert, W.J.A., Albias, J., *Sustained Release of BMP-2 in Bioprinted Alginate for Osteogenicity in Mice and Rats.* PloS one, 2014. **8**(8): p. 1-9.
7. Rujitanaroj, P.-o., et al., *Controlling fibrous capsule formation through long-term down-regulation of collagen type I (COL1A1) expression by nanofiber-mediated siRNA gene silencing.* Acta Biomaterialia, 2013. **9**(1): p. 4513-4524.
8. Cao, H., Mchugh, K. Chew, S.Y., Anderson, J.M., *The topographical effect of electrospun nanofibrous scaffolds on the in vivo and in vitro foreign body reaction.* Journal of Biomedical Materials Research Part A, 2009. **93A**(3): p. 1151-1159.
9. Anderson, J.M., *BIOLOGICAL RESPONSES TO MATERIALS.* Annual Review of Materials Research, 2001. **31**(1): p. 81-110.
10. Spiller, K.L., et al., *The role of macrophage phenotype in vascularization of tissue engineering scaffolds.* Biomaterials, 2014. **35**(15): p. 4477-4488.
11. Ratner, B.D., *Reducing capsular thickness and enhancing angiogenesis around implant drug release systems.* Journal of Controlled Release, 2002. **78**(1–3): p. 211-218.
12. Telemeco, T.A., et al., *Regulation of cellular infiltration into tissue engineering scaffolds composed of submicron diameter fibrils produced by electrospinning.* Acta Biomaterialia, 2005. **1**(4): p. 377-385.
13. Rivet, C.J., et al., *Cell infiltration into a 3D electrospun fiber and hydrogel hybrid scaffold implanted in the brain.* Biomatter, 2015. **5**(1): p. e1005527.
14. Leong, M.F., Rasheed, M.Z. Lim, T.C., Chian, K.S, *In vitro cell infiltration and in vivo infiltration and vascularization in a fibrous, highly porous poly(D,L-lactide) scaffold fabricated by cryogenic electrospinning technique.* Journal of Biomedical Materials Research Part A, 2008. **91A**(1): p. 231-240.
15. Bañobre-López, M., et al., *Poly(caprolactone) based magnetic scaffolds for bone tissue engineering.* Journal of Applied Physics, 2011. **109**(7): p. 07B313.

CHAPTER 6: CONCLUSION AND FUTURE DIRECTIONS

6.1. Key Findings

6.1.2. Osteoinductive Trabecular Scaffold

The purpose of the trabecular scaffold was to provide a porous structure of cellular infiltration and nutrient transport and promote the osteogenic differentiation of hMSCs. First, we explored the effect of various FDA approved crosslinking agents, EDC, glutaraldehyde, and microbial transglutaminase (mTG) on the mechanical properties of gelatin-based scaffolds. mTG proved to be the optimal crosslinking agent by creating more stable collagen bonds and a stronger matrix. SEM images and energy dispersive X-ray fluorescence confirmed the presence of embedded hydroxyapatite (HAp) crystals in the scaffold. This was achieved by mixing HAp into the polymeric solution prior to electrospinning. Sintering then leaching the scaffolds creating a more stable structure with a pore range of 5 to 200μm. This pore range is desirable for osteoblastic infiltration and vascular integration [1-3]. Electrodeposition mineralization deposited 3x more mineral content than the static and flow mineralization techniques. A co-electrospinning set-up was utilized to increase the gelatin content in the scaffold. Scaffolds with increased gelatin demonstrated had higher mechanical strength and mineral content after mineralization. Additionally, we concluded scaffolds with fibers angles ranging from 15° to 45° exhibited greater mechanical strength due to the angled fibers acting as opposing internal forces. Lastly, the osteogenic potential of the scaffold with HAp was validated qualitatively and quantitatively through the detection bone marker proteins alkaline phosphate, calcium, and osteocalcin.

6.1.3. Pre-Vascularized Cortical Scaffold

The rationale behind the pre-vascularized cortical scaffold was to provide the native cells with a biomimetic pro-angiogenic endothelial lumen. The findings presented in this dissertation highlight the material and biological characterization of a scaffold that mimics the hollow cylindrical architecture of native osteons and promotes angiogenic differentiation. The scaffolds' architecture promoted cellular attachment and proliferation of human microvascular endothelial cells (HMECs) and endothelial vein umbilical cells (HUVECs). The concentric electrospun fibers also guided cellular growth circumferentially and organized collagen network within the canal of the cortical scaffold. A FDA freeze-thaw decellularization was employed and yielded an 86% decrease in cellular response with a 96% maintained collagenous/non-collagenous protein matrix. hMSCs exhibited cellular morphology indicative of endothelial lumens in 2D in response to the decellularized scaffold. Furthermore, the maintained pro-angiogenic collagenous matrix promoted differentiation of hMSCs which was confirmed by the presence of vascular endothelial growth factor, an early marker for angiogenesis. The pre-vascularized cortical scaffold combines the advantages of cell-based therapies, pro-angiogenic factors, and a stable biomimetic construct to promote the early vascularization necessary for long-term graft viability and integration.

6.1.4. HAp Columns

HAp is naturally occurring minerals with inherit osteoinductive properties. Sintered HAp has been shown to exhibit mechanical properties comparable to native bone. We investigated the integration of sintered HAp columns with the polymeric trabecular and cortical scaffold to increase the overall mechanical properties. Instron packed

nanopowder HAp sintered for 5hrs at 1200°C yielded the most mechanical enhanced HAp columns with a compressive modulus of 1079.07 ± 58.34 MPa. Finite element analysis (FEA) predicted four 1mm in diameter cylindrical HAp columns would be the optimal HAp column shape and arrangement in terms of Von Misses stress. Complete scaffolds that were constructed according to the FEA results were testing in compression. The addition of the HAp columns increases the compressive strength of the scaffolds by by 77%. Findings also concluded the active flow of mineral solution via electrodeposition mineralization was successful increasing the mineral content by 25%; yielding a complete scaffold with 62% inorganic content. In conclusion, the synthetic bone scaffold with HAp columns exhibited mechanics necessary for load-bearing applications.

6.1.5. Subcutaneous *In Vivo* Evaluation

Scaffolds, with and without the pre-vascularized lumen or mineral content, were implanted into the dorsum of BALB/c mice and qualitatively and quantitatively assessed for cellular infiltration and tissue development at 4 and 8 weeks. At 4 weeks, the scaffolds not previously with hMSCs were enveloped in an average 50μm thick fibrotic capsule and infiltration with vascularized tissue. Histology confirmed significant infiltration of cells from a mix population and the presence of erythrocytes in developed blood vessels. The compressive moduli, yield strengths, ultimate compressive strengths and toughness of the excised scaffolds was calculated and compared to determine the impact of the *in vivo* conditions on the structural integrity of the scaffolds. The mechanical testing results concluded there was no significant decrease in the scaffold's mechanical properties. The scaffolds seeded with hMSCs exhibited significantly greater strength and toughness than the control scaffolds, possibly due to tissue integration.

Additionally, the mechanical properties significantly increased from 4 to 8 weeks. The results from this study confirm the biocompatibility of the scaffold and its ability to maintain its structure *in vivo*.

6.2. Future Directions

The work featured in this dissertation focuses mainly on the in *vitro* characterization of the scaffold. While we have shown the osteoblastic differentiation and angiogenic differentiation, the interaction between endothelial cells and mineralization was not thoroughly investigated. Recent findings have concluded human endothelial cells inhibit mesenchymal stem cell differentiation into mature osteoblasts *in vitro*. To test the influence of the endothelial cells on osteoblastic differentiation of the hMSCs, a future study could be performed by co-culturing endothelial cells and pre-osteoblasts cells in the appropriate scaffolds sections, cortical and trabecular respectively, and evaluate the cell markers over time using flow cytometry and gating analysis. Flow cytometry will enable the researcher to stain the cells with multiple markers and quantify the cells based on cell type and protein expression. Furthermore, a long-term growth factor release profile of the pre-vascularized cortical scaffold will provide additional information about the presence of pro-angiogenic proteins present and the continued release over time. Along with this study, the decellularized scaffold should be freeze dried for storage and evaluated over a period of time to determine the sustainability of the pre-vascularized lumen. Future directions for the HAp columns would be to include beta-Tricalcium phosphatase with the HAp to control the degradation rates. Biphasic calcium phosphate nanocomposite

scaffolds have been shown to have mechanics comparable to bone with desirable degradation for *in vivo* load-bearing application [4].

In addition to the *in vitro* future work, scaffold implantation in a critical-size defect model is highly recommended in order to further validate the long-term graft mechanics and viability *in vivo.* Protocols have already been approved for a rabbit radial defect repair and sheep tibial defect repair. New Zealand White rabbits (~ 4kg) would be used for this study. Studies using rabbit radial models have shown successful scaffold implantation results [5]. The scaffold groups (n=8) for the rabbit study are (I) autologous bone grafts, (II) BMSC seeded scaffolds without decellularized pre-vascularized lumens and HAp, (III) BMSC seeded scaffolds with decellularized lumens and HAp, and (IV) acellular scaffolds with decellularized lumens and HAp. The scaffold will be secured with a surgical steel suture to fit a 18 mm critical size defect in the rabbit's radial bone. Half of the rabbits in each group will be sacrificed at 6 weeks and the rest at 12 week postoperatively. The foreleg bones will be removed and tested for mechanical properties and histological analysis.

In the sheep long bone resection *in vivo* study, Dorset Cross sheep approximately 4-6 years old should be used due to their mature bone structure [6]. The sheep critical-sized defect is a model that closely resembles human bone formation and structure [7-8]. The scaffold groups would be as follows (I) No Scaffold (open defect), (II) autologous bone graft, (III) acellular complete scaffold and (IV) complete scaffold with autologous sheep BMSCs. The scaffolds will be created as previously described in Chapter 2-5, but at a larger size: 30 mm in length and 22 mm. The scaffolds will have an additional 10 mm of length at each end with a smaller diameter to fit into the medullary canal and within a 30

mm long tibial defect. After fabrication, the grafts will be treated, sterilized, and seeded with autologous sheep BMSCS, if necessary, and implanted into a hind limb defect. X-ray images of the bone defect area will be taken at 4, 8 and 12 weeks. The sheep will be sacrificed at 12 weeks and the tibias will be removed and assigned to micro-computerized tomography CT analysis, mechanical and histological studies.

6.3. Contribution to Science

This technology is the first synthetic bone graft to contain biomimetic architectures and be designed for vascularized bone growth and load-bearing applications. This scaffold mimics the native trabecular and cortical bone architectures, making it a viable option for whole bone replacements. Most TE bone treatments seek to only replicate trabecular or cortical bone. The individual bone structures varying in density, location, and mechanical strength, therefore having the two structures present is physiological relevant in bone function. This technology also has the ability to promote simultaneous osteogenic and angiogenic differentiation of human stem cells. This feature will promote early graft integration and bone healing *in vivo.* Additionally, this technology can be utilized for load-bearing applications with the inclusion of HAp columns. Furthermore, the versatility of this technology makes it an option for non load-bearing applications or as a healing aid in addition to an allograft. This transformative technology is the first of its kind and has the potential to revolutionize the bone grafting industry.

6.4. References

1. Rho, J.-Y., L. Kuhn-Spearing, and P. Zioupos, *Mechanical properties and the hierarchical structure of bone.* Medical Engineering & Physics, 1998. **20**(2): p. 92-102.
2. An, Y.H. and R.A. Draughn, *Mechanical testing of bone and the bone-implant interface*. 2000, Boca Raton: CRC Press.
3. Novosel, E.C., C. Kleinhans, and K. P.J., *Vascularization is the key challenge in tissue engineering.* Adv Drug Deliv Rev, 2011. **63**(4-5): p. 300-311.
4. Ramay, H.R.R. and M. Zhang, *Biphasic calcium phosphate nanocomposite porous scaffolds for load-bearing bone tissue engineering.* Biomaterials, 2004. **25**(21): p. 5171-5180.
5. Kang, S.H., et al., *Bone regeneration potential of allogeneic or autogeneic mesenchymal stem cells loaded onto cancellous bone granules in a rabbit radial defect model.* Cell and tissue research, 2014. **355**(1): p. 81-8.
6. Marcacci, M., et al., *Reconstruction of extensive long-bone defects in sheep using porous hydroxyapatite sponges.* Calcif Tissue Int, 1999. **64**: p. 83-90.
7. Nuss, K.M., et al., *An animal model in sheep for biocompatibility testing of biomaterials in cancellous bones.* BMC musculoskeletal disorders, 2006. **7**: p. 67.
8. Reichert, J.C., et al., *A tissue engineering solution for segmental defect regeneration in load-bearing long bones.* Science translational medicine, 2012. **4**(141): p. 141ra93.